



РОССИЙСКИЙ ГОСУДАРСТВЕННЫЙ ПЕДАГОГИЧЕСКИЙ УНИВЕРСИТЕТ им. А. И. ГЕРЦЕНА  
HERZEN STATE PEDAGOGICAL UNIVERSITY of RUSSIA

ISSN 2687-153X

# PHYSICS OF COMPLEX SYSTEMS

T. 3 № 1 2022

VOL. 3 No. 1 2022



Herzen State Pedagogical University of Russia

ISSN 2687-153X (online)

[physcomsys.ru](http://physcomsys.ru)

<https://www.doi.org/10.33910/2687-153X-2022-3-1>

2022. Vol. 3, no. 1

## PHYSICS OF COMPLEX SYSTEMS

Mass Media Registration Certificate El No. FS77-77889, issued by Roskomnadzor on 10 February 2020

Peer-reviewed journal

Open Access

Published since 2020

4 issues per year

### Editorial Board

*Editor-in-chief* Alexander V. Kolobov (Saint Petersburg, Russia)

*Deputy Editor-in-chief* Andrey K. Belyaev (Saint Petersburg, Russia)

*Deputy Editor-in-chief* Yuri A. Gorokhovatsky (Saint Petersburg, Russia)

*Assistant Editor* Alexey A. Kononov (Saint Petersburg, Russia)

Vachagan T. Avanesyan (Saint Petersburg, Russia)

Alexander P. Baraban (Saint Petersburg, Russia)

Paul Barklem (Uppsala, Sweden)

Sergey P. Gavrilov (Saint Petersburg, Russia)

Dmitry M. Gitman (São Paulo, Brazil)

Vladimir M. Grabov (Saint Petersburg, Russia)

Andrey A. Grib (Saint Petersburg, Russia)

Elisabeth Dalimier (Paris, France)

Alexander Z. Devdariani (Saint Petersburg, Russia)

Vadim K. Ivanov (Saint Petersburg, Russia)

Rene A. Castro Arata (Saint Petersburg, Russia)

Miloš Krbal (Pardubice, the Czech Republic)

Sergey A. Nemov (Saint Petersburg, Russia)

Albina Nikolaeva (Chişinău, Moldova)

Oleg Yu. Prikhodko (Almaty, Kazakhstan)

Igor P. Pronin (Saint Petersburg, Russia)

Mikhail Yu. Puchkov (Saint Petersburg, Russia)

Alexey E. Romanov (Saint Petersburg, Russia)

Pavel P. Seregin (Saint Petersburg, Russia)

Nicole Feautrier (Paris, France)

Koichi Shimakawa (Gifu, Japan)

### Advisory Board

Gennady A. Bordovsky (Saint Petersburg, Russia)

Alexander V. Ivanchik (Saint Petersburg, Russia)

Vladimir V. Laptev (Saint Petersburg, Russia)

Alexander S. Sigov (Moscow, Russia)

Publishing house of Herzen State Pedagogical University of Russia

48 Moika Emb., Saint Petersburg 191186, Russia

E-mail: [izdat@herzen.spb.ru](mailto:izdat@herzen.spb.ru)

Phone: +7 (812) 312-17-41

Data size 4,70 Mbyte

Published at 29.03.2022

The contents of this journal may not be used in any way without a reference to the journal "Physics of Complex Systems" and the author(s) of the material in question.

Editors of the English text *I. A. Nagovitsyna, A. S. Samarsky*

Cover design by *O. V. Rudneva*

Layout by *A. M. Khodan, L. N. Kliuchanskaya*



Saint Petersburg, 2022

© Herzen State Pedagogical University of Russia, 2022

## CONTENTS

<b>Condensed Matter Physics</b> .....	<b>3</b>
<i>Shishkin N. D., Guliakova A. A.</i> Ferroelectric polymers with improved performance. ....	3
<i>Salnikova Zh. A., Kononov A. A., Smirnov A. P., Castro Arata R. A.</i> Application of the complex electrical module method for the determination of the relaxation parameters of dielectrics with high electrical conductivity .....	11
<i>Timoshnev S. N., Benemanskaya G. V.</i> The electronic structure of the K/AlN nanointerface. ....	21
<b>Theoretical physics</b> .....	<b>25</b>
<i>Belyaev A. K.</i> Reprojection method for inelastic processes in atomic collisions within Born-Oppenheimer approach .....	25
<i>Bagmutov A. S., Popov I. Y.</i> Bound states for two delta potentials supported on parallel lines on the plane .....	37
<b>Physics of Semiconductors</b> .....	<b>43</b>
<i>Castro Arata R. A., Ilinskiy A. V., Klimov V. A., Pashkevish M. E., Shadrin E. B.</i> Dielectric spectroscopy of VO <sub>2</sub> nanocrystalline films .....	43
<b>Summaries in Russian</b> .....	<b>51</b>



Check for updates

Condensed Matter Physics. Dielectric Physics

UDC 538.9

<https://www.doi.org/10.33910/2687-153X-2022-3-1-3-10>

# Ferroelectric polymers with improved performance

N. D. Shishkin<sup>1</sup>, A. A. Guliakova<sup>✉1</sup>

<sup>1</sup> Herzen State Pedagogical University of Russia, 48 Moika Emb., Saint Petersburg 191186, Russia

## Authors

Nikolay D. Shishkin, e-mail: [expert.shishkin2012@yandex.ru](mailto:expert.shishkin2012@yandex.ru)

Anna A. Guliakova, ORCID: 0000-0002-0193-7298, e-mail: [a.guliakova@gmail.com](mailto:a.guliakova@gmail.com)

**For citation:** Shishkin, N. D., Guliakova, A. A. (2022) Ferroelectric polymers with improved performance. *Physics of Complex Systems*, 3 (1), 3–10. <https://www.doi.org/10.33910/2687-153X-2022-3-1-3-10>

**Received** 29 December 2021; reviewed 13 January 2022; accepted 13 January 2022.

**Funding:** The study did not receive any external funding.

**Copyright:** © N. D. Shishkin, A. A. Guliakova (2022). Published by Herzen State Pedagogical University of Russia. Open access under [CC BY-NC License 4.0](https://creativecommons.org/licenses/by-nc/4.0/).

**Abstract.** This article offers a short overview of the unique properties of PVDF-based electroactive polymers and their applications. Ferroelectric materials are widely used in modern electronics. Relaxor-ferroelectric terpolymers are multifunctional materials with high electrostrictive strain which, in turn, leads to large actuation capability. The terpolymer with chlorofluoroethylene shows relaxor-ferroelectric behavior with vanishing hysteresis effect but considerably higher polarization. Therefore, such material is a potential candidate for energy-storage devices (supercapacitors).

**Keywords:** ferroelectric polymers, polyvinylidene fluoride, polarization, energy conversion, energy storage

## Introduction

Polyvinylidene fluoride (PVDF) and its copolymer with trifluoroethylene P(VDF-TrFE) are ferroelectric polymers which exhibit pronounced polarization-versus-field hysteresis and related electromechanical and thermoelectrical response, in particular the piezo- and pyroelectric effect. The terpolymer with chlorofluoroethylene P(VDF-TrFE-CFE) shows relaxor-ferroelectric behavior with vanishing hysteresis effect, but considerably higher polarization (Bauer et al. 2004; Klein et al. 2005). Therefore, this terpolymer is a promising candidate for energy-storage devices (supercapacitors) and—given its low elastic modulus—for electromechanical actuators, which use the electrostrictive effect or the Maxwell strain caused by application of a strong DC field.

Since the discovery of piezoelectricity of PVDF in 1969 (Kawai 1969), PVDF and its copolymers have been the subject of numerous structural, dynamic-mechanical, thermal and electrical studies focused on investigating how their preparation-induced microstructure determines their mechanical and electrical behaviour and how this microstructure can be changed by external loads and fields. These studies have been summarized in several review articles and monographs (Furukawa 1989; 1994; 1997; Kepler, Anderson 1992; Kochervinskii 1996; Lovinger 1983; Nalwa 1995).

There have been many successful attempts to use these properties commercially in sensor and actuator applications (piezoelectric transducers, motion detectors, ultrasonic detectors, micro-actuators) and in organic electronics (OFETs) (Bauer, Bauer 2008; Furukawa et al. 2010; Park et al. 2008). An important advantage of ferroelectric polymers in comparison with inorganic ferroelectrics is that they can be processed as flexible free-standing films of only a few micrometers in thickness or as thin submicrometer films on a substrate.

As in inorganic ferroelectrics, the ferroelectricity of PVDF and P(VDF-TrFE) is a property of a polar crystalline phase, but the structure and the elastic properties of the amorphous phase embedding the polar crystallites strongly determines the macroscopic ferroelectric behaviour of the polymers. There exist several polar and non-polar crystalline phases depending on processing conditions and pre-history of the film. Moreover, the intermediate phases between amorphous and crystalline phases must be considered in order to explain the polymers' dynamic-mechanical and electro-mechanical properties. Chemical modification of P(VDF-TrFE) with CFE considerably reduces the crystallite size, leading to a transformation of the ferroelectric-to-paraelectric phase transition into a process that shows features of a strong relaxation. This process determines the high polarization with only little polarization-versus-field hysteresis.

### **Preparation of ferroelectric polymer films**

Films of PVDF and its copolymers can be obtained by solution casting, doctor blading or spin coating from a solution in a polar solvent. With the exception of the copolymer of PVDF with TrFE and the terpolymer, which can both be prepared as (relaxor)-ferroelectric films without further treatment; the other known ferroelectric polymers need subsequent mechanical stretching in order to induce the formation of a ferroelectric phase. This treatment aligns the polymer chains of the amorphous phase in parallel, thus transforming the thermodynamically preferred but nonpolar crystalline  $\alpha$  phase into the polar  $\beta$  phase. It is the same polar phase which is formed spontaneously for sterical reasons in the copolymer with TrFE. In order to induce a ferroelectric polarization, the molecular dipoles in the polar phase must afterwards be oriented in an electric field higher than a certain threshold (the coercive field).

During this field treatment, the dipole alignment is stabilized by Coulomb interaction with interface charges accumulated on the phase boundaries between the polar crystallites and their amorphous environment, which are injected from the metal contacts or generated by dissociation of fluorine or impurities (Sessler et al. 1992).

### **Electro-mechanical response of PVDF and its derivatives in relation to their structure**

Up to now, the majority of applications have been based on PVDF-TrFE because of its easy processing as a ferroelectric free-standing thin film or as a ferroelectric film on a substrate and its relatively high piezo- and pyroelectric response, which is only slightly lower than that of the homopolymer PVDF. The piezoelectric  $d_{33}$  coefficient of PVDF-TrFE is about 20 pC/N, about ten times higher than the piezoelectric response of quartz. However, the thermal stability of PVDF-TrFE ferroelectric polarization is relatively low; it cannot be used at elevated temperatures for longer periods of time. Though there exists a Curie transition at about 100 °C (depending on the TrFE/VDF ratio), the domain orientation decays gradually, because the stabilizing charges flow away or become neutralized at temperatures above the glass transition and because secondary crystallization disturbs the parallel-chain all-trans configuration above 50 °C (Fruebing et al. 2012). The homopolymer is thermally more stable, but in principle exhibits similar mechanisms of polarization decay.

The terpolymer is characterized by a low elastic modulus, which enables a considerable and reversible change of film thickness under mechanical or electrical stress or a deformation of a clamped film, which can be used for the design of micro-actuators. The underlying physical processes are the electrostrictive effect and the Maxwell strain, which is caused by Coulomb attraction between the oppositely charged electrodes.

### **From normal ferroelectric copolymer into a ferroelectric relaxor**

Molecular conformations for PVDF-based polymers are shown in Fig. 1 (Bachmann, Lando 1981). A significant change in various properties, as well as polarization and strain change could be caused by a reversible molecular change from nonpolar to polar forms. Unfortunately, this is not the case for traditional ferroelectric PVDF and copolymers.

It has been shown (Fig. 2) that by introducing defects via high electron irradiation of P(VDF-TrFE) copolymers, the copolymer is converted from a normal ferroelectric to a relaxor ferroelectric. (Bauer 2012; Zhang et al. 1998).

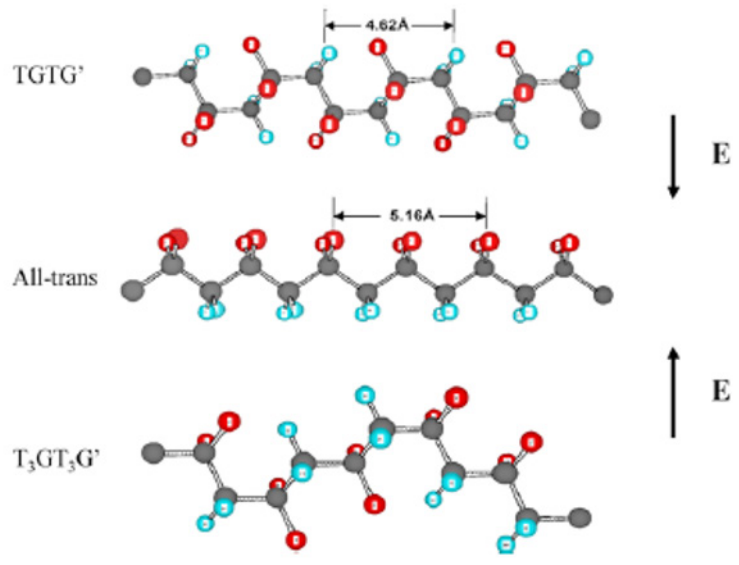


Fig. 1. The conformations of P(VDF-TrFE) copolymer (Bauer 2012)

Here, the polarization practically disappears and the dielectric response shows typical ferroelectric relaxor behavior. The main reason for the observed large electrostrictive strain is the change in conformation from the disordered TG and  $T_3G$  to the all-trans conformation.

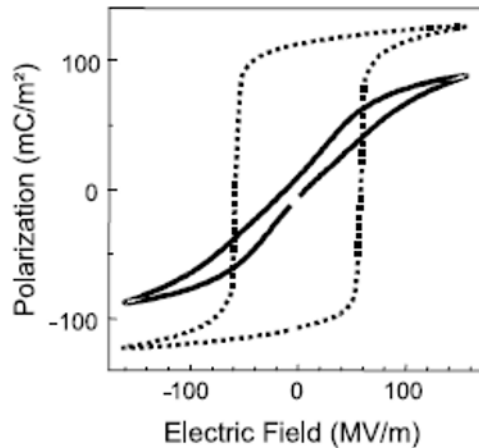


Fig. 2. Influence of defect modifications (Zhang et al. 1998)

Defect modification is another effective way to produce relaxor ferroelectric polymers from P(VDF-co-TrFE) and to modify the Curie transition (Yang, Li et al. 2013). Thus, a new class of ferroelectric polymers, i. e., the terpolymers of P(VDF-TrFE-CFE) and P(VDF-TrFE-CTFE), were synthesized. When the third monomer is introduced into the polymer chain, it interrupts the ferroelectric domains, reducing their size and forcing a conformation change from the all-trans ( $T_m \geq 4$ ) or conformation to the trans-gauche (TG) and  $T_3G$  conformations. Such an introduction broadens the ferroelectric transition and reduces the ferroelectric–paraelectric transition temperature (Bachmann, Lando 1981; Bobnar et al. 2003; Huang et al. 2004; Klein et al. 2005; Petchsuk 2003). These relaxor-ferroelectric terpolymers exhibit a room temperature dielectric constant greater than 50 (Bauer, Fousson et al. 2004; Huang et al. 2004; Lu et al. 2006; Xia et al. 2002).

The observed high electrostrictive strain, together with relatively high modulus, makes polymers suitable as structural components in addition to their electroactive functions (actuators and sensors). The amount of monomers added to the P(VDF-TrFE) has a great influence on the strain response and

the polarization hysteresis by changing the spontaneous polarization, the crystallinity, the Young's modulus, the dielectric properties, and the structural conformations (Petchsuk 2003).

### Some important applications

#### *Pyroelectric applications*

Ferroelectric polymers are a good choice for sensors and energy harvesting devices (Ploss, Domig 1994; Pecora et al. 2012; Setiadi et al. 1999; Whatmore 1986). The most successful ferroelectric polymers for pyroelectric energy harvesting are copolymers and terpolymers, due to their high pyroelectric coefficients ( $\approx 60 \mu\text{C m}^{-2} \text{K}^{-1}$  for the terpolymer) (Li, Wang 2016).

#### *Electrocaloric refrigeration*

Ferroelectrics are preferred electrocaloric materials as they demonstrate large spontaneous electrical polarizations and ferroelectric–paraelectric phase transition, where significant changes in spontaneous electrical polarization take place. They became even more relevant in energy efficient and environmentally-friendly refrigeration (Mischenko et al. 2006; Neese et al. 2008). Here, the idea is to use electrocaloric effect as a technology alternative to conventional vapor-compression, since ferroelectric polymers have much higher breakdown strength in comparison with inorganic materials. Therefore, when a high driving field is applied to the polymers for sizable electrocaloric heat; ferroelectric polymers produce larger Q values. Relaxor ferroelectric polymers show remarkable electrocaloric performance over a wider temperature range than normal ferroelectric polymers (Li et al. 2011; 2012; Peng et al. 2013).

#### *Application in electric energy storage*

Polymer-based capacitors demonstrate high energy density, low loss, high reliability, easy processing, and feasibility. Due to the ferroelectricity of (PVDF)-based polymers, they exhibit much higher polarization response under an electric field, in comparison with other linear dielectric polymers for capacitor applications.

The stored and discharged electric energy density for a non-linear dielectric polymer is easily calculated. Fig. 3 shows the polarization hysteresis loop for terpolymer, from which the stored and discharged energy density can be obtained (Bauer et al. 2006). The implementation of defect modifications stabilizes the paraelectric  $\alpha$  phase and reduces the remnant polarization (Chu et al. 2006). The discharged energy density of these PVDF-based copolymers is greatly improved over that of the PVDF homopolymer (Chu et al. 2006; Li, Wang 2016).

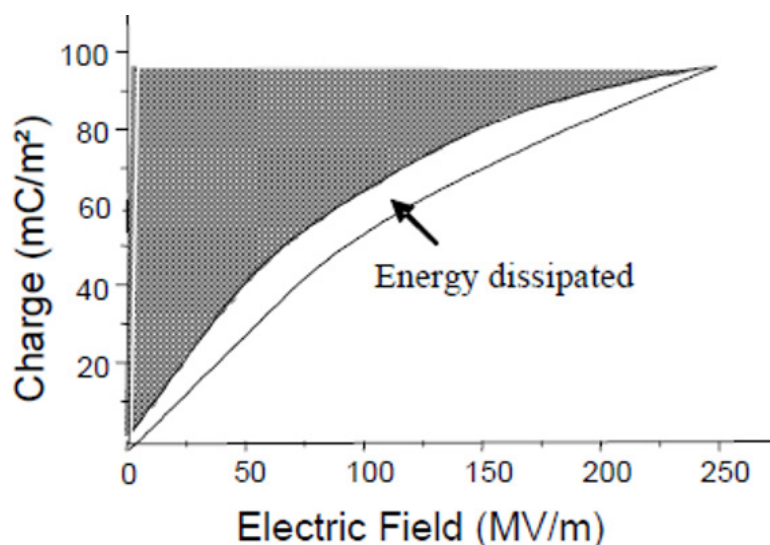


Fig. 3. Determination of discharged/released energy density (shaded area) and dissipation energy (open area) for terpolymer film (Bauer et al. 2006)

Incorporating a third monomer, such as CTFE and CFE, into P(VDF-TrFE) reduces the ferroelectric domain size and the energy barrier in phase transition, and thereby the normal ferroelectric copolymer is converted to a terpolymer with relaxor ferroelectric behaviour (Bauer et al. 2006; Li, Wang 2016). Relaxor ferroelectricity helps to reduce hysteresis loss and improves the charge–discharge efficiency, while their high dielectric constants promote polarizations.

### Actuators

Electromechanical properties of different ferroelectric materials—such as, for example, the maximum strain and the elastic modulus—were compared (Bauer et al. 2007; Cross 1996; Park, Shrout 1997). Terpolymer was found to demonstrate high strain change and high elastic energy density which, in turn, can lead to high motion of a based terpolymer unimorph (Bauer 2012; Zhang et al. 1998). The large electrostrictive strains, which can be induced by an external electric field, are a unique feature of such materials ( Bauer et al. 2006; Zhang et al. 2004). These terpolymer properties are very important for the developments of actuators; one of the possible configurations is shown on Fig. 4.

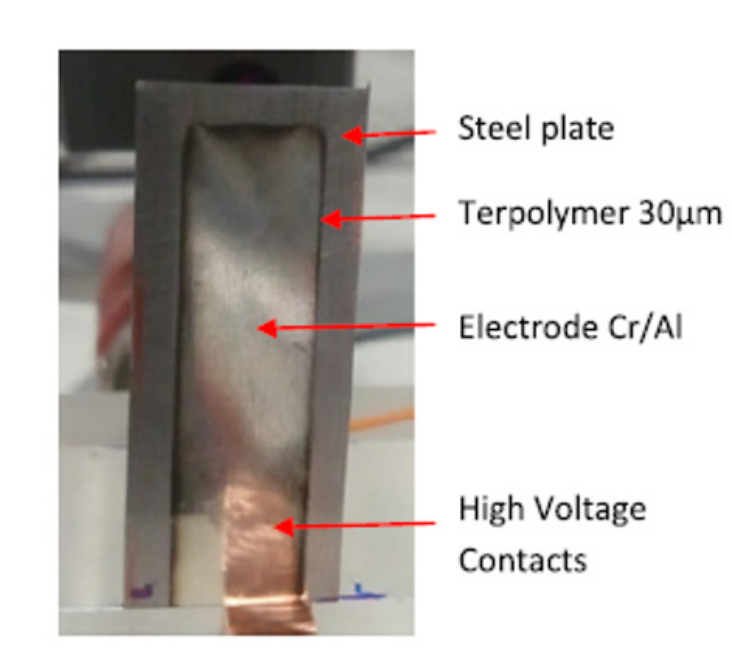


Fig. 4. Actuator configuration for the control of micro pulsed air jet from the shell of a projectile (Bauer 2012; Zngan et al. 1998; Xia et al. 2002)

Terpolymers are also promising materials for tactile display applications (Bar-Cohen 2010). It is important to develop a miniature actuator that can meet both the Braille displacement and force requirements while operating at low voltage. Due to the large transverse electrostrictive strains and high elastic modulus, P(VDF-TrFE)-based terpolymers could be successfully used for compact actuation devices (Xia et al. 2002; Zhang et al. 1998). These actuator polymers can be fabricated into thin films (down to 1  $\mu\text{m}$ ) enabling low operation voltages for practical commercial devices. Actuators made from P(VDF-TrFE-CFE) and Braille cell design is shown in Fig. 5 (Levard et al. 2012; Bauer 2012). The actuators may also be suitable for a wide range of other applications, including artificial muscles, mechanisms, smart structures, and robotics (Chuc et al. 2008; Rajamani et al. 2008; Ren et al. 2007).

Another device based on electroactive polymer was developed by (Choi et al. 2009) (see Fig. 6). Here, actuators push the optical fluid in the chambers into the lens part, which produces a bending deformation of the elastomer membrane corresponding to the change of focal length (Bauer 2012; Choi et al. 2009).

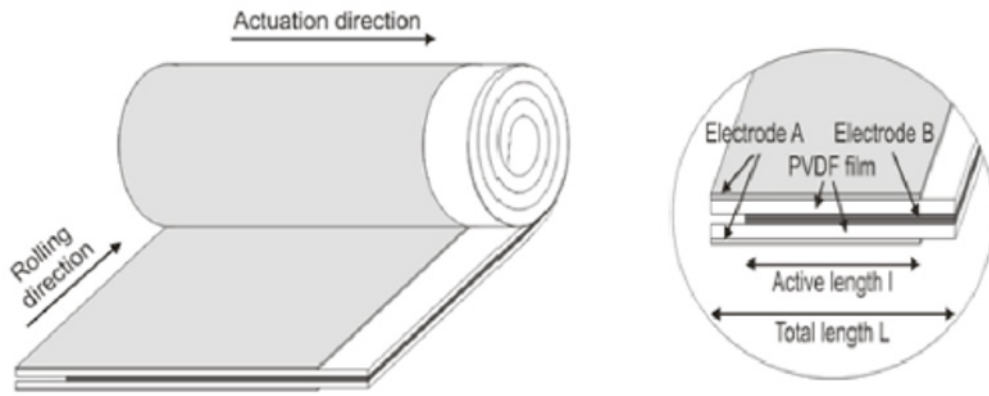


Fig. 5. Actuator design (Levard et al. 2012)

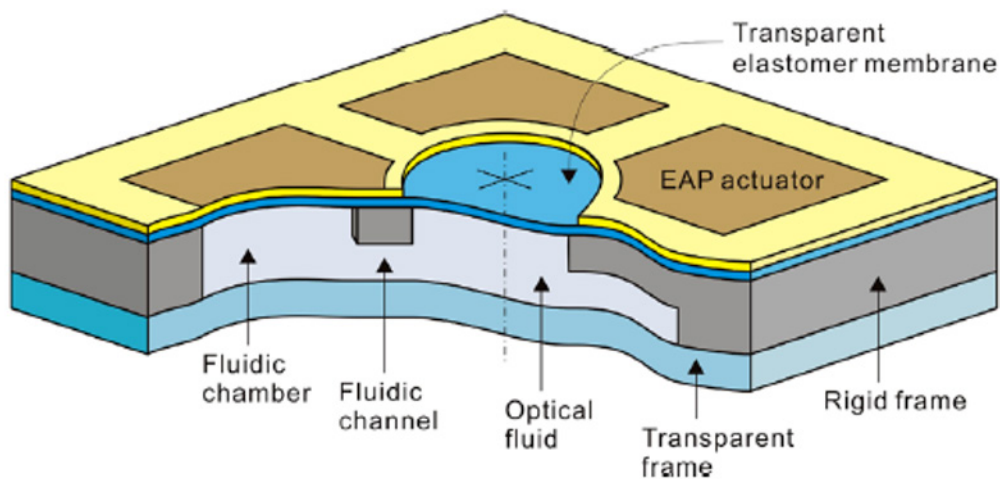


Fig. 6. Scheme of the liquid-filled varifocal lens (Bauer 2012; Choi et al. 2009)

## Conclusion

Ferroelectric polymers possess unique physical properties, as well as plenty of advantages of organic materials (processability, flexibility, etc.). Relaxor-ferroelectric terpolymers based on PVDF have become an essential part of advanced electronics, as well as energy storage and conversion devices. Here, some applications of such materials have been presented.

## Conflict of Interest

The authors declare that there is no conflict of interest, either existing or potential.

## References

- Bachmann, M., Lando, J. (1981) A reexamination of the crystal structure of phase II of poly(vinylidene fluoride). *Macromolecules*, 14 (1), 40–46. <https://doi.org/10.1021/ma50002a006> (In English)
- Bar-Cohen, Y. (2010) Refreshable Braille displays using EAP actuators. In: Y. Bar-Cohen (ed.). *SPIE Proceedings. Vol. 7642. Electroactive Polymer Actuators and Devices (EAPAD)*. Bellingham: SPIE Publ., article 764206. <https://doi.org/10.1117/12.844698> (In English)
- Bauer, F. (2012) Review on the properties of the ferrorelaxor polymers and some new recent developments. *Applied Physics A*, 107 (3), 567–573. <https://doi.org/10.1007/s00339-012-6831-8> (In English)

- Bauer, F., Fousson, E., Zhang, Q. M. (2006) Recent advances in highly electrostrictive P(VDF-TrFE-CFE) terpolymers. *IEEE Transactions on Dielectrics and Electrical Insulation*, 13 (5), 1149–1154. <https://doi.org/10.1109/TDEI.2006.247843> (In English)
- Bauer, F., Fousson, E., Zhang, Q. M., Lee, M. L. (2004) Ferroelectric copolymers and terpolymers for electrostrictors: Synthesis and properties. *IEEE Transactions on Dielectrics and electrical insulation*, 11 (2), 293–298. <https://doi.org/10.1109/TDEI.2004.1285900> (In English)
- Bauer, F. (2007) Brevet 05 08050, US-Patent 2007/0167590 A1, Method for the Production of Terpolymers based on VDF, TrFE and CFE, or CFTE. (In English)
- Bauer, F., Fousson, E., Zhang, Q. M., Lee, M. L. (2004) Ferroelectric copolymers and terpolymers for electrostrictors: Synthesis and properties. *IEEE Transactions on Dielectrics and Electrical Insulation*, 20 (2), 293–297. <https://doi.org/10.1109/TDEI.2004.1285900> (In English)
- Bauer, S., Bauer, F. (2008) Piezoelectric polymers and their applications. In: *Piezoelectricity. Springer Series in Materials Science. Vol. 114*. Berlin; Heidelberg: Springer Verlag, pp. 157–177. [https://doi.org/10.1007/978-3-540-68683-5\\_6](https://doi.org/10.1007/978-3-540-68683-5_6) (In English)
- Bobnar, V., Vodopivec, B., Levstik, A. (2003) Dielectric properties of relaxor-like vinylidene fluoride-trifluoroethylene-based electroactive polymers. *Macromolecules*, 36 (12), 4436–4442. <https://doi.org/10.1021/ma034149h> (In English)
- Choi, S. T., Lee, J. Y., Kwon, J. O. et al. (2009) Liquid-filled varifocal lens on a chip. In: D. L. Dickensheets, H. Schenk, W. Piyawattanametha (eds.). *SPIE Proceedings. Vol. 7208. MOEMS and Miniaturized Systems VIII*. Bellingham: SPIE Publ., article 72080. <https://doi.org/10.1117/12.811401> (In English)
- Chu, B., Zhou, X., Ren, K. et al. (2006) A dielectric polymer with high electric energy density and fast discharge speed. *Science*, 313 (5785), 334–336. <https://doi.org/10.1126/science.1127798> (In English)
- Chuc, N. H., Chuc, J., Choon, K., Lee, Y. (2008) Artificial muscle actuator based on the synthetic elastomer. *International Journal of Control, Automation, and Systems*, 6 (6), 894–903. (In English)
- Cross, L. E. (1996) Ferroelectric ceramics: Materials and application issues. In: K. M. Nair, V. N. Shukla (eds.). *Ceramic Transactions. Vol. 68. Hybrid microelectronic materials*. Westerville: American Ceramic Society Publ., pp. 15–55. (In English)
- Fruebing, P., Wang, F., Wegener, M. (2012) Relaxation processes and structural transitions in stretched films of polyvinylidene fluoride and its copolymer with hexafluoropropylene. *Applied Physics A*, 107 (3), 603–611. <https://doi.org/10.1007/s00339-012-6838-1> (In English)
- Furukawa, T. (1989) Ferroelectric properties of vinylidene fluoride copolymers. *Phase Transitions. A Multinational Journal*, 18 (3–4), 143–211. <https://doi.org/10.1080/01411598908206863> (In English)
- Furukawa, T. (1994) Structure and properties of ferroelectric polymers. *Key Engineering Materials*, 92–93, 15–30. <https://doi.org/10.4028/www.scientific.net/KEM.92-93.15> (In English)
- Furukawa, T. (1997) Structure and functional properties of ferroelectric polymers. *Advances in Colloid and Interface Science*, 71–72, 183–208. [https://doi.org/10.1016/S0001-8686\(97\)90017-8](https://doi.org/10.1016/S0001-8686(97)90017-8) (In English)
- Furukawa, T., Takahashi, Y., Nakajima, T. (2010) Recent advances in ferroelectric polymer thin films for memory applications. *Current Applied Physics*, 10 (1), e62–e67. <https://doi.org/10.1016/j.cap.2009.12.015> (In English)
- Huang, C., Klein, R., Xia, F. et al. (2004) Poly(vinylidene fluoride-trifluoroethylene) based high performance electroactive polymers. *IEEE Transactions on Dielectrics and Electrical Insulation*, 11 (2), 299–311. <http://dx.doi.org/10.1109/TDEI.2004.1285901> (In English)
- Kawai, H. (1969) The Piezoelectricity of Poly (vinylidene Fluoride). *Japanese Journal of Applied Physics*, 8 (7), 975–976. <https://doi.org/10.1143/JJAP.8.975> (In English)
- Kepler, R. G., Anderson, R. A. (1992) Ferroelectric polymers. *Advances in Physics*, 41 (1), 1–57. <https://doi.org/10.1080/00018739200101463> (In English)
- Klein, R. J., Xia, F., Zhang, Q. M. (2005) Influence of composition on relaxor ferroelectric and electromechanical properties of poly(vinylidene fluoride-trifluoroethylene-chlorofluoroethylene). *Journal of Applied Physics*, 97 (9), article 094105. <https://doi.org/10.1063/1.1882769> (In English)
- Kochervinskii, V. V. (1996) The structure and properties of block poly(vinylidene fluoride) and systems based on it. *Russian Chemical Review*, 65 (10), article 865913. <https://doi.org/10.1070/RC1996v065n10ABEH000328> (In English)
- Levard, T., Diglio, P. J., Lu, Sh-G. et al. (2012) Core-free rolled actuators for Braille displays using P(VDF-TrFE-CFE), *Smart Materials Structure*, 21 (1), article 012001. <https://doi.org/10.1088/0964-1726/21/1/012001> (In English)
- Li, Q., Wang, Q. (2016) Ferroelectric polymers and their energy-related applications. *Macromolecular Chemistry and Physics*, 217 (11), 1228–1244. <https://doi.org/10.1002/macp.201500503> (In English)
- Li, X., Qian, X-sh., Lu, S. G. et al. (2011) Tunable temperature dependence of electrocaloric effect in ferroelectric relaxor poly(vinylidene fluoride-trifluoroethylene-chlorofluoroethylene terpolymer). *Applied Physics Letters*, 99 (5), article 052907. <https://doi.org/10.1063/1.3624533> (In English)

- Li, X., Qian, X-sh., Gu, H. et al. (2012) Giant electrocaloric effect in ferroelectric poly(vinylidene fluoride-trifluoroethylene) copolymers near a first-order ferroelectric transition. *Applied Physics Letters*, 101 (13), article 132903. <https://doi.org/10.1063/1.4756697> (In English)
- Lovinger, A. J. (1983) Ferroelectric polymers. *Science*, 220 (4602), 1115–1121. <https://doi.org/10.1126/science.220.4602.1115> (In English)
- Lu, Y., Claude, J., Neese, B. et al. (2006) A modular approach to ferroelectric polymers with chemically tunable curie temperatures and dielectric constants. *Journal of the American Chemical Society*, 128 (25), 8120–8121. <https://doi.org/10.1021/ja062306x> (In English)
- Mischenko, A., Zhang, Q., Scott, J. F. et al. (2006) Giant electrocaloric effect in thin-film  $\text{PbZr}_{0.95}\text{Ti}_{0.05}\text{O}_3$ . *Science*, 311 (5765), 1270–1271. <https://doi.org/10.1126/science.1123811> (In English)
- Nalwa, H. S. (1995) *Ferroelectric polymers: Chemistry, physics and applications*. New York: Dekker Publ., 895 p. (In English)
- Neese, B., Chu, B., Lu, S. G. et al. (2008) Large electrocaloric effect in ferroelectric polymers near room temperature. *Science*, 321 (5890), 821–823. <https://doi.org/10.1126/science.1159655> (In English)
- Park, S.-E., Shrout, T. (1997) Ultrahigh strain and piezoelectric behavior in relaxor based ferroelectric single crystals. *Journal of Applied Physics*, 82 (4), article 1804. <https://doi.org/10.1063/1.365983> (In English)
- Park, Y. J., Jeong, H. J., Chang, J. et al. (2008) Recent development in polymer ferroelectric field effect transistor memory. *Journal of Semiconductor Technology and Science*, 8 (1), 51–65. <https://doi.org/10.5573/JSTS.2008.8.1.051> (In English)
- Pecora, A., Maiolo, L., Maita, F., Minotti, A. (2012) Flexible PVDF-TrFE pyroelectric sensor driven by polysilicon thin film transistor fabricated on ultra-thin polyimide substrate. *Sensors and Actuators A: Physical*, 185, 39–43. <https://doi.org/10.1016/j.sna.2012.07.013> (In English)
- Peng, B., Fan, H., Zhang, Q. (2013) A giant electrocaloric effect in nanoscale antiferroelectric and ferroelectric phases coexisting in a relaxor  $\text{Pb}_{0.8}\text{Ba}_{0.2}\text{ZrO}_3$  thin film at room temperature. *Advanced Functional Materials*, 23 (23), 2987–2992. <https://doi.org/10.1002/adfm.201202525> (In English)
- Petchsuk, A. (2003) *Ferroelectric terpolymers, based on semicrystalline VDF/TRFE/chloro-containing termonomers: Synthesis, electrical properties, and functionalization reactions. Thesis in Materials Science and Engineering*. Pennsylvania, Pennsylvania State University, 182. (In English)
- Ploss, B., Domig, A. (1994) Static and dynamic pyroelectric properties of PVDF. *Ferroelectrics*, 159 (1), 263–268. <https://doi.org/10.1080/00150199408007583> (In English)
- Rajamani, A., Grissom, M., Rahn, Ch. D, Zhang, Q. (2008) Wound roll dielectric elastomer actuators: Fabrication, analysis, and experiments. *IEEE/ASME Transactions on Mechatronics*, 13 (1), 117–124. <https://doi.org/10.1109/TMECH.2008.915825> (In English)
- Ren, K., Liu, Sh., Lin, M. et al. (2007) A compact electroactive polymer actuator suitable for refreshable Braille display. *Sensors and Actuators A: Physical*, 143 (2), 335–342. <https://doi.org/10.1016/j.sna.2007.10.083> (In English)
- Sessler, G. M., Das-Gupta, D. K., DeReggi, A. S. et al. (1992) Piezo and pyroelectricity in electrets: Caused by charges, dipoles, or both? *IEEE Transactions on Electrical Insulation*, 27, 872–897. <https://doi.org/10.18419/opus-4986> (In English)
- Setiadi, D., Weller, H., Binnie, T. D. (1999) A pyroelectric polymer infrared sensor array with a charge amplifier readout. *Sensors and Actuators A: Physical*, 76 (1–3), 145–151. [https://doi.org/10.1016/S0924-4247\(98\)00372-0](https://doi.org/10.1016/S0924-4247(98)00372-0) (In English)
- Whatmore, R. W. (1986) Pyroelectric devices and materials. *Reports on Progress in Physics*, 49 (12), article 1335. <https://doi.org/10.1088/0034-4885/49/12/002> (In English)
- Xia, F., Cheng, Z.-Y., Xu, H. S. et al. (2002) High electromechanical responses in terpolymer of poly(vinylidene fluoridetrifluoroethylene-chlorofluoroethylene). *Advanced Materials*, 14 (21), 1574–1577. [https://doi.org/10.1002/1521-4095\(20021104\)14:21%3C1574::AID-ADMA1574%3E3.0.CO;2-%23](https://doi.org/10.1002/1521-4095(20021104)14:21%3C1574::AID-ADMA1574%3E3.0.CO;2-%23) (In English)
- Yang, L., Li, X., Allahyarov, E. et al. (2013) Novel polymer ferroelectric behavior via crystal isomorphism and the nanoconfinement effect. *Polymer*, 54 (7), 1709–1728. <https://doi.org/10.1016/j.polymer.2013.01.035> (In English)
- Zhang, Q. M., Huang, Ch., Xia, F., Su, J. (2004) Electric EAP. In: Y. Bar-Cohen (ed.). *Electroactive polymer (EAP) Actuators as artificial muscles: Reality, potential, challenges*. Bellingham: SPIE Press, 816 p. <https://doi.org/10.1117/3.547465.ch4> (In English)
- Zhang, Q. M., Bharti, V., Zhao, X. (1998) Giant electrostriction and relaxor ferroelectric behavior in electron-irradiated poly(vinylidene fluoride-trifluoroethylene) copolymer. *Science*, 280 (5372), 2101–2104. <https://doi.org/10.1126/science.280.5372.2101> (In English)



Check for updates

Condensed Matter Physics. Dielectric Physics

UDC 538.956

<https://www.doi.org/10.33910/2687-153X-2022-3-1-11-20>

# Application of the complex electrical module method for the determination of the relaxation parameters of dielectrics with high electrical conductivity

Zh. A. Salnikova<sup>✉1</sup>, A. A. Kononov<sup>1</sup>, A. P. Smirnov<sup>1</sup>, R. A. Castro Arata<sup>1</sup>

<sup>1</sup> Herzen State Pedagogical University of Russia, 48 Moika Emb., Saint Petersburg 191186, Russia

## Authors

Zhanna A. Salnikova, ORCID: 0000-0002-8244-7513, e-mail: [jannete90@mail.ru](mailto:jannete90@mail.ru)

Alexey A. Kononov, ORCID: 0000-0002-5553-3782, e-mail: [kononov\\_aa@icloud.com](mailto:kononov_aa@icloud.com)

Alexander P. Smirnov, ORCID: 0000-0003-2463-2056, e-mail: [Smirnov\\_Alexander\\_hspu@mail.ru](mailto:Smirnov_Alexander_hspu@mail.ru)

Rene Alejandro Castro Arata, ORCID: 0000-0002-1902-5801, e-mail: [recastro@mail.ru](mailto:recastro@mail.ru)

**For citation:** Salnikova, Zh. A., Kononov, A. A., Smirnov, A. P., Castro Arata, R. A. (2022) Application of the complex electrical module method for the determination of the relaxation parameters of dielectrics with high electrical conductivity. *Physics of Complex Systems*, 3 (1), 11–20. <https://www.doi.org/10.33910/2687-153X-2022-3-1-11-20>

**Received** 23 December 2021; reviewed 13 January 2022; accepted 14 January 2022.

**Funding:** The study did not receive any external funding.

**Copyright:** © Zh. A. Salnikova, A. A. Kononov, A. P. Smirnov, R. A. Castro Arata (2022). Published by Herzen State Pedagogical University of Russia. Open access under [CC BY-NC License 4.0](https://creativecommons.org/licenses/by-nc/4.0/).

**Abstract.** The paper submits that the method of a complex electrical module allows to investigate the characteristics of relaxation processes in dielectrics having high electrical conductivity. The method makes it possible to determine the relaxation parameters of dielectrics when relaxation peaks are absent in the frequency dependence of dielectric losses  $\varepsilon''(f)$ . In turn, relaxation peaks can be detected on the frequency dependences  $M''(f)$ . In addition, a function graph  $M'(f)$  is plotted. Simultaneous approximation of the curves  $M''(f)$  and  $M'(f)$  in the frequency range corresponding to the maximum  $M''$  by the Havriliak–Negami equation for the electrical module makes it possible to determine the relaxation parameters  $\alpha$ ,  $\beta$ ,  $\tau_0$ .

**Keywords:** electrical module, relaxation parameters, the Havriliak–Negami equation for the electrical module

## Introduction

Dielectric spectroscopy, i. e., investigation of frequency dependences of dielectric permittivity and dielectric loss factor, is widely used in the physics of dielectrics. This method is used to study both synthetic (Castro et al. 2017; Kremer, Schonhals 2002; Nikonorova et al. 2016; 2019; Rychkov et al. 2005; Sazhin 1977) and biological dielectrics (Annus, Min 2021; Asami 2002; Chelidze 2002; Raicu, Feldman 2015; Romanov et al. 2008; Wolf et al. 2011). The analysis of the relaxation peaks on the frequency dependence of the dielectric loss factor makes it possible to determine the relaxation parameters of dielectrics. However, in case of high electrical conductivity, the relaxation peaks on the frequency dependence of the dielectric loss factor cannot be detected. The method of the complex electrical module, proposed in (McCrum et al. 1967), is used to detect such peaks. The purpose of the paper is to show how the complex electrical module method is applied in the analysis of dielectric spectroscopy measurements for synthetic and biological dielectrics under high electrical conductivity. The use of the method is illustrated by specific examples.

## Dielectric Spectroscopy

### Relaxation equations

The concept of a complex dielectric permittivity  $\varepsilon^*(f)$  is used for the analysis of the relaxation properties of dielectrics. It is determined by the expression:

$$\varepsilon^*(f) = \varepsilon'(f) - i\varepsilon''(f),$$

where  $f$  is the frequency of the applied electric field,  $\varepsilon'(f)$  is the real part of the complex dielectric constant called dielectric permittivity characterising the degree of electric field shielding,  $\varepsilon''(f)$  is the imaginary part of the complex dielectric constant called dielectric loss factor characterising absorption energy transferring into the thermal form. The values  $\varepsilon'(f)$  and  $\varepsilon''(f)$  are determined experimentally using dielectric spectrometers. For example, the spectrometer "Novocontrol Technology Concept 81" allows to make dielectric measurements in the frequency range  $f = 10^{-3} - 10^{10}$  Hz at different temperatures.

Generally, relaxation processes are described by the Havriliak–Negami (H–N) equation (Havriliak, Negami 1966):

$$\varepsilon^*(\omega) = \varepsilon_\infty + \frac{\varepsilon_s - \varepsilon_\infty}{(1 + (i\omega\tau_0)^{1-\alpha})^\beta} \quad (1)$$

where  $\varepsilon_s$  and  $\varepsilon_\infty$  are the static and high-frequency permittivity  $\varepsilon'(f)$  respectively, i. e.,  $\varepsilon_s$  corresponds  $f \rightarrow 0$ ,  $\varepsilon_\infty$  corresponds  $f \rightarrow \infty$ ,  $\omega = 2\pi f$  is the cyclic frequency,  $\tau_0$  is the most probable relaxation time of the electrical response of molecular aggregates or sample molecules,  $\alpha$  is the width of the relaxation time spectrum,  $\beta$  is the asymmetry of this spectrum. These parameters can correspond to the following values:  $0 \leq \alpha < 1$ ,  $0 < \beta \leq 1$ . In this case, the larger the value  $\alpha$ , the greater is the frequency dispersion of the numerical values of the relaxation times of the sample molecules  $\tau$ , that is, the wider the relaxation spectrum, the smaller the value  $\beta$ , the greater the degree of its asymmetry. For the Debye spectrum  $\alpha = 0$ ,  $\beta = 1$ .

According to Formula (1), it possible to write analytical formulas for  $\varepsilon'(\omega)$  and  $\varepsilon''(\omega)$  (Salnikova, Kononov 2020):

$$\varepsilon'(\omega) = \varepsilon_\infty + \frac{(\varepsilon_s - \varepsilon_\infty)(\cos(\beta\varphi))}{\left[1 + 2(\omega\tau_0)^{1-\alpha} \cos \frac{\pi(1-\alpha)}{2} + (\omega\tau_0)^{2(1-\alpha)}\right]^{\frac{1}{2}}}, \quad (2)$$

$$\varepsilon''(\omega) = \frac{(\varepsilon_s - \varepsilon_\infty)(\sin(\beta\varphi))}{\left[1 + 2(\omega\tau_0)^{1-\alpha} \cos \frac{\pi(1-\alpha)}{2} + (\omega\tau_0)^{2(1-\alpha)}\right]^{\frac{1}{2}}}, \quad (3)$$

$$\text{where } \varphi = \arctg \left[ \frac{(\omega\tau_0)^{1-\alpha} \sin \frac{\pi(1-\alpha)}{2}}{1 + (\omega\tau_0)^{1-\alpha} \cos \frac{\pi(1-\alpha)}{2}} \right].$$

Parameters  $\alpha$ ,  $\beta$ ,  $\tau_0$  are the fundamental relaxation parameters of the samples under study. These parameters are determined by the approximation of functions  $\varepsilon'(f)$  and  $\varepsilon''(f)$ . For example, Figure (1a) shows the dispersion of the dielectric permittivity. In turn, Figure (1b) presents the example of function  $\varepsilon''(f)$ . In this image the relaxation peaks are seen very well. These four peaks are associated with different forms of internal molecular motion of macromolecules. For the analysis of the data, the experimental values  $\varepsilon''(f)$  are approximated by a curve according to Formula (3). In this case, the variable parameters of the approximation are  $\alpha$ ,  $\beta$ , and  $\tau_0$ . These parameters are selected according to the principle of the maximum coincidence of the experimental and approximating curves. This approximation is made by the software which uses the least square method.

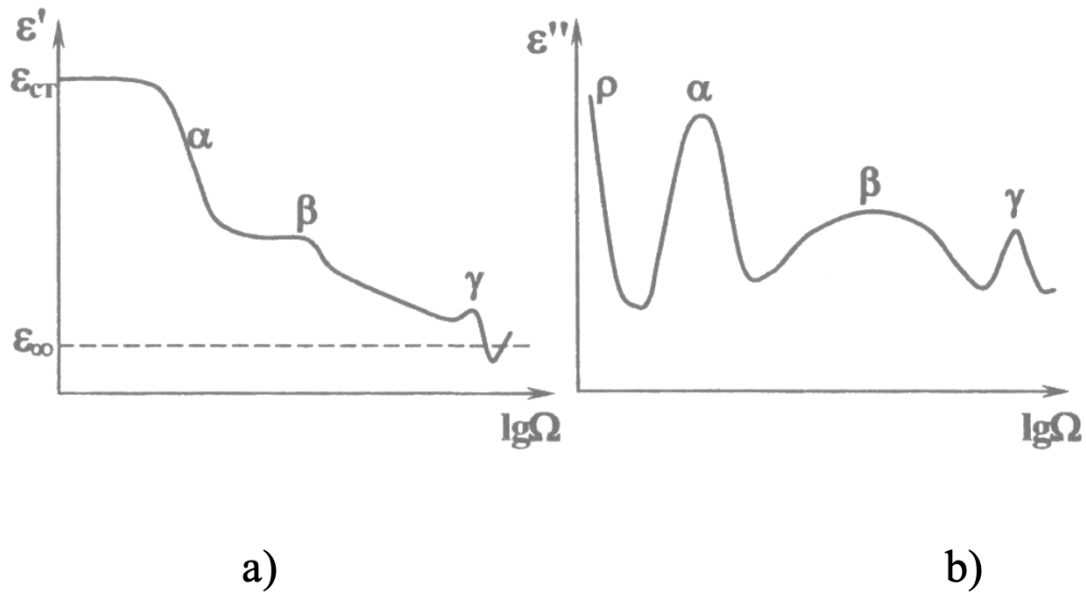


Fig. 1. Frequency  $\Omega$  dependences for a polar polymer in a highly elastic state (Rychkov et al. 2005):  
 a) dielectric permittivity  $\varepsilon'$  b) dielectric loss factor  $\varepsilon''$

For dielectrics having high electrical conductivity, relaxation peaks in the  $\varepsilon''(f)$  plot are often not observed. To detect them, the dielectric losses associated with electrical conductivity are subtracted from the total dielectric losses (Sazhin 1977):

$$\varepsilon''(f) = \frac{1.8 \times 10^{10} \sigma(f)}{f},$$

where  $\sigma(f)$  is the specific electrical conductivity of the dielectric. The remaining value is equal to the relaxation losses  $\varepsilon''_{rel}(f)$ :

$$\varepsilon''_{rel}(f) = \varepsilon''(f) - \frac{1.8 \times 10^{10} \sigma(f)}{f}. \quad (4)$$

However, in case of electrical conductivity, this method does not allow to detect relaxation peaks in the  $\varepsilon''_{rel}(f)$  plot. Consequently, the determination of the relaxation parameters  $\alpha, \beta, \tau_0$  by this method becomes impossible.

In this case, it is advisable to use the complex electrical module method. It is known, that the application of this method allows to detect relaxation peaks. In turn, mathematical methods allow to determine the values of the relaxation parameters.

#### Complex electrical module method

The complex electrical module  $M^*(\omega)$  is the value of the inverse complex dielectric permittivity determined by the expression (McCrum et al. 1967):

$$M^*(\omega) = M'(\omega) + iM''(\omega).$$

The quantities  $M'(\omega), M''(\omega)$  are called the real and imaginary components of the complex electrical module, respectively. They are equal to:

$$M'(\omega) = \frac{\varepsilon'(\omega)}{\varepsilon'^2(\omega) + \varepsilon''^2(\omega)}, \quad (5)$$

$$M''(\omega) = \frac{\varepsilon''(\omega)}{\varepsilon'^2(\omega) + \varepsilon''^2(\omega)}. \quad (6)$$

From Equation H-N (1) it is possible to derive formulas for  $M'(\omega)$  and  $M''(\omega)$  (Salnikova, Kononov 2020):

$$M'(\omega) = \frac{M_\infty M_s A^\beta (M_\infty - M_s) \sin\beta\phi}{A^{2\beta} M_s^2 + 2A^\beta (M_\infty - M_s) M_s \cos\beta\phi + (M_\infty - M_s)^2} \quad , \quad (7)$$

$$M''(\omega) = \frac{M_\infty M_s A^\beta (M_\infty - M_s) \sin\beta\phi}{A^{2\beta} M_s^2 + 2A^\beta (M_\infty - M_s) M_s \cos\beta\phi + (M_\infty - M_s)^2} \quad , \quad (8)$$

where  $M_\infty = \frac{1}{\varepsilon_\infty}$  ,  $M_s = \frac{1}{\varepsilon_s}$  ,

$$A = \left[ 1 + 2(\omega\tau_0)^{1-\alpha} \sin\frac{\pi\alpha}{2} + (\omega\tau_0)^{2(1-\alpha)} \right]^{\frac{1}{2}} \quad ,$$

$$\phi = \operatorname{arctg} \left[ \frac{(\omega\tau_0)^{1-\alpha} \cos\frac{\pi\alpha}{2}}{1 + (\omega\tau_0)^{1-\alpha} \sin\frac{\pi\alpha}{2}} \right] \quad .$$

In this case, the parameters  $\alpha$ ,  $\beta$ ,  $\tau_0$  have the same physical meaning as in Equation (1).

### Experiment

#### Practical application of the complex electrical module method for copolyamide films SPA-3

Let us consider the practical application of the complex electrical module method to determine relaxation parameters of dielectrics with high electrical conductivity. The sample under study is aliphatic copolyamide SPA-3 films, whose dielectric spectra were derived in our previous work (Avanesyan, Salnikova 2020). If we plot the frequency dependences  $\varepsilon'(f)$  and  $\varepsilon''(f)$ , then the diagrams shown in Fig. 2 will be obtained. It is seen that the  $\varepsilon''(f)$  plot does not have relaxation peaks.

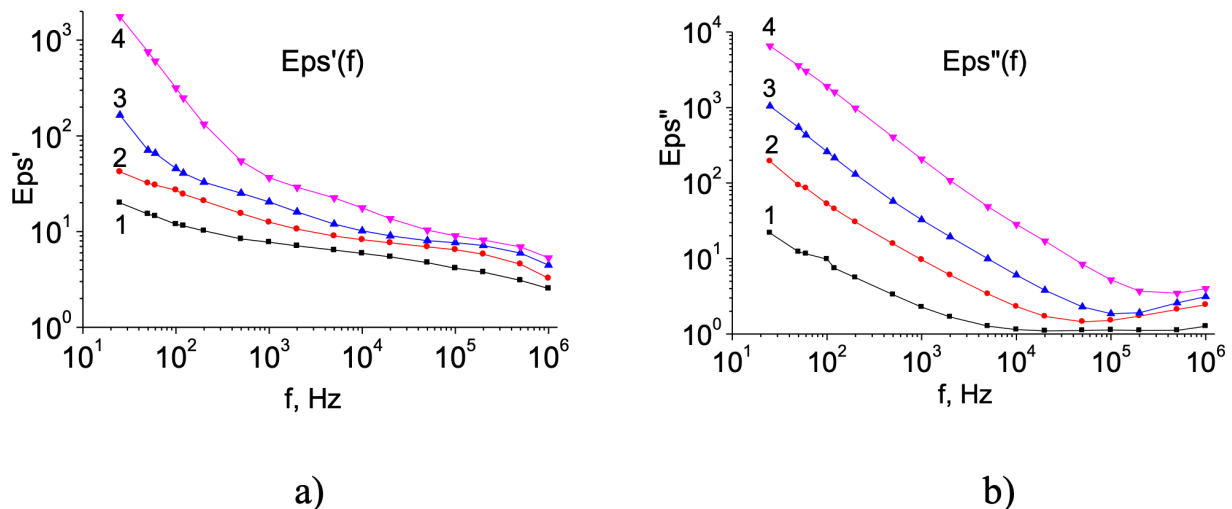


Fig. 2. Frequency dependences for SPA-3 a) dielectric permittivity  $\varepsilon'(f)$ , b) dielectric loss factor  $\varepsilon''(f)$  at different temperatures: 1—350 K, 2—375 K, 3—405 K, 4—440 K

Figure (3a) shows the frequency dependence of the specific electrical conductivity  $\sigma(f)$ . After subtracting the contribution of conductivity from dielectric losses, the  $\varepsilon''_{rel}(f)$  diagram changes (Fig. 3b). There are no relaxation peaks in the diagram, and negative values are explained by high electrical conductivity.

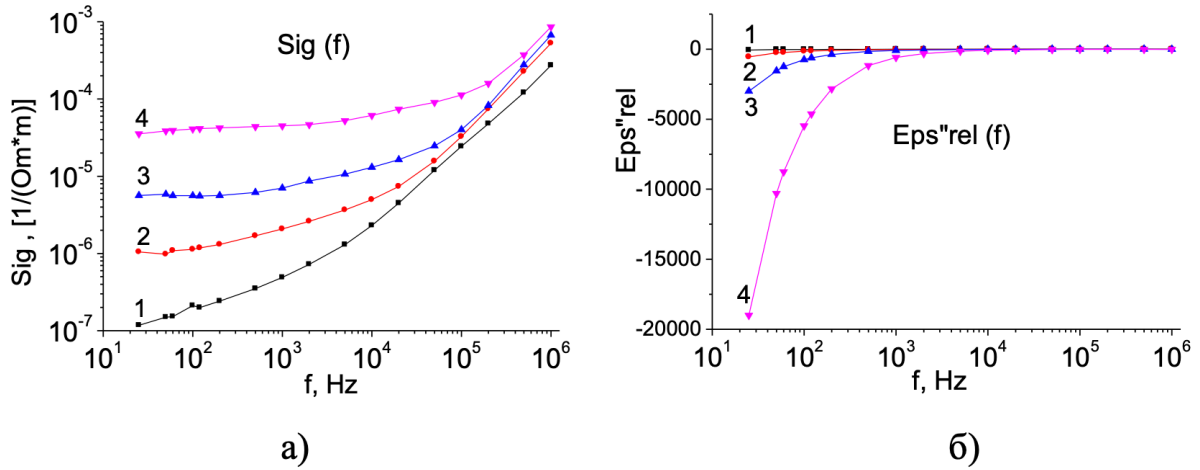


Fig. 3. Frequency dependence for SPA-3 a) specific electrical conductivity  $\sigma(f)$ , b) relaxation dielectric losses  $\varepsilon''_{rel}(f)$  at different temperatures: 1 — 350 K, 2 — 375 K, 3 — 405 K, 4 — 440 K

Let us consider the complex electrical module for this sample. Figure 4 shows the experimental diagrams  $M'(f)$  and  $M''(f)$  (the values of the electrical module are calculated using Formulas (5, 6); the approximating curves are obtained using Formulas (7, 8)).

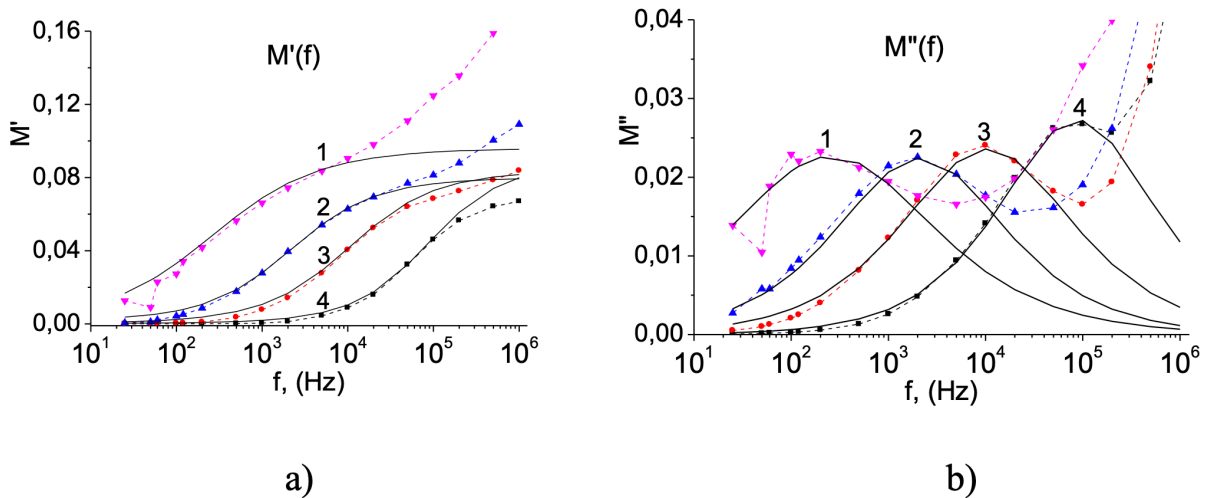


Fig. 4. Frequency dependences of the electrical module for SPA-3 a) the real component of the electrical module  $M'(f)$ , b) the imaginary component of the electrical module  $M''(f)$  at different temperatures: 1 — 350 K, 2 — 375 K, 3 — 405 K, 4 — 440 K. Black lines mark the approximating curves obtained from H–N equation (7, 8) (Avanesyan, Salnikova 2020)

The experimental data are presented by color lines, the approximating curves are shown by black lines. Relaxation peaks are observed on the  $M''(f)$  dependence, and a sharp increase is observed in the  $M'(f)$  dependence in the frequency range corresponding to the  $M''$  maximum. The approximating curves are obtained using the H–N equation for the electrical module. The parameters  $\alpha$ ,  $\beta$ ,  $\tau_0$  are selected so as to achieve the maximum coincidence of the experimental and approximating curves simultaneously for both diagrams  $M'(f)$  and  $M''(f)$ . It is seen that the simultaneous approximation of both  $M'(f)$  and  $M''(f)$  in the region of the maximum  $M''$  gives good results. This algorithm allows to determine the parameters  $\alpha$ ,  $\beta$ ,  $\tau_0$ . The relaxation parameters obtained by this method are presented in Table 1.

The relaxation peaks illustrated in Fig. 4b shift toward high frequencies when temperatures rise. This confirms the relaxation type of the polarisation process of the sample. With an increase in temperature, the width of the peaks decreases, but the peaks stay rather wide, their width at half maximum is two frequency decades. This means that the sample has a wide relaxation spectrum typical of polar polymers.

Table 1. Temperature dependence of the relaxation parameters  $\alpha$ ,  $\beta$ ,  $\tau_0$  for SPA-3 (Avanesyan, Salnikova 2020)

$T$ K	$\alpha$	$\beta$	$\tau_0$ (s)
350	0.35	0.87	$1.5 \times 10^{-2}$
375	0.29	0.93	$2.5 \times 10^{-3}$
405	0.30	0.94	$2.4 \times 10^{-4}$
440	0.27	0.97	$1.0 \times 10^{-5}$

These results show that the sample has a relatively wide ( $\alpha \geq 0.27$ ) and almost symmetric ( $\beta \geq 0.87$ ) relaxation spectrum typical of polar polymers.

Using the obtained values  $\tau_0(T)$ , it is possible to calculate the activation energy of dipole polarization.

Besides, for the complex electrical module it is possible to plot a Cole-Cole diagram, i. e., the dependence  $M''(M')$ . Fig. 5 shows the diagram for SPA-3 sample.

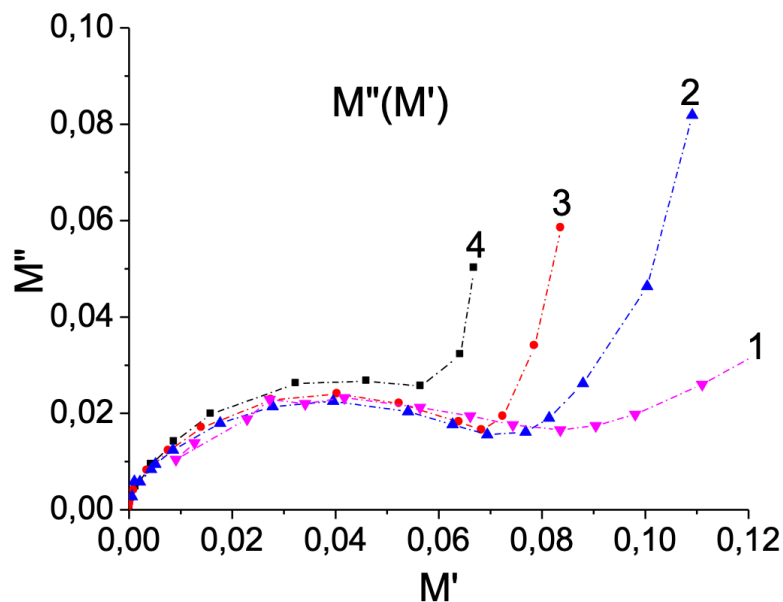


Fig. 5. Cole-Cole diagram for the complex electrical module at different temperatures for SPA-3: 1 — 350 K, 2 — 375 K, 3 — 405 K, 4 — 440 K

It is seen that the experimental points are approximated well by semicircles, the centers of which are located below the  $M'$  axis. This corresponds to polymers with a broad, symmetric relaxation spectrum, i. e.,  $\alpha \neq 0, \beta \approx 1$ . With an increase in temperature, the curves approach the semicircles, which corresponds to the Debye spectrum, i. e., with an increase in  $T$ , the parameter  $\alpha$  decreases and the parameter  $\beta$  increases.

*Practical application of the complex electrical module method for blood serum of patients with chronic lymphocytic leukemia*

Let us consider the practical application of the complex electrical method for the investigation of blood serum (BS) in patients with cancer—chronic lymphocytic leukemia (CLL) (Salnikova et al. 2020a; 2020b). BS has high electrical conductivity ( $\sigma \sim 0.01 \text{ Ohm}^{-1} \cdot \text{m}^{-1}$ ) because it contains  $\text{Na}^+$  and  $\text{Cl}^-$  ions. The dependences  $\epsilon'(f)$  and  $\epsilon''(f)$  constructed according to the data obtained in our work (Salnikova et al. 2020a) will result in the diagrams shown in Fig. 6. It is seen that there are no relaxation peaks in the  $\epsilon''(f)$  plot.

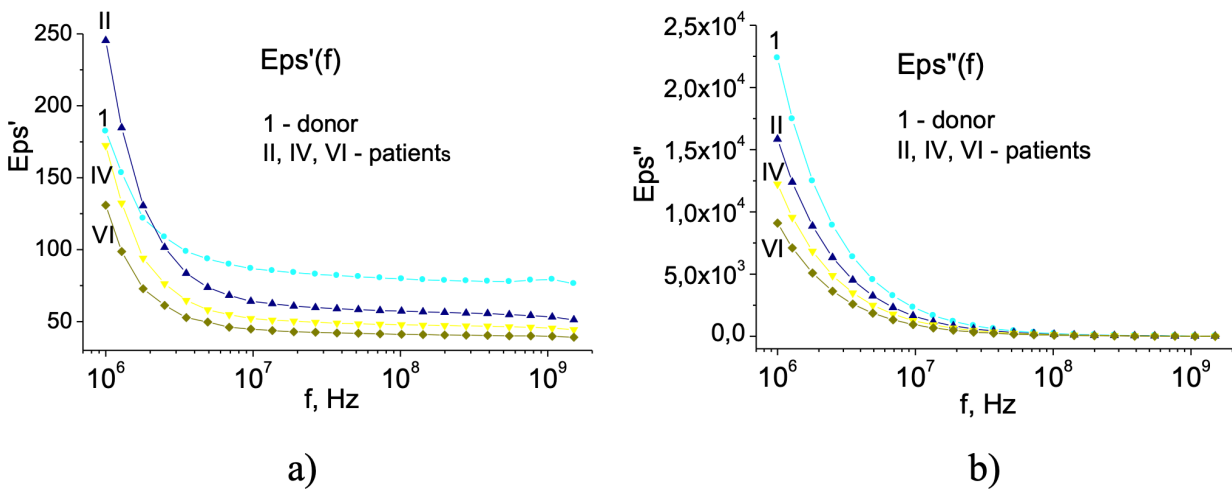


Fig. 6. Frequency dependence for BS in patients with CLL a) dielectric permittivity  $\epsilon'(f)$ , b) dielectric losses  $\epsilon''(f)$

Figure (7a) shows the frequency dependence of the specific electrical conductivity  $\sigma(f)$ . Figure (7b) shows the frequency dependence  $\epsilon''_{rel}(f)$  obtained by subtracting the contribution of specific electrical conductivity  $\sigma(f)$  from the dielectric loss factor using Formula (4). The absence of the relaxation peaks in the diagrams and negative values are explained by high electrical conductivity.

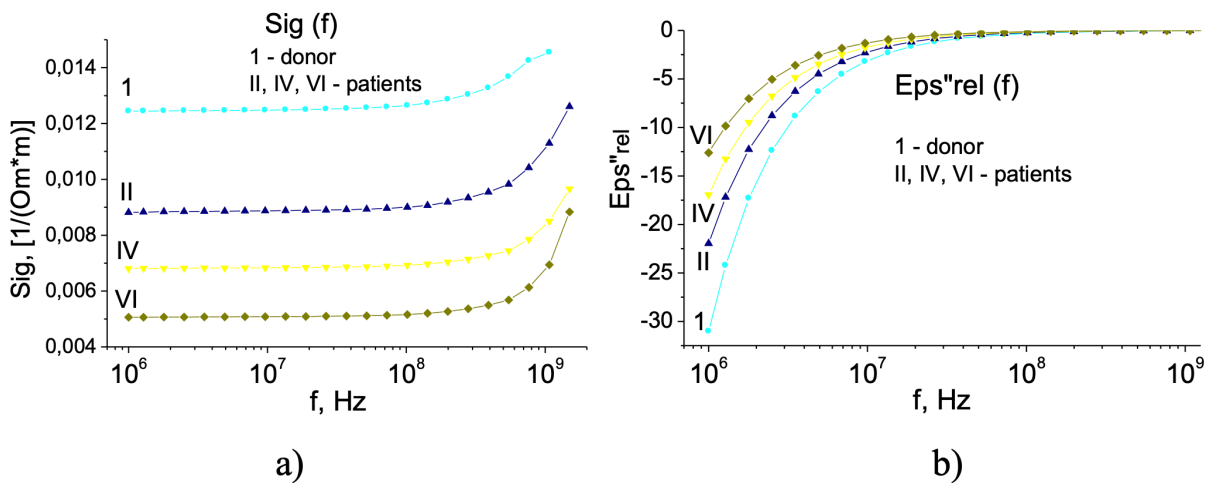


Fig. 7. Frequency dependence for BS in patients with CLL a) specific electrical conductivity  $\sigma(f)$ , b) dielectric losses  $\epsilon''_{rel}(f)$

Let us move on to the complex electrical module. The values of the real and imaginary components of the electrical module  $M'(f)$ ,  $M''(f)$  are calculated by Formulas (5, 6) and are represented by colored lines (Fig. 8) (Salnikova et al. 2020a). Relaxation peaks are observed on the  $M''(f)$  dependence, and a sharp increase is observed in the  $M'(f)$  dependence in the frequency range corresponding to the  $M''$  maximum. The approximating curves obtained using the H–N equation for the electrical module Formulas (7, 8) are represented by solid black lines. It is seen that the simultaneous approximation of both  $M'(f)$  and  $M''(f)$  in the region of the maximum  $M''$  gives good results. This algorithm allows to determine the parameters  $\alpha$ ,  $\beta$  with an accuracy no worse than  $\pm 0.01$ . The relaxation parameters obtained this way are presented in Table 2 (Salnikova et al. 2020a).

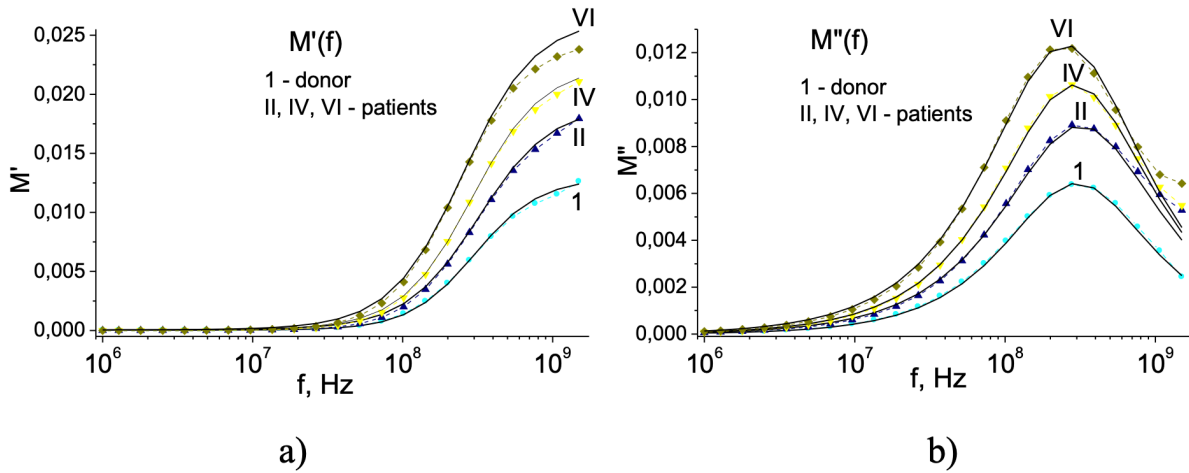


Fig. 8. Frequency dependence for BS in patients with CLL a) the real component of the electrical module  $M'(f)$ , b) the imaginary component of the electrical module  $M''(f)$ ; 1 — donor, II, IV, VI — patients. Black lines indicate approximating curves obtained using the H–N equation (7, 8)

Table 2. Relaxation parameters  $\alpha$ ,  $\beta$ ,  $\tau_0$  of BS for patients with CLL (Salnikova et al. 2020a)

Sample	$\alpha$	$\beta$	$\tau_0$ (s)
1	0	1	$6.3 \times 10^{-5}$
II	0.03	0.99	$1.2 \times 10^{-4}$
IV	0.03	0.99	$1.7 \times 10^{-4}$
VI	0.04	0.99	$2.9 \times 10^{-4}$

\*1–4—donors, I–VI—patients

Figure 9 shows the Cole-Cole diagram of the electrical module  $M''(M')$  for BS in patients with CLL and donors (Salnikova et al. 2020b). The semicircles are observed clearly. The semicircles are remarkably different for donors and patients with CLL.

We assume that the complex electrical module method can be used for any BS samples. In our opinion, future application of this method will make it possible to diagnose and monitor various diseases by analyzing changes in the relaxation parameters  $\alpha$ ,  $\beta$ ,  $\tau_0$  of blood serum. The parameters will not change over time for healthy individuals, while patients will see a change in the parameters. Moreover, the parameters will change more intensively if the disease gets more acute. In case of remission (weakening of the disease), these parameters will begin to return to the normal values typical for a particular individual.

### Conclusion

The complex electrical module method allows to determine the relaxation parameters  $\alpha$ ,  $\beta$ ,  $\tau_0$  of dielectrics having high electrical conductivity when there are no relaxation peaks on the frequency dependence of dielectric losses  $\epsilon''(f)$ . Relaxation peaks can be found in the  $M''(f)$  diagram. In the  $M'(f)$

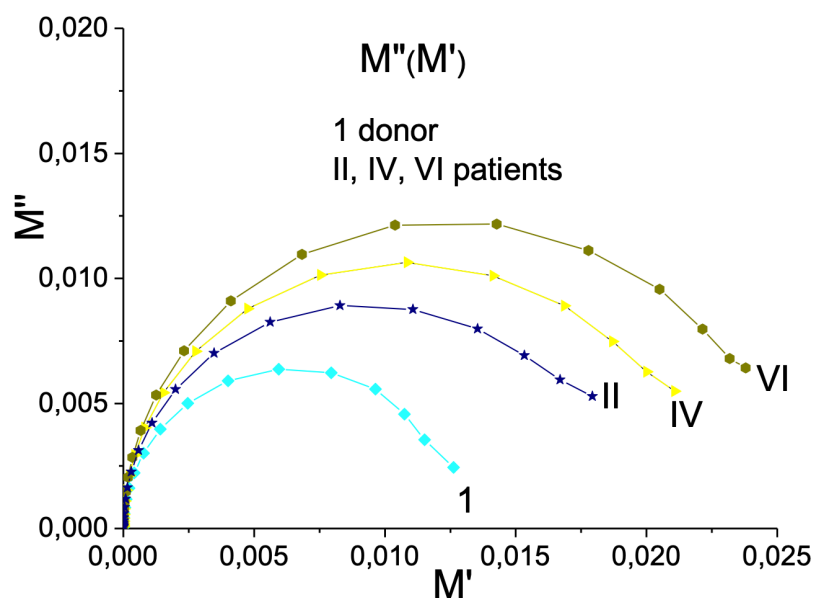


Fig. 9. Cole-Cole diagram of the electrical module for BS in patients with CLL and donors. 1–4 — donors, II, IV, VI — patients

diagram, one can find a sharp rise in the area of the maximum  $M''$ . Simultaneous approximation of the curves  $M''(f)$  and  $M'(f)$  in the frequency range corresponding to the maximum  $M''$  according to the Havriliak–Negami equation for the electrical module allows to determine the relaxation parameters for the sample under investigation. Thus, the method of the complex electrical module makes it possible to research the characteristics of relaxation processes hidden by the high electrical conductivity of dielectrics.

### Conflict of interest

The authors declare that they have no conflicts of interest.

### References

- Annus, P., Min, M. (eds.). (2021) *Bioimpedance and Spectroscopy*. London: Academic Press, 452 p. (In English)
- Asami, K. (2002) Characterization of biological cells by dielectric spectroscopy. *Journal of Non-Crystalline Solids*, 305 (1–3), 268–277. [https://doi.org/10.1016/S0022-3093\(02\)01110-9](https://doi.org/10.1016/S0022-3093(02)01110-9) (accessed 15.10.2021). (In English)
- Avanesyan, V. T., Salnikova, Zh. A. (2020) Electric modulus spectroscopy of PA6/PA66 aliphatic polyamide. In: Yu. Gorokhovatsky, D. Temnov, V. Kapralova (eds.). *AIP Conference Proceedings. Vol. 2308. Proceedings of The XV International Conference "Physics of dielectrics" (St. Petersburg, Russia, 5–8 October 2020)*. [S. l.]: AIP Publ., article 030013. [Online]. Available at: <https://doi.org/10.1063/5.0035258> (accessed 15.10.2021). (In English)
- Castro, R. A., Ignatiev, A. I., Nikonorov, N. V. et al. (2017). Dielectric properties of silver-containing photo-thermorefractive glass in temperature range of – 50 to + 250 °C: The role of hybrid molecular clusters. *Journal of Non-Crystalline Solids*, 461, 72–79. <https://doi.org/10.1016/j.jnoncrysol.2017.01.041> (In English)
- Chelidze, T. (2002) Dielectric spectroscopy of blood. *Journal of Non-Crystalline Solids*, 305 (1–3), 285–294. [https://doi.org/10.1016/S0022-3093\(02\)01101-8](https://doi.org/10.1016/S0022-3093(02)01101-8) (accessed 15.10.2021) (In English)
- Havriliak, S., Negami, S. (1966) A complex plane analysis of  $\alpha$ -dispersions in some polymer systems. *Journal of Polymer Science Part C: Polymer Symposia*, 14 (1), 99–117. <https://doi.org/10.1002/polc.5070140111> (In English)
- Kremer, K., Schonhals, A. (eds.). (2002) *Broadband dielectric spectroscopy* (accessed 15.10.2021) (In English)
- McCrum, N. G., Read, B. E., Williams, G. (1967) *Anelastic and dielectric effects in polymeric solids*. London: Wiley Publ., 617 p., <https://doi.org/10.1002/app.1969.070130214> (In English)
- Nikonorova, N. A., Balakina, M. Y., Fominykh, O. D. et al. (2016) Dielectric spectroscopy and molecular modeling of branched methacrylic (co)polymers containing nonlinear optical chromophores. *Materials Chemistry and Physics*, 181, 217–226. <https://doi.org/10.1016/j.matchemphys.2016.06.052> (In English)

- Nikonorova, N. A., Kononov, A. A., Dao, H. T., Castro, R. A. (2019) Molecular mobility of thermoplastic aromatic polyimides studied by dielectric spectroscopy. *Journal of Non-Crystalline Solids*, 511, 109–114. <https://doi.org/10.1016/j.jnoncrysol.2018.12.032> (In English)
- Raicu, V., Feldman, Y. (eds.). (2015) *Dielectric relaxation in biological systems: Physical principles, methods, and applications*. Oxford: Oxford University Press, 432 p. (In English)
- Romanov, A. N., Vinokurova, E. Yu., Kovrigin, A. O. et al. (2008) *Dielektricheskie kharakteristiki biologicheskikh zhidkostej cheloveka pri razvitií onkologicheskikh zabolevanij [Dielectric characteristics of human biological fluids in the development of oncological diseases]*. Barnaul: Azbuka Publ., 72 p. (In Russian)
- Rychkov, A. A., Rychkov, D. A., Trifonov, S. A. (2005) *Polimernye dielektriki [Polymer dielectrics]*. Saint Petersburg: Knizhnyj Dom Publ., 156 p. (In Russian)
- Salnikova, Zh. A., Kononov, A. A. (2020) Derivation of the Havriliak—Negami equation for the complex electrical modulus. In: Yu. Gorokhovatsky, D. Temnov, V. Kapralova (eds.). *AIP Conference Proceedings. Vol. 2308. Proceedings of The XV International Conference “Physics of dielectrics” (St. Petersburg, Russia, 5–8 October 2020)*. [S. l.]: AIP Publ., article 030017. [Online]. Available at: <https://doi.org/10.1063/5.0034028> (accessed 15.10.2021). (In English)
- Salnikova, Zh. A., Plotnikova, L. V., Smirnov, A. P. et al. (2020a) Dielectric spectroscopy of blood serum of patients with chronic lymphocytic leukemia. In: Yu. Gorokhovatsky, D. Temnov, V. Kapralova (eds.). *AIP Conference Proceedings. Vol. 2308. Proceedings of The XV International Conference “Physics of dielectrics” (St. Petersburg, Russia, 5–8 October 2020)*. [S. l.]: AIP Publ., article 030018. [Online]. Available at: <https://doi.org/10.1063/5.0035270> (accessed 15.10.2021) (In English)
- Salnikova, Zh. A., Plotnikova, L. V., Smirnov, A. P. et al. (2020b) Diagramma Koul-Koula elektricheskogo modulya syvorotki krovi bol'nykh khronicheskim limfolejkozom [Cole-Cole diagram of the electrical module of blood serum of patients with chronic lymphocytic leukemia]. In: *Materialy 54-j shkoly PIYaF po fizike kondensirovannogo sostoyaniya (16–20 Marta 2020 g.) [Materials of the 54<sup>th</sup> PNPI School on Condensed Matter Physics (16–20. March 2020)]*. Saint Petersburg: NRC “Kurchatov Institute”—PNPI Publ., p. 157 (In Russian)
- Sazhin, B. I. (ed.). (1977) *Elektricheskie svoystva polimerov [Electrical properties of polymers]*. 2<sup>nd</sup> ed. Leningrad: Khimiya Publ., 192 p. (In Russian)
- Wolf, M., Gulich, R., Lunkenheimer, P. et al. (2011) Broadband dielectric spectroscopy on human blood. *Biochimica et Biophysica Acta (BBA)—General Subjects*, 1810 (8), 727–740. <https://doi.org/10.1016/j.bbagen.2011.05.012> (In English)



Check for updates

Condensed Matter Physics. Physics of Transport  
Phenomena in Condensed Matter

UDC 538.9+538.95

<https://www.doi.org/10.33910/2687-153X-2022-3-1-21-24>

# The electronic structure of the K/AlN nanointerface

S. N. Timoshnev<sup>1</sup>, G. V. Benemanskaya<sup>✉2</sup>

<sup>1</sup> Alferov University, 8/3 Khlopina Str., Saint Petersburg 194021, Russia

<sup>2</sup> Ioffe Institute, 26 Politekhnikeskaya Str., Saint Petersburg 194021, Russia

## Authors

Sergei N. Timoshnev, ORCID: 0000-0002-9294-3342, e-mail: [timoshnev@mail.ru](mailto:timoshnev@mail.ru)

Galina V. Benemanskaya, ORCID: 0000-0002-2399-3223, e-mail: [galina.benemanskaya@mail.ru](mailto:galina.benemanskaya@mail.ru)

**For citation:** Timoshnev, S. N., Benemanskaya, G. V. (2022) The electronic structure of the K/AlN nanointerface. *Physics of Complex Systems*, 3 (1), 21–24. <https://www.doi.org/10.33910/2687-153X-2022-3-1-21-24>

**Received** 3 December 2021; reviewed 13 January 2022; accepted 13 January 2022.

**Funding:** The study did not receive any external funding.

**Copyright:** © S. N. Timoshnev, G. V. Benemanskaya (2022). Published by Herzen State Pedagogical University of Russia. Open access under [CC BY-NC License 4.0](https://creativecommons.org/licenses/by-nc/4.0/).

**Abstract.** The electronic structure of the AlN surface and the ultrathin K/AlN interface was studied using *in situ* photoelectron spectroscopy under ultra-high vacuum conditions. Core level spectra from the N 1s, Al 2p and K 3p and from the valence band were studied for the clean AlN surface and for the K/AlN interface in the regime of K submonolayer coatings. During K adsorption, significant changes in all the spectra were found. Surface states in the valence band region below the  $E_{VBM}$  were found. It was determined that the K/AlN interface has the semiconductor-like character.

**Keywords:** III-nitrides, aluminum nitride (AlN), interfaces, surface, photoelectron spectroscopy, electronic structure

## Introduction

III-nitrides are widely used in modern micro- and optoelectronics. They are highly important for building heterostructures used in optical and high-power electronic devices (DenBaars et al. 2013). In the group of III-nitrides, AlN has a wide band gap of  $\sim 6.2$  eV, low coefficient of thermal expansion, and high thermal conductivity. AlN is a favorable material for the development of UV light-emitting diodes and lasers (Taniyasu, Kasu 2008). Despite significant technical progress in the creation of high-quality materials, theoretical and experimental data on the electronic properties of AlN surface are scarce, including data on surface states, interface formation, band bending, etc. These properties are critical because they play a major role in nanostructures, where interfaces are of major importance. The electronic structure of the AlN surface has been studied in many aspects (Loughin et al. 1993; Magnuson et al. 2009; Strak et al. 2015), but information on the structure and electronic properties of metal/AlN interface is very limited (Kempisty et al. 2020; Kiranjot et al. 2020; Sznajder 2020). Recently, the electronic and photoemission properties of metal/ $\text{Al}_x\text{Ga}_{1-x}\text{N}$  interfaces, namely Cs/GaN, Ba/GaN, Ba/ $\text{Al}_{0.16}\text{Ga}_{0.84}\text{N}$ , Ba/ $\text{Al}_{0.42}\text{Ga}_{0.58}\text{N}$ , have been investigated (Benemanskaya et al. 2014; 2018a; 2018b; Timoshnev et al. 2020).

Photoelectron spectroscopy (PES) is one of the main techniques used to study the properties of atoms, molecules and solids, and the most important experimental technique to obtain the most complete information about the band structure of occupied electronic states because of its high sensitivity to chemical states. Recently, the surface and interface properties of group III nitrides have attracted close attention of researchers. Nitrides are widely used in the development and manufacture of optoelectronic devices in a wide spectral range from visible to UV light.

The aim of this work is to study the modification of the electronic structure of the K/AlN interface as a function of the K submonolayer coverage using photoelectron spectroscopy.

### Materials and methods

Photoemission studies were carried out on an experimental RGL-station at the Russian-German beamline at BESSY II synchrotron radiation facility (Berlin, Germany) using the photon energies in the range from 100 eV to 650 eV. Studies were performed *in situ* in a high vacuum of  $5 \times 10^{10}$  Torr at room temperature. The photoelectrons emitted along the normal to the sample surface were recorded. The exciting beam fell on the sample surface at an angle of  $45^\circ$ . The normal photoemission spectra for the valence band area and from the N 1s, Al 2p and K 3p core levels were measured.

The AlN samples were grown on 6H-SiC/Si(111) substrates by chemical vapour deposition. The band-gap width corresponds to  $E_g = 6.2$  eV. The samples of AlN were annealed *in situ* directly in a vacuum chamber at  $T \sim 900$  K. Atomically clean potassium was adsorbed on the surface of the AlN sample from a standard calibrated source. Submonolayer coating from 0.1 monolayer (ML) to 0.9 ML of K was deposited on the clean AlN surface.

### Results and discussion

Figure 1 shows normal photoemission spectra in the valence band area for the clean AlN surface (1) and for the K/AlN interface at the K monolayer coverage (2) – 0.9 ML. The excitation energy is  $h\nu = 100$  eV. The energy position of the  $E_{VBM} = 0$  eV at the surface is determined by linear approximation of the low-energy shoulder of the spectrum of the valence band (VB). It is clear that, upon the adsorption of potassium, the intensity of photoemission from the valence band slightly decreases. In addition, a peak of the K 3p core level appears in the spectrum at binding energy of  $\sim 15.3$  eV.

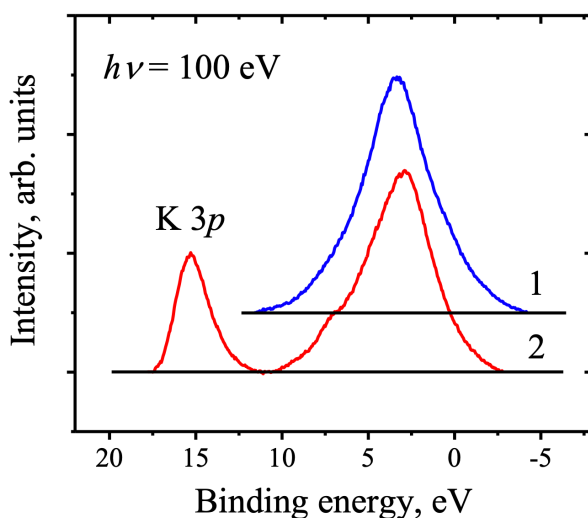


Fig.1. Normalized photoemission spectra from the VB for the clean AlN surface (1) and for the K/AlN interface (2) at the K coverage of 0.9 ML

For the clean AlN surface, the spectrum of the valence band area is described by the faintly structured bands S1 and S2 at the binding energies of  $-0.1$  eV and  $5.9$  eV relatively  $E_{VBM}$  with main VB maximum at  $\sim 2.9$  eV (see fig. 2). The shape and the width of the spectrum of the valence band and surface states S1 and S2 spectra coincide well with the GaN and AlGaN photoemission results reported earlier (Benemanskaya et al. 2014; 2018a; 2018b; Timoshnev et al. 2020).

Figure 3 represents the photoemission spectra from the core level of N 1s for a clean AlN surface (fig. 3a) and a K/AlN interface (fig. 3b). The excitation energy is 470 eV. It is shown that the shape of the spectrum changes slightly upon adsorption of K. At the same time, the peak intensity decreases abruptly and its shift towards higher energies is observed. There is an intensity reduction of the N 1s peak by

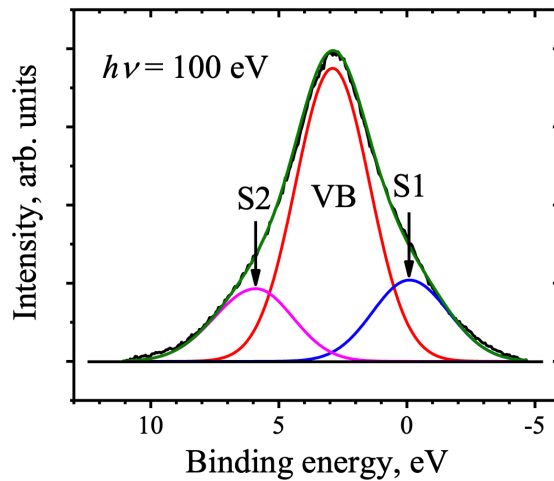


Fig. 2. Decomposition of the photoemission spectrum for the VB and surface states S1 and S2 for the clean AlN surface. The excitation energy is  $h\nu = 100$  eV

of  $\sim 2.1$  times at the K coverage is 0.9 ML. The intensity of the peak of Al  $2p$  decreased by  $\sim 1.4$  times at 0.9 ML of K coverage (spectrum not shown). Since the photoemission intensity of the N  $1s$  peak upon K adsorption decreased more than Al  $2p$  peak it can be assumed that the AlN sample has a predominantly N-polar surface. The shift of the N  $1s$  peak ( $\sim 0.7$  eV) towards higher binding energy was found, originating from the charge transfer with increasing the N-ionicity. Thus, changes in the Al  $2p$  spectrum clearly show that K adsorbed atoms interact exclusively with the N atoms in the upper layer of the substrate AlN.

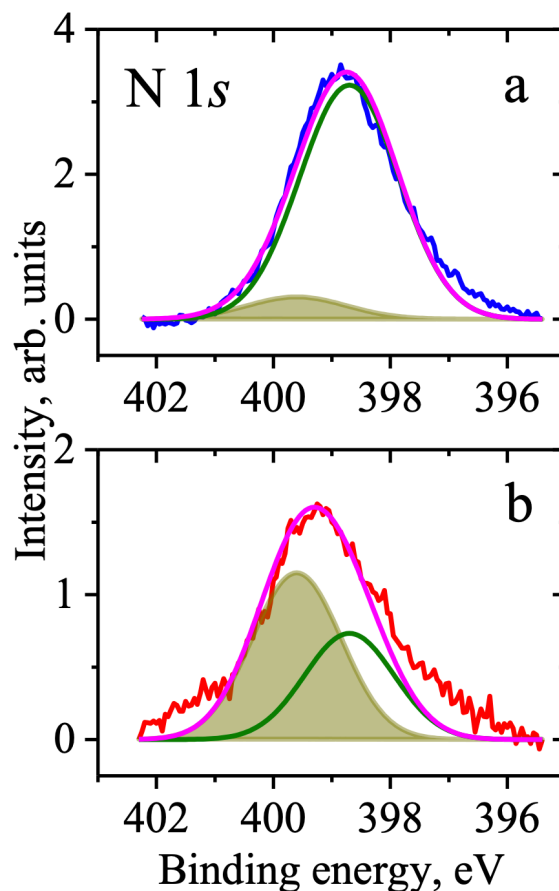


Fig. 3. Decomposition of the normalized photoemission spectra of the core level of N  $1s$  for the clean AlN surface (a) and for K/AlN interface at K coating of 0.9 ML (b). Excitation energy  $h\nu = 470$  eV

## Conclusions

The K adsorption on the AlN surface has been studied by synchrotron radiation photoelectron spectroscopy at different excitation energy in the range from 100 eV to 470 eV. The K deposition is found to modify the N 1s core level spectrum and the surface states spectra. For the pure AlN surface, the intrinsic surface states at the  $E_B$  of  $-0.1$  eV and  $5.9$  eV below  $E_{VBM}$  are found. The positive shift of the N 1s peak toward higher binding energy originates from charge transfer with increasing the N-ionicity.

## Conflict of interest

The authors declare that there is no conflict of interest, either existing or potential.

## Acknowledgements

The authors would like to thank Helmholtz Zentrum Berlin and the staff of the Russian-German laboratory for providing beamtime and assistance during the experiments. The authors are grateful to P.A. Dementev for help in the preparation of the experiments.

## References

- Benemanskaya, G. V., Kukushkin, S. A., Dementev, P. A. et al. (2018a) Synchrotron-based photoemission study of electronic structure of the Cs/GaN ultrathin interface. *Solid State Communications*, 271, 6–10. <https://doi.org/10.1016/j.ssc.2017.12.004> (In English)
- Benemanskaya, G. V., Lapushkin, M. N., Marchenko, D. E., Timoshnev S. N. (2018b) The electronic structure of the Cs/n-GaN(0001) Nano-Interface. *Technical Physics Letters*, 44 (3), 247–250. <https://doi.org/10.1134/S106378501803015X> (In English)
- Benemanskaya, G. V., Timoshnev, S. N., Ivanov, S. V. et al. (2014) Modification of the electronic structure and formation of an accumulation layer in ultrathin Ba/n-GaN and Ba/n-AlGaIn interfaces. *Journal of Experimental and Theoretical Physics*, 118 (4), 600–610. <https://doi.org/10.1134/S1063776114040098> (In English)
- DenBaars, S. P., Feezell, D., Kelchner, K. et al. (2013) Development of gallium-nitride-based light-emitting diodes (LEDs) and laser diodes for energy-efficient lighting and displays. *Acta Materialia*, 61 (3), 945–951. <https://doi.org/10.1016/j.actamat.2012.10.042> (In English)
- Kempisty, P., Strak, P., Sakowski, K. et al. (2020) *Ab initio* and thermodynamic picture of Al adsorption of AlN(000-1) surface—Role of bond creation and electron transition contributions. *Applied Surface Science*, 532, article 147419. <https://doi.org/10.1016/j.apsusc.2020.147419> (In English)
- Kiranjot, Dhawan, R., Gupta, R. K. et al. (2020) Interface asymmetry in AlN/Ni and Ni/AlN interfaces: A study using resonant soft X-ray reflectivity. *Applied Surface Science*, 529, article 147199. <https://doi.org/10.1016/j.apsusc.2020.147199> (In English)
- Loughin, S., French, R. H., Ching, W. Y. et al. (1993) Electronic structure of aluminum nitride: Theory and experiment. *Applied Physics Letters*, 63 (9), 1182–1184. <https://doi.org/10.1063/1.109764> (In English)
- Magnuson, M., Mattesini, M., Höglund, C. et al. (2009) Electronic structure and chemical bonding anisotropy investigation of wurtzite AlN. *Physical Review B*, 80 (15), article 155105. <https://doi.org/10.1103/PhysRevB.80.155105> (In English)
- Strak, P., Sakowski, K., Kempisty, P., Krukowski, S. (2015) Structural and electronic properties of AlN(0001) surface under partial N coverage as determined by *ab initio* approach. *Journal of Applied Physics*, 118 (9), article 095705. <https://doi.org/10.1063/1.4929823> (In English)
- Sznajder, M. (2020) DFT-based modelling of carbon adsorption on the AlN surfaces and influence of point defects on the stability of diamond/AlN interfaces. *Diamond and Related Materials*, 103, article 107694. <https://doi.org/10.1016/j.diamond.2020.107694> (In English)
- Taniyasu, Y., Kasu, M. (2008) Aluminum nitride deep-ultraviolet light-emitting *p-n* junction diodes. *Diamond and Related Materials*, 17 (7–10), 1273–1277. <https://doi.org/10.1016/j.diamond.2008.02.042> (In English)
- Timoshnev, S., Benemanskaya, G., Iluridze, G., Minashvili, T. (2020) Photoelectron spectroscopy of electronic surface structure of the Cs/GaN and Cs/InN interfaces. *Surface and Interface Analysis*, 52 (10), 620–625. <https://doi.org/10.1002/sia.6801> (In English)



UDC 539.186.3+539.196.3

<https://www.doi.org/10.33910/2687-153X-2022-3-1-25-36>

# Reprojection method for inelastic processes in atomic collisions within Born–Oppenheimer approach

A. K. Belyaev<sup>✉1</sup>

<sup>1</sup> Herzen State Pedagogical University of Russia, 48 Moika Emb., Saint Petersburg 191186, Russia

## Authors

Andrey K. Belyaev, ORCID: [0000-0001-8834-1456](https://orcid.org/0000-0001-8834-1456), e-mail: [akbelyaev@herzen.spb.ru](mailto:akbelyaev@herzen.spb.ru)

**For citation:** Belyaev, A. K. (2022) Reprojection method for inelastic processes in atomic collisions within Born–Oppenheimer approach. *Physics of Complex Systems*, 3 (1), 25–36. <https://www.doi.org/10.33910/2687-153X-2022-3-1-25-36>

**Received** 29 December 2021; reviewed 13 January 2022; accepted 13 January 2022.

**Funding:** The research was supported by the Ministry of Education of the Russian Federation as part of state task (Project No. FSZN-2020-0026).

**Copyright:** © A. K. Belyaev (2022). Published by Herzen State Pedagogical University of Russia. Open access under [CC BY-NC License 4.0](https://creativecommons.org/licenses/by-nc/4.0/).

**Abstract.** The paper provides a detailed description of the reprojection method for the exact solution of the nonadiabatic nuclear dynamics within the Born–Oppenheimer formalism. In particular, it discusses the asymptotic behaviour of a state-to-state transition probability when a nonadiabatic radial coupling for this transition has a nonzero asymptotic value—a fundamental feature of the Born–Oppenheimer approach. It is known that the conventional Born–Oppenheimer approach leads to divergency of inelastic cross sections and inelastic rate coefficients, while the reprojection method provides convergences. The article describes physical background of the reprojection method.

**Keywords:** scattering theory, inelastic collision processes, nonadiabatic transitions, atomic data

## Introduction

Inelastic atomic collisions govern the behaviour of gaseous and plasma media in many important domains, e. g., stellar and planetary atmospheres, interstellar media, laser media, etc. Consequently, there is a constant demand for inelastic collisional processes data, especially for low energies. In the great majority of cases, the required atomic data are not available. In general, information about inelastic collisions can be obtained from both experimental measurements and theoretical calculations. Experiments in this field are often very difficult, and numerical calculations remain the main source for inelastic collisional process data. It is therefore highly desirable to use reliable methods for numerical calculations of state-to-state transition probabilities, corresponding inelastic cross sections and rate constants.

The quantum studies of atomic collisions have been accomplished practically since the beginning of the quantum mechanics foundations (Born, Oppenheimer 1997), and now the atomic collision theory seems to be a well-developed part of quantum mechanics. The approaches to study atomic collisions include the conventional Born–Oppenheimer (BO) approach (Born, Oppenheimer 1997; Macías, Riera 1982; Mott, Massey 1949; Nikitin, Umansky 1984), the approach based on the Faddeev equations (Faddeev 1961; Faddeev, Merkuriev 1993), the hyperspherical adiabatic approach (Lin 1995; Macek et al. 1987), to mention a few. However, a vast majority of the theoretical studies in inelastic heavy-particle collision processes is performed within the Born–Oppenheimer approach, which is based on the idea of (Born, Oppenheimer 1997) about the separation of electronic and nuclear motion. The appropriate BO procedure was first formulated by (Mott, Massey 1949). The solution of the problem falls into two

steps. First, the electronic fixed-nuclei Hamiltonian is treated and the electronic molecular states are determined, and then the nuclear dynamics is studied using an expansion of the total wave functions in terms of electronic molecular-state wave functions. The first step (“quantum chemical” treatment) yields the potential energy curves of the collisional quasimolecule and a number of coupling matrix elements. These data enter into a set of coupled channel equations solved in the second step. Thus, the BO approach treats a heavy-particle (atomic, ionic, molecular, etc.) collision in terms of molecular states. In general, one should distinguish between the Born-Oppenheimer approach and the Born–Oppenheimer approximation: the BO approach treats a single molecular state, while the BO approximation takes into account an infinite number of molecular states.

Although the BO approach looks straightforward, it is difficult to put it into practice. The problem was first recognized by (Bates, McCarroll 1958). The most severe problem is that the coupling matrix elements can remain nonzero as the internuclear distance  $R$  goes to infinity, providing inelastic transitions between molecular states under the influence of a collision partner at an arbitrarily large distance. So, the problem can be called the molecular-state problem. The nonzero asymptotic couplings are a fundamental feature of the BO approach. It was found (Belyaev 2009; 2010; 2015; Belyaev et al. 2001; Grosser et al. 1999) that the asymptotic couplings are required to obtain exact asymptotic wave functions within the molecular state representation. Using this idea, the so-called reprojection method (Belyaev 2009; 2010; 2015; Belyaev et al. 2001; Grosser et al. 1999) was developed within a full quantum BO approach to solve the molecular-state problem, including the nonvanishing asymptotic couplings.

The efforts to solve the molecular-state problem have continued, and resulted, in particular, in the development of the quantum reprojection method (Belyaev 2009; 2010; 2015; Belyaev et al. 2001; Grosser et al. 1999). Initially, the method was proposed for a single-electron case. Later, it was scaled out for a multi-electron case (Belyaev 2010). Conceptually, the method is rather simple. It uses BO molecular potential energies and nonadiabatic couplings as they come from quantum-chemical calculations, including nonvanishing couplings. The method has been applied to a number of heavy-particle inelastic collisions, including charge-exchange. The rigorous reprojection method is discussed below.

It is worth emphasizing the importance of taking nonvanishing asymptotic nonadiabatic radial couplings into account correctly. Ref. (Belyaev 2010) shows that if a nonvanishing asymptotic coupling is taken into account the common way within the conventional BO approach, then a corresponding state-to-state transition probability remains nonzero up to infinity, and inelastic cross section and rate coefficient diverge. Finally, such results have no meaning at all. On the contrary, if the reprojection method is used, convergences are reached and the calculated state-to-state transition probabilities, inelastic cross sections and rate coefficients are reliable. Moreover, calculations performed by the reprojection method are the most accurate among those computed within the BO formalism.

## General idea of the Born–Oppenheimer approach

A quantum treatment of an atomic collision represents a many-body problem (at least a three-body one) and, hence, is a complicated challenge for the quantum scattering theory. A quantum study of a many-body problem requires an appropriate approach. As mentioned in the Introduction, the most widely used approach to inelastic heavy-particle collision processes is the standard adiabatic Born–Oppenheimer approach.

The general idea of the BO approach is to separate electronic and nuclear motion (Born, Oppenheimer 1992). The problem is handled in two stages: (i) electronic structure calculations of the adiabatic BO fixed-nuclei molecular-state potentials and corresponding nonadiabatic couplings, (ii) a quantum treatment of the nonadiabatic nuclear dynamics.

A detailed derivation of the basic equations within the BO formalism can be found elsewhere, see, e. g., (Belyaev 2009; 2010; Belyaev et al. 2001; Bransden, McDowell 1992; Grosser et al. 1999, Macías, Riera 1982) and references therein. The present paper provides only final equations.

The stationary Schrödinger equation is solved in the form of expansion into partial waves for the total wave function. Each partial wave with given total angular momentum quantum numbers  $J$  and  $M_J$ , also satisfies the Schrödinger equation. The information about inelastic transition probabilities contains in asymptotical parts of the radial nuclear wave functions.

## Single-electron collisional system with radial couplings

Let us consider a heteronuclear atomic-collisional system of two nuclei A and B with masses  $M_A$  and  $M_B$  and one electron  $e$  (mass  $m_e$ ). For the sake of simplicity, let us consider only radial couplings first and

neglect a number of small terms. For this purpose, we assume that only electronic  $\Sigma$  molecular states should be considered.

### Jacobi coordinates and Hamiltonian

After some manipulation with coordinates, Hamiltonian, and the Schrödinger equation, one has the following: in the interaction region, the system is treated in the molecular Jacobi coordinates, see Fig. 1 (m). In these coordinates the internuclear vector  $R$  connects the nuclei, and the electronic coordinate  $r$  is measured from the center of nuclear mass (CNM).

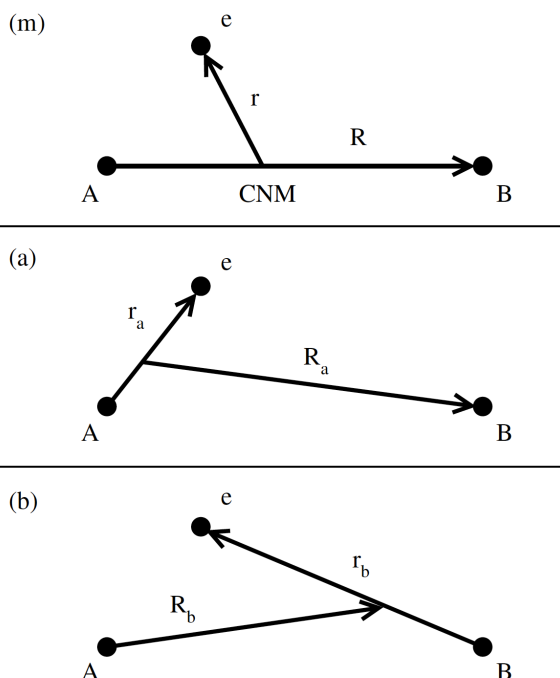


Fig. 1. The 3-body Jacobi relative coordinates. A and B are nuclei,  $e$ —an electron. (m)—the molecular coordinates  $r, R$ ; the vector  $R$  connects the nuclei and the electron is measured from the center of nuclear mass. (a)—the scattering (atomic) coordinates  $r_a, R_a$ ; the electron is measured from the nucleus A and the nucleus B is measured from the center of mass of A and e. (b)—the scattering (atomic) coordinates  $r_b, R_b$ ; the electron is measured from the nucleus B and the vector  $R_b$  connects the nucleus A and the center of mass of B and e

It is worth pointing out the differences between the internuclear and interatomic vectors first noticed by (Bates, McCarroll 1958). Although the differences are small, they do not disappear even in the asymptotic ( $R \rightarrow \infty$ ) region (Table 1). They result in certain physical effects discussed below.

Table 1. The definitions of the reduced masses and the scaling factors  $\gamma_j$ . The channel specific masses  $m_j$  and  $M_j$  are required in the region of large atomic distances. Their values are different for states traveling with nucleus A or B. The differences  $m_j - m$  and  $M_j - M$  are small throughout

	$m$	$M$	$m_j$	$M_j$	$\gamma_j$
Electron travels with nucleus A	$\frac{m_e(M_A + M_B)}{m_e + M_A + M_B}$	$\frac{M_A M_B}{M_A + M_B}$	$m_a = \frac{m_e M_A}{m_e + M_A}$	$M_a = \frac{(M_A + m_e) M_B}{m_e + M_A + M_B}$	$\gamma_a = -\frac{M_B}{M_A + M_B}$
Electron travels with nucleus B	$\frac{m_e(M_A + M_B)}{m_e + M_A + M_B}$	$\frac{M_A M_B}{M_A + M_B}$	$m_b = \frac{m_e M_B}{m_e + M_B}$	$M_b = \frac{(M_B + m_e) M_A}{m_e + M_A + M_B}$	$\gamma_b = \frac{M_A}{M_A + M_B}$

There are three sets of the Jacobi coordinates for a 3-body system, as shown in Fig. 1. For applying the BO approach, there is the only set of the Jacobi coordinates, that is, the molecular coordinates depicted in Fig. 1 (m), provides a fixed-nuclei treatment in the interaction region. In the molecular coordinates, the Hamiltonian for the entire system in the center of mass frame reads

$$H = -\frac{\hbar^2}{2M} \frac{\partial^2}{\partial R^2} - \frac{\hbar^2}{2m} \frac{\partial^2}{\partial r^2} + H_{int}(r, R) \quad (1)$$

$$= -\frac{\hbar^2}{2M} \frac{\partial^2}{\partial R^2} + H_e,$$

and the electronic fixed-nuclei Hamiltonian is defined as follows

$$H_e = -\frac{\hbar^2}{2m} \frac{\partial^2}{\partial r^2} + H_{int}(r, R), \quad (2)$$

$H_{int}(r, R)$  being the interaction potential

$$H_{int}(r, R) = V_{eA} + V_{eB} + V_{AB} \quad (3)$$

$V$  being 2-body potentials. The reduced masses are defined in Table 1.

In the adiabatic representation, adiabatic fixed-nuclei electronic molecular wave functions  $\phi_j(r; R)$  are defined as the eigenfunctions of the electronic Hamiltonian (2)

$$H_e \phi_j(r; R) = U_j(R) \phi_j(r; R). \quad (4)$$

The eigenvalues  $U_j(R)$  of the electronic Hamiltonian are the adiabatic potential energies. The molecular wave functions  $\phi_j(r; R)$  form a set of suitable electronic basis functions.

### Coupled channel equations

According to the general idea of the BO approach, the total (electronic and nuclear) scattering wave function for the entire system  $\Psi_{JM_j}(r, R)$  is expanded over the electronic molecular basis functions. For practical applications it is convenient to single out wave functions  $F_k(R)$  for the description of the radial motion of the nuclei. More specifically, for  $\Sigma$  molecular states treated in the present paper, the expansion of the total wave function has the form (Grosser 1986; Grosser et al. 1999; Macías, Riera 1982)

$$\Psi_{JM_j}(r, R) = Y_{JM_j}(\Theta, \Phi) \sum_k \frac{F_k(R)}{R} \phi_k(r, R). \quad (5)$$

$Y_{JM_j}$  are the spherical harmonics, while  $R, \Theta, \Phi$ , are the spherical coordinates for  $R$ . The wave functions  $F_k(R)$  are found to obey a system of equations, which can be derived from the Schrödinger equation by using the expansion (5). In the adiabatic representation, the set of coupled channel equations for the radial nuclear wave functions  $F_j(R)$  reads (Grosser et al. 1999)

$$\left[ -\frac{\hbar^2}{2M} \frac{d^2}{dR^2} + U_j^{eff}(R) - E_{tot} \right] F_j = \quad (6)$$

$$\frac{\hbar^2}{M} \sum_{k \neq j} \left\langle \phi_j \left| \frac{\partial}{\partial R} \right| \phi_k \right\rangle \frac{dF_k}{dR} + \frac{\hbar^2}{2M} \sum_{k \neq j} \left\langle \phi_j \left| \frac{\partial^2}{\partial R^2} \right| \phi_k \right\rangle F_k,$$

where the effective potentials  $U_j^{eff}(R)$  are defined as

$$U_j^{eff}(R) = U_j(R) + \frac{J(J+1)\hbar^2}{2MR^2} - \frac{\hbar^2}{2M} \left\langle \phi_j \left| \frac{\partial^2}{\partial R^2} \right| \phi_j \right\rangle. \quad (7)$$

The angular components of the matrix elements  $\langle \phi_j | \partial / \partial R | \phi_k \rangle$  do not appear any more, because they do not couple  $\Sigma$  states with the others. The matrix elements in Eq. (6) depend on  $R$ , but not on the angular coordinates.  $U_j(R)$  depends on the distance  $R$  alone now, and it is written correspondingly. Equations (5) and (6) are the basis of the following treatment.

### Boundary conditions and R-matrix

The coupled channel equations (6) should be solved with proper boundary conditions. For regular solutions, the correct boundary conditions at  $R \rightarrow 0$  read

$$F_j(R) \rightarrow 0 \text{ as } R \rightarrow 0 \quad (8)$$

At large distances, the boundary condition consists in matching a numerical solution of the coupled channel equations at a large distance with an asymptotic (analytical) solution at larger distances.

At present, the numerical solution of the coupled channel equations is obtained in the form of an  $R$ -matrix. Suppose that the coupled channel equations (6) have been solved between small distances and a fixed large distance  $R_0$ .  $R_0$  should be so large that the coupled channel equations have their asymptotic form at  $R_0$  and hence the radial functions have an asymptotic form discussed below. The solutions have to obey the usual boundary conditions Eq. (8) as  $R \rightarrow 0$ . All solutions with this property are characterized by the  $R$ -matrix, elements of which,  $R_{jk}$ , relate the values of the radial functions at the upper integration limit and their derivatives

$$F_j = \sum_k R_{jk} \frac{dF_k}{dR} \text{ at } R_0 \quad (9)$$

The  $R$ -matrix forms a convenient and well-established way to express all properties of the solutions  $F_j(R)$  needed for their continuation into the asymptotic region  $R > R_0$  (Burke, Noble 1995; Lane, Thomas 1958; Light 1979).

Usually, a set of the coupled channel equations is truncated. A truncated system of  $N$  coupled channel equations possesses  $2N$  linearly independent solutions. Normally, there exist  $N$  independent regular solutions  $F_j^{(n)}(R)$  ( $j, n = 1, \dots, N$ ), which obey the correct boundary condition (8) at small  $R$ ,  $j$ , being the channel number,  $n$  the number of the solution. Assume that these solutions are known at a distance  $R_0$  and denote

$$P_{jn} = F_j^{(n)}(R_0) \quad (10)$$

and

$$Q_{jn} = \left. \frac{dF_j^{(n)}}{dR} \right|_{R=R_0}. \quad (11)$$

Provided  $\underline{Q}^{-1}$  exists, it easily shown that Eq. (9) holds for every regular solution of the coupled equations (that is, every linear combination of the  $F_j^{(n)}$ ) at  $R_0$ , with

$$\underline{R} = \underline{P} \underline{Q}^{-1}. \quad (12)$$

Under the present conditions,  $N$  regular solutions are easily obtained by numerical computation. Equation (12) is used to compute the  $R$ -matrix from the numerical solutions. The  $R$ -matrix is a convenient way to match the numerical solution at the boundary  $R_0$  to the analytic solution at  $R > R_0$ .

### Asymptotic couplings

The most important information about an inelastic process, in particular inelastic transition probabilities, is contained in regular solutions of the coupled channel equations in the asymptotic ( $R \rightarrow \infty$ ) region. Both initial and final states of an inelastic collisional process are determined by the free motion of colliding partners in some or other eigenstates, that is, by scattering channels when colliding partners before and after a collision (in the asymptotic region) are in well-defined electronic atomic states.

It has been shown, see, e. g., (Belyaev 2010; Belyaev et al. 2001; 2002; Grosser et al. 1999), that the asymptotic values of the radial nonadiabatic couplings calculated with the electron origin at the Center of Nuclear Mass (CNM) read

$$\left\langle \phi_j \left| \frac{\partial}{\partial R} \right| \phi_k \right\rangle_{\infty} = \gamma_k \frac{m}{\hbar^2} [U_j(\infty) - U_k(\infty)] \left\langle \phi_j \left| z^{at} \right| \phi_k \right\rangle, \quad (13)$$

$\langle \phi_j | z^{at} | \phi_k \rangle$  being the atomic transition dipole moment for an atom with which an active electron travels in the asymptotic region. Therefore, the coupling matrix elements  $\langle \phi_j | \partial/\partial R | \phi_k \rangle$  can remain nonzero as  $R \rightarrow \infty$ .

### Asymptotic wave functions

Inelastic transition (state-to-state) probabilities of a collisional process are determined by asymptotic wave functions in scattering (atomic-state) channels with well defined electronic states of colliding atoms or/and ions. In the asymptotic region, electronic molecular-state wave functions are converted into atomic eigenfunctions, so it looks natural to assume that incoming and outgoing wave functions in a scattering channel and in a molecular channel coincide. Equations (5) and (6) seem to have a straightforward interpretation. When one uses, for  $R \rightarrow \infty$ , atomic eigenstates for the electronic basis states  $\phi_j$ , the single terms in Eq. (5) are expected to represent, at large  $R$ , the free motion of the atoms in one or the other of their eigenstates. It seems natural that only one of the terms should contain an incoming wave, and outgoing waves in the other terms occur because the right hand sides in Eq. (6) are nonzero; they represent inelastic transitions. This tentative interpretation is not correct, however.

In the general case, the total (electronic and nuclear) wave function  $\Psi_{JM_j}(r, R)$  in the asymptotic ( $R \rightarrow \infty$ ) region is a superposition of the incoming  $\Psi_j^-$  and outgoing  $\Psi_j^+$  wave functions describing the free motion of the atomic particle in atomic eigenstates

$$\Psi_{JM_j}(r, R) = \sum_j K_j^{-1/2} (a_j^+ \Psi_j^+ + a_j^- \Psi_j^-), \quad (14)$$

with

$$K_j = \sqrt{2M_j (E_{tot} - U_j^{eff}(\infty))} / \hbar \quad (15)$$

being the wave number in the scattering channel  $j$ .  $a_j^{\pm}$  are the outgoing and incoming amplitudes in the scattering (atomic-state) channel  $j$ , they are constants. The channel-specific reduced masses  $M_j$  are listed in Table 1; they are equal to  $M_a$  or  $M_b$  depending on the nucleus binding the electron in the asymptotic region. The factor  $K_j^{-1/2}$  in Eq. (14) has been introduced because in this way the  $|a_j^{\pm}|^2$  represent the outgoing and incoming probability currents in the scattering channel  $j$ .

In the asymptotic region, the outgoing and incoming spherical waves have the form

$$\Psi_j^{\pm} = Y_{JM_j}(\Theta_j, \Phi_j) \frac{\exp(\pm iK_j R_j^{sc})}{R_j^{sc}} \phi_j(r_j^{at}). \quad (16)$$

$R_j^{sc}$ ,  $\Theta_j$  and  $\Phi_j$  are polar coordinates for the scattering (interatomic) vector  $R_j^{sc}$  which connects the center of mass of the atom with the free nucleus, in contrast to the vector  $R$  which connects the nuclei, see Fig. 1.  $R_j^{sc}$  is a channel specific coordinate, which is different when the electron travels with a nucleus A or B, respectively. In fact,

$$R_j^{sc} = R_a \quad (17)$$

or

$$R_j^{sc} = R_b, \quad (18)$$

see Fig. 1(a) and (b).

The asymptotic radial nuclear wave functions in each scattering channel can be written in terms of the exponential functions, as in Eq. (16) or somehow else, but the important point is that the radial

nuclear wave functions must be the functions of the interatomic distance  $R_j^{sc}$ , not of the internuclear distance  $R$  (Bates, McCarroll 1958; Belyaev 2010; Belyaev et al. 2001; 2002; Bransden, McDowell 1992; Grosser et al. 1999). The exponential functions (16) have the simple form and represent the incoming and outgoing asymptotic wave functions in each scattering (atomic-state) channel.

The scattering (interatomic) vector  $R_j^{sc}$  can be written as follows:

$$R_j^{sc} = R + b_j, \quad (19)$$

where the vector  $b$  equals

$$b_j = \gamma_j \frac{m_j}{M} (r - \gamma_j R). \quad (20)$$

The channel specific reduced masses  $m_j$  and the scaling factors  $\gamma_j$  are collected in Table 1. The vector  $b_j$  depends on the asymptotic rearrangement in the channel  $j$  and hence can be different for different channels. This vector is small compared to  $R$ , but it does not vanish at infinity and therefore must be taken into account. It is worth emphasizing that the vector  $b_j$  depends on both molecular coordinates  $r$  and  $R$ .

Although the adiabatic electronic molecular-state wave functions  $\phi_k$  convert into atomic eigenfunctions in the asymptotic region, a single term in the expansion (5), describing a wave function in the molecular state  $k$ , does not coincide with a single term in Eq. (14), describing an asymptotic wave function in the corresponding scattering (atomic-state) channel, see Eq. (16). Indeed, the basic electronic wave functions are the same, despite being written in different coordinates, but the radial nuclear wave functions are the functions of different coordinates,  $R$  and  $R_j^{sc}$ , respectively, where the latter depends not only on  $R$ , but also on  $r$ , see Eqs. (19) and (20).

Due to the dependence of the vector  $b_j$  on the electronic coordinate  $r$ , an incoming/outgoing current in a single scattering channel is distributed among several molecular states and vice versa. Projecting the asymptotic scattering-channel wave functions (16) on the molecular asymptotic wave functions (5) gives

$$\Psi_j^\pm = Y_{JM_j}(\Theta, \Phi) \frac{\exp(\pm iK_j R)}{R} \sum_k t_{kj}^\pm \phi_k(r, R), \quad (21)$$

where the elements of the matrices  $t^\pm$  represent the reprojection coefficients (Belyaev, Dalgarno, McCarroll 2002; Belyaev 2009; Belyaev 2010)

$$t_{kj}^\pm = \left\langle \phi_k \left| \exp(\pm iK_j b_{jz}) \right| \phi_j \right\rangle_\infty, \quad (22)$$

$b_{jz}$  being a projection of the vector  $b_j$  onto the molecular axis, which coincides with the axis  $z$ :

$$b_{jz} = \gamma_j \frac{m_j}{M} (z - \gamma_j R). \quad (23)$$

Expanding the exponential in Eq. (22) at low collision energies, the matrix elements  $t_{kj}^\pm$  can be evaluated via corresponding atomic transition dipole moments

$$t_{kj}^\pm = \delta_{kj} \left( 1 - \frac{\tilde{x}_j}{2} \right) \pm i x_{kj}, \quad (24)$$

where

$$x_{kj} = K_j \gamma_j \frac{m_j}{M} \left\langle \phi_k \left| z - \gamma_j R \right| \phi_j \right\rangle \Bigg|_{R \rightarrow \infty}, \quad (25)$$

and

$$\tilde{x}_j = K_j^2 \gamma_j^2 \frac{m_j^2}{M^2} \left\langle \phi_j \left| (z - \gamma_j R)^2 \right| \phi_j \right\rangle \Bigg|_{R \rightarrow \infty}. \quad (26)$$

All the values are taken in the asymptotic region,  $R \rightarrow \infty$ .  $\delta_{kj}$  is the Kronecker delta symbol. Furthermore, taking into account Eq. (13), the matrix elements  $t_{kj}^\pm$  (24) can be written via asymptotic values of the derivative couplings calculated in the Jacobi molecular coordinates

$$x_{kj} = \frac{K_j \hbar^2}{M [U_k(\infty) - U_j(\infty)]} \left\langle \phi_k \left| \frac{\partial}{\partial R} \right| \phi_j \right\rangle_{\infty} \quad (27)$$

and

$$\tilde{x}_j = \sum_l x_{lj}^2. \quad (28)$$

Thus, Eqs. (24), (27) and (28) allow one to calculate the matrix elements  $t_{kj}^{\pm}$ , which are in turn needed for the construction of the correct asymptotic wave functions (21) via asymptotic values of adiabatic potential energies  $U_j(\infty)$  and asymptotic values of nonadiabatic radial couplings  $\langle \phi_k | \partial/\partial R | \phi_j \rangle_{\infty}$ .

It is worth noting that the coefficients  $t_{kj}^{\pm}$  are  $R$ -independent, but they depend on the collision energy  $E$  via the wave numbers  $K_j$ . In the zero collision energy limit, the matrices  $t^{\pm}$  transfer into the unit matrix. Thus, the asymptotic radial nonadiabatic couplings are responsible for the construction of the correct asymptotic wave functions in the molecular coordinates  $r, R$ .

At low collision energies, the  $\tilde{x}_j$  are small and the diagonal matrix elements  $t_{jj}^{\pm}$  are close to unit. In this case, one can keep the terms of the order of  $\sqrt{m}/M$ , and the expansion coefficients  $t_{kj}^{\pm}$  can be approximately calculated via the nonadiabatic couplings

$$t_{kj}^{\pm} = \delta_{kj} \pm \frac{iK_j \hbar^2}{M [U_k(\infty) - U_j(\infty)]} \left\langle \phi_k \left| \frac{\partial}{\partial R} \right| \phi_j \right\rangle_{\infty} \quad (29)$$

or via the corresponding atomic transition dipole moments

$$t_{kj}^{\pm} = \delta_{kj} \pm iK_j \gamma_j \frac{m_j}{M} \left\langle \phi_k \left| z - \gamma_j R \right| \phi_j \right\rangle \Big|_{R \rightarrow \infty}. \quad (30)$$

Note that in the asymptotic region  $z - \gamma_j R = z^{at}$ , so  $\langle \phi_k | z - \gamma_j R | \phi_j \rangle_{R \rightarrow \infty}$  represents an atomic transition dipole moment  $\langle \phi_k | z^{at} | \phi_j \rangle$ .

Equations (22) and (23) give the most general formula for calculating the expansion coefficients  $t_{kj}^{\pm}$ , but they require some additional quantum chemical calculations, while Eqs. (24), (27), (28), and, in particular, Eq. (29), allow one to easily calculate the expansion coefficients via the asymptotic limits of corresponding adiabatic potentials and nonadiabatic couplings, that is, without additional quantum chemical calculations. Estimates show that Eq. (29) is typically applicable for collision energies up to at least 1 keV.

The incoming and outgoing asymptotic wave functions  $\Psi_j^{\pm}$  in Eq. (21) continue to represent the free motion of the atoms in the  $j$ -th atomic eigenstate (the scattering channel  $j$ ). They are now written in the form of the original expansion, Eq. (5), and, therefore, have an unexpected appearance: the sum (21) consists not only of a leading term with the molecular state  $\phi_j$ , but it contains additional terms with other electronic molecular states, which are typically smaller by a factor of  $\sqrt{m}/M$ . The additional terms are obviously required as an adjustment for the use of the inadequate coordinates  $r$  and  $R$  in the asymptotic region. The point is that the molecular coordinates  $r$  and  $R$  used to describe molecular states of the collision complex at small and intermediate distances are not suitable for the description of free atoms in the asymptotic region.

Writing  $\Psi$  in the form of Eq. (5), the radial wave functions  $F_k$  in the molecular state  $k$  at large  $R$  are found to be written as follows (Belyaev 2009; Belyaev et al. 2001; Grosser et al. 1999):

$$F_k = \sum_j K_j^{-1/2} \left[ t_{kj}^+ a_j^+ \exp(iK_j R) + t_{kj}^- a_j^- \exp(-iK_j R) \right] \text{ for } R \rightarrow \infty \quad (31)$$

One easily sees that the  $F_k$  satisfies the coupled channel equations Eq. (6) for large  $R$ . As this is true for any arbitrary choice of the  $a_j^{\pm}$ , Eq. (31) is the general form for the asymptotic behaviour of the solutions. Note that we refer here to the coupled channel equations in the correct form, which possesses nonvanishing asymptotic couplings.

To summarise so far, Eq. (31) represents the asymptotic form for the solutions of the coupled equations. The corresponding asymptotic total wave function can be written in the form of Eq. (14), where every single term represents the free motion of an atom in an atomic eigenstate (in a scattering channel). The factors  $a_j^{\pm}$  represent the probability amplitudes to find the atoms in the corresponding atomic eigenstates. Therefore, equation (31) constitutes the relation between the solutions  $F_k$  of the coupled channel equations and the true probability amplitudes. The remaining task is to find the relations between  $a_j^+$  and  $a_k^-$ , once the coupled equations have been solved.

## Scattering matrix

The amplitudes  $a_j^+$  and  $a_k^-$  are related to each other by a scattering  $S$ -matrix (Grosser et al. 1999),

$$a_j^+ = (-1)^{J+1} \sum_k S_{jk} a_k^- \quad (32)$$

The  $S$ -matrix can be expressed by the  $R$ -matrix.  $\underline{R}$ ,  $\underline{S}$  and  $\underline{t}^\pm$  represent the corresponding matrices, and  $\underline{K}$ ,  $\underline{K}^{\pm 1/2}$ , and  $\exp(-i\underline{K}R)$  stand for diagonal matrices with elements  $K_j$ ,  $K_j^{\pm 1/2}$ , and  $\exp(-iK_j R)$  (Belyaev 2010; Belyaev et al. 2001; Grosser et al. 1999):

$$\begin{aligned} \underline{S} = & (-1)^J \exp(-i\underline{K}R_0) \underline{K}^{-1/2} \left( \underline{t}^- + i\underline{R} \underline{t}^- \underline{K} \right) \\ & \times \left( \underline{t}^+ - i\underline{R} \underline{t}^+ \underline{K} \right)^{-1} \underline{K}^{1/2} \exp(-i\underline{K}R_0). \end{aligned} \quad (33)$$

The  $a_j^\pm$  are the incoming and outgoing amplitudes for the scattering channel  $j$  when the correct asymptotic wave functions are used, that is, the functions of the interatomic distances, not the internuclear ones. Equation (33) shows how the correct  $S$ -matrix is obtained from the regular solutions of the coupled channel equations expressed by the matrix  $\underline{R}$  even when asymptotic nonadiabatic couplings are nonzero. This approach is called the reprojection method (Belyaev 2010).

Equation (33) can be compared to the relation between the  $R$ - and the  $S$ -matrices used in the conventional BO method. When one disregards the difference between the interatomic and internuclear coordinates and neglects asymptotic nonadiabatic couplings, the  $\underline{t}^\pm$ -matrices are replaced by the unit matrix  $\underline{1}$ . In this case, Eq. (33) reduces to the relation

$$\begin{aligned} \underline{S}^{conv} = & (-1)^J \exp(-i\underline{K}R_0) \underline{K}^{-1/2} \left( \underline{1} + i\underline{R} \underline{K} \right) \\ & \times \left( \underline{1} - i\underline{R} \underline{K} \right)^{-1} \underline{K}^{1/2} \exp(-i\underline{K}R_0). \end{aligned} \quad (34)$$

This expression is the conventional relation between the  $R$ - and  $S$ -matrices. Comparison of the two expressions for  $\underline{S}$  shows that the present procedure (33) is only slightly more complicated than the usual procedure to obtain the  $S$  from the  $R$ -matrix. It is worth noting that the conventional BO method assumes (i) that all asymptotic nonadiabatic couplings calculated in the molecular coordinates are equal to zero (which is not correct) and (ii) that asymptotic nuclear radial wave functions have the form of single functions of the internuclear distance (which is not correct either). As pointed out above, nonzero asymptotic couplings (13) are a fundamental feature of the BO approach and the correct asymptotic radial nuclear wave functions in molecular coordinates have the form of a superposition of functions of the internuclear distance, Eq. (31), so both assumptions of the conventional BO method are not fulfilled. The reprojection method takes into account nonvanishing asymptotic couplings in the coupled channel equations and uses the correct forms (16) for the asymptotic incoming and outgoing wave functions.

## Transition probability, cross section and rate coefficient

Having the  $S$ -matrix known at a given collision energy  $E = E_{tot} - U_i^{eff}(\infty)$  in the initial scattering channel  $i$  and at a given total angular momentum quantum number  $J$ , a probability  $P_{if}(J, E)$  for an inelastic state-to-state transition  $i \rightarrow f$  is calculated by the following formula

$$P_{if}(J, E) = \left| S_{if}(J, E) \right|^2 \quad (35)$$

An inelastic cross section  $\sigma_{if}(E)$  is calculated as a sum over the total angular momentum quantum number  $J$

$$\sigma_{if}(E) = \frac{\pi \hbar^2 p_i^{stat}}{2ME} \sum_{J=0}^{\infty} P_{if}(J, E) (2J+1), \quad (36)$$

where  $p_i^{stat}$  is the statistical probability for population of the initial channel  $i$ .

An inelastic rate coefficient  $K_{if}(T) = \langle \sigma_{if} v \rangle$  is then obtained by integrating over a collision energy  $E$  assuming that the Maxwellian distribution is valid

$$K_{if}(T) = \sqrt{\frac{8}{\pi M (k_B T)^3}} \int_0^\infty \sigma_{if}(E) E \exp\left(-\frac{E}{k_B T}\right) dE, \quad (37)$$

$T$  being a temperature,  $k_b$  the Boltzmann constant.

It is worth emphasizing that in order to calculate accurate nonadiabatic transition probabilities  $P_{if}$ , one has to reach a convergence for these probabilities with respect to variation of the upper integration limit for a solution of the coupled channel equations, since scattering matrix elements  $S_{if}$ , as well as the corresponding wave functions, are defined in the asymptotic ( $R \rightarrow \infty$ ) region, see Eqs. (5), (14), (31), and (32). In order to calculate reliable cross sections, one has to reach an additional convergence for  $\sigma_{if}(E)$  with respect to a number of partial waves taken into account, that is, to the upper summation value for the total angular momentum quantum number  $J \rightarrow \infty$ , see Eq. (36).

## Reprojection method and conventional BO approach

### Conventional BO: A theoretical extract

Let us compare the results of applications of the reprojection method and the conventional BO approach. As mentioned above, one of the fundamental features of the BO approach is nonzero asymptotic matrix elements of the radial nonadiabatic coupling between the molecular states which asymptotically correlate to scattering channels with nonzero transition dipole moments between corresponding atomic states. Let us consider how the conventional BO approach treats this feature.

The total asymptotic wave functions written in terms of the asymptotic incoming and outgoing scattering-channel wave functions Eq. (14) can be re-written in terms of the asymptotic incoming and outgoing molecular-state wave functions and in the molecular coordinates by using the expansion (21) as follows

$$\Psi_{JM_J}(r, R) = \sum_k K_k^{-1/2} (A_k^+ \tilde{\Psi}_k^+ + A_k^- \tilde{\Psi}_k^-), \quad (38)$$

where

$$\Psi_k^\pm = Y_{JM_J}(\Theta, \Phi) \frac{\exp(\pm i K_k R)}{R} \phi_k(r, R) \quad (39)$$

and

$$A_k^\pm = \sum_j a_j^\pm T_{kj}^\pm. \quad (40)$$

The  $R$ -dependent coefficients  $T_{kj}^\pm$  read

$$\begin{aligned} T_{kj}^\pm &= t_{kj}^\pm \frac{\sqrt{K_k}}{\sqrt{K_j}} \exp[\pm i(K_k - K_j)R] \\ &= \delta_{kj} \left(1 - \frac{\tilde{X}_j}{2}\right) \pm i X_{kj}^\pm, \end{aligned} \quad (41)$$

where

$$X_{kj}^\pm = \frac{\sqrt{K_j K_k} \hbar^2 \exp[\pm i(K_j - K_k)R]}{M[U_k(\infty) - U_j(\infty)]} \left\langle \phi_k \left| \frac{\partial}{\partial R} \right| \phi_j \right\rangle_\infty \quad (42)$$

and

$$\tilde{X}_j = \tilde{x}_j, \quad (43)$$

see Eq. (28).

Finally, as distinct from the  $R$ -independent incoming and outgoing amplitudes  $a_j^\pm$  in the scattering channels, the incoming and outgoing probability-current amplitudes  $A_k^\pm$  in molecular channels, Eq. (38), depend on the internuclear distance  $R$ , see Eqs. (40)-(42). This results in  $R$ -dependence of inelastic transition probabilities between molecular states unlike the  $R$ -independent inelastic probabilities between scattering states which are expressed via the amplitudes  $a_j^\pm$ , see Eq. (14).

### Na + Li collisional example

Let us consider the collisions of Na + Li as an example. For the sake of simplicity, let us take into account only three lowest molecular  $^1\Sigma^+$ , which asymptotically correspond to the following interactions: Na( $3s$ ) + Li( $2s$ ) the ground state  $X$ , Na( $3s$ ) + Li( $2p$ ) the excited state  $A$ , and Na( $3p$ ) + Li( $2s$ ) the excited state  $C$ . It is shown in Ref. (Belyaev 2010) that two of these three matrix elements have nonzero asymptotic nonadiabatic couplings.

The  $R$  dependence of the probability-current amplitudes in molecular states means no convergency with respect to the upper integration limit for the coupled channel equations. One expects the oscillatory behaviour of the transition probability up to infinity, and the numerical calculations confirm this conclusion, see Ref. (Belyaev 2010). Nonzero transition probabilities in the asymptotic region at any angular momentum quantum numbers result in no convergency with respect to the upper summation limit for the cross sections of the excitation processes in these collisions, see Eq. (36). Finally, the inelastic (excitation) cross sections increase up to infinity, although this is not physically correct at all. In contrast to the convergent BO approach, the reprojection method provides the convergency and correct results for the transition probabilities, cross sections and rate coefficients.

## Conclusion

Possible sources of deviation between the experimental and numerical data can have different origin: (i) A major shortcoming of the experimental data consists in the highly indirect procedure used for determining the absolute cross section scale. The data were normalized for this purpose to the results published by other authors, which, in turn, relied on a similar normalization. The error of the experimental data was estimated to be of the order of 40% (Grosser, Krüger 1984). However, a larger error of the absolute scale seems possible. It offers a straightforward explanation for a large part of the observed discrepancy. (ii) The neglect of higher excited states in the system of coupled equations. Inclusion of the higher-lying molecular states can therefore be expected to have some effect on the numerical results, but would probably not lead to changes beyond a few tens of percent. Generally, one expects errors of this type to be less relevant for the range of energies near the threshold, compared to the 1 keV range. (iii) Errors in the calculated potentials and coupling matrix elements are expected to be smaller than for the Na + Li system referred to above and should, in general, result in correspondingly smaller deviations.

In summary, the numerical treatment of the present system offers no severe conceptual or mathematical difficulties, neither at the quantum chemical nor at the dynamical level. The degree of agreement with the experimental data makes a repetition of the experiment highly desirable.

## Conflict of Interest

The author declares that there is no conflict of interest, either existing or potential.

## References

- Bates, D. R., McCarroll, R. (1958) Electron capture in slow collisions. *Proceedings of the Royal Society of London. Series A. Mathematical and Physical Sciences*, 245 (1241), 175–183. <https://doi.org/10.1098/rspa.1958.0075> (In English)
- Belyaev, A. K. (2009) Nonadiabatic effects in inelastic collisional processes. *Physica Scripta*, 80 (4), article 048113. <https://doi.org/10.1088/0031-8949/80/04/048113> (In English)
- Belyaev, A. K. (2010) Revised Born–Oppenheimer approach and a reprojection method for inelastic collisions. *Physical Review A*, 82 (6), article 060701. <https://doi.org/10.1103/PhysRevA.82.060701> (In English)
- Belyaev, A. K. (2015) Excitation cross sections in low-energy hydrogen-helium collisions. *Physical Review A*, 91 (6), article 062709. <https://doi.org/10.1103/PhysRevA.91.062709> (In English)
- Belyaev, A. K., Dalgarno, A., McCarroll, R. (2002) The dependence of nonadiabatic couplings on the origin of electron coordinates. *The Journal of Chemical Physics*, 116 (13), 5395–5400. <https://doi.org/10.1063/1.1457443> (In English)
- Belyaev, A. K., Egorova, D., Grosser, J., Menzel, T. (2001) Electron translation and asymptotic couplings in low-energy atomic collisions. *Physical Review A*, 64 (5), article 052701. <https://doi.org/10.1103/PhysRevA.64.052701> (In English)
- Born, M., Oppenheimer, R. (1927) Zur Quantentheorie der Molekeln [On the quantum theory of molecules]. *Annalen der Physik*, 389 (20), 457–484. <https://doi.org/10.1002/andp.19273892002> (In German)

- Brandsen, B. H., McDowell, M. R. C. (1992). *Charge exchange and the theory of ion-atom collisions*. Oxford: Clarendon Press; New York: Oxford University Press, 474 p. (In English)
- Burke, V. M., Noble, C. J. (1995) FARM—A flexible asymptotic R-matrix package. *Computer Physics Communications*, 85 (3), 471–500. [https://doi.org/10.1016/0010-4655\(94\)00178-5](https://doi.org/10.1016/0010-4655(94)00178-5) (In English)
- Faddeev, L. D. (1961) Scattering theory for a three-particle system. *Soviet Physics—JETP*, 12 (5), 1014–1019. (In English)
- Faddeev, L. D., Merkuriev, S. P. (1993) *Quantum scattering theory for several particle systems*. Dordrecht: Springer Publ., 406 p. <https://doi.org/10.1007/978-94-017-2832-4> (In English)
- Grosser, J. (1986) Angular momentum coupling in atom-atom collisions. *Zeitschrift für Physik D. Atoms, Molecules and Clusters*, 3 (1), 39–58. <https://doi.org/10.1007/BF01442346> (In English)
- Grosser, J., Krüger, W. (1984) Hydrogen 2s and 2p excitation in low energy H, D+ He collisions. *Zeitschrift für Physik A. Atoms and Nuclei*, 318 (1), 25–30. (In English)
- Grosser, J., Menzel, T., Belyaev, A. K. (1999) Approach to electron translation in low-energy atomic collisions. *Physical Review A*, 59 (2), article 1309. <https://doi.org/10.1103/PhysRevA.59.1309> (In English)
- Lane, A. M., Thomas, R. G. (1958) R-matrix theory of nuclear reactions. *Reviews of Modern Physics*, 30 (2), article 257. <https://doi.org/10.1103/RevModPhys.30.257> (In English)
- Light, J. C. (1979). Reactive scattering cross sections I: Theory. In: R. B. Bernstein (ed.). *Atom-Molecule Collision Theory*. Boston: Springer Verlag, pp. 239–257. [https://doi.org/10.1007/978-1-4613-2913-8\\_6](https://doi.org/10.1007/978-1-4613-2913-8_6) (In English)
- Lin, C. D. (1995) Hyperspherical coordinate approach to atomic and other Coulombic three-body systems. *Physics Reports*, 257 (1), 1–83. [https://doi.org/10.1016/0370-1573\(94\)00094-J](https://doi.org/10.1016/0370-1573(94)00094-J) (In English)
- Macek, J., Cavagnero, M., Jerjian, K., Fano, U. (1987) Bypassing translation factors in molecular dissociation and reactions. *Physical Review A*, 35 (9), article 3940. <https://doi.org/10.1103/PhysRevA.35.3940> (In English)
- Macías, A., Riera, A. (1982) Ab initio quantum chemistry in the molecular model of atomic collisions. *Physics Reports*, 90 (5), 299–376. [https://doi.org/10.1016/0370-1573\(82\)90173-9](https://doi.org/10.1016/0370-1573(82)90173-9) (In English)
- Mott, N. F., Massey, H. S. W. (1949) *The theory of atomic collisions*. Oxford: Clarendon Press, 388 p. (In English)
- Nikitin, E. E., Umansky, S. Ya. (1984) *Theory of slow atomic collisions*. Berlin: Springer Verlag, 432 p.



UDC 517.938

<https://www.doi.org/10.33910/2687-153X-2022-3-1-37-42>

## Bound states for two delta potentials supported on parallel lines on the plane

A. S. Bagmutov<sup>1</sup>, I. Y. Popov<sup>✉1</sup>

<sup>1</sup> ITMO University, 49 Kronverkskii Ave., Saint Petersburg 197101, Russia

### Authors

Alexander S. Bagmutov, e-mail: [Bagmutov94@mail.ru](mailto:Bagmutov94@mail.ru)

Igor Y. Popov, ORCID: [0000-0002-5251-5327](https://orcid.org/0000-0002-5251-5327), e-mail: [popov1955@gmail.com](mailto:popov1955@gmail.com)

**For citation:** Bagmutov, A. S., Popov, I. Y. (2022) Bound states for two delta potentials supported on parallel lines on the plane. *Physics of Complex Systems*, 3 (1), 37–42. <https://www.doi.org/10.33910/2687-153X-2022-3-1-37-42>

**Received** 21 November 2021; reviewed 10 January 2022; accepted 12 January 2022.

**Funding:** The research was supported by the Russian Foundation for Basic Research (Grant No. 20-31-90050).

**Copyright:** © A. S. Bagmutov, I. Y. Popov (2022). Published by Herzen State Pedagogical University of Russia. Open access under [CC BY-NC License 4.0](https://creativecommons.org/licenses/by-nc/4.0/).

**Abstract.** We consider a singular  $\delta$ -potential supported on two parallel lines in  $R^2$  as a model of two interacting macromolecules. The intensity of the potential is constant, but each line contains a finite segment with a variation. Using variational approach, we study continuous and discrete spectra and estimate the gap between the eigenvalue and the continuous spectrum as a function of shift between the line segments. The existence of bound states for the system is proven by test function with separated variables.

**Keywords:** spectrum, variational approach, potential supported on line.

### Introduction

A great deal of recent research has focused on potentials supported on line in  $R^3$  or  $R^2$ . Apart from the mathematical interest, the problem attracts researches due to its physical application as a potential can be considered a model of a long molecule. There is a series of works exploring the potentials supported on sets of zero measure (see, e. g.: Behrndt, Frank et al. 2017; Brasche, Teta 1992; Brasche et al. 1994; Exner, Ichinose 2001; Exner, Jex 2013; Exner, Kondej 2002; 2004; 2005; 2015; Exner, Pankrashkin 2014; Exner, Vugalter 2016; Exner, Yoshitomi 2002; Posilicano 2001; 2004). The background of the model is the theory of self-adjoint extensions of symmetric operators. An analogous model was also developed for narrow slits in the surfaces (Popov 1992a; 1993) and for potentials supported on hypersurfaces (Behrndt et al. 2016; 2017a; Exner et al. 2018). In the present paper we deal with 2D strip which boundaries are formed by potentials supported on lines. These potentials look like semitransparent boundaries (see, e. g., Bagmutov, Popov 2020; Popov 1992b; Vorobiev et al. 2020). The potentials are assumed to be negative (i. e., attractive, having a local perturbation and identical at each side of the strip but having some shift along the strip at one line in respect to the second line (Fig. 1). We prove the existence of eigenvalue caused by the local perturbation of the potentials and look after its behaviour if the shift of the perturbation changes.

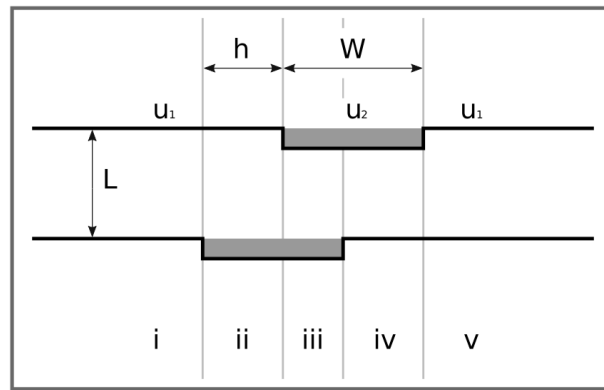


Fig. 1. System of two parallel lines with delta-potentials of varying intensity on them

The result has a biophysical character. It is related to molecule coupling, e. g., viruses coupling with cells or coupling of two DNA chains. Roughly speaking, the process looks as follows. One molecule recognises some label at the second molecule, keeps close to this position and forms a bond. In our simple model, molecules are represented by lines with potentials, a “label” is a perturbation of the potentials. A reasonable question begs itself: which factors can assist molecules to keep a small distance in proper position? If one considers electron in this system of two attractive potentials, there is a bound state due to its local perturbations. This state assists to keep molecules close. In real system this state can be destroyed by external perturbations (e. g., thermal vibration). The state is more stable if there is sufficient gap between the eigenvalue and the lower bound of the continuous spectrum. In our model, we show that an increase in the shift leads to a decrease in the gap, i. e., the most stable position is in the case of the shift absence. It means that the electron bound state is a factor assisting molecules to be in proper position.

Let us consider a system shown in Fig. 1. It consists of two infinitely-stretching parallel lines at a distance  $L$ , on a 2D plane. Attractive delta-potential of a constant intensity  $-u_1 < 0$  is located along the lines, except for a region of finite width  $W$  on each line, where intensity changes to  $-u_2$ , such as  $-u_2 < -u_1$ . Let us denote by  $h < W$  a distance to which a region  $W$  on one line is shifted relative to the second line. We use the atomic system of units in which one has  $m = 0.5$ ,  $\hbar = 1$ . Correspondingly, the Hamiltonian of the system is the Laplacian  $H\hat{\psi} = -\Delta\psi$ , with the domain consisting of continuous functions  $\psi \in L^2(R)$  that satisfy the following conditions on the lines:

$$\frac{\partial\psi}{\partial y}(x, y_l + 0) - \frac{\partial\psi}{\partial y}(x, y_l - 0) = -\alpha_x \psi(x, y_l) \quad (1)$$

where  $y_l = 0$  or  $L$ , and  $\alpha_x = u_2$  is inside the perturbed region of the line  $W$  and  $\alpha_x = u_1$ , outside.

### Continuous spectrum

Let us consider the continuous spectrum of the operator. As the system is a local perturbation of the corresponding one with two constant potentials  $-\alpha = -u_1$  supported on two parallel lines, the continuous spectrum is the same as without this perturbation. In case of two parallel lines ( $y = 0, y = L$ ) with constant potentials, separation of variables can be made, i. e., one can consider the wave function in the form  $\psi(x, y) = \chi(x) \zeta(y)$ . Correspondingly, the lower bound of the continuous spectrum for the Laplacian  $\hat{H}$  with conditions (1) on the lines is given by the lowest eigenvalue for the transversal problem (for function  $\zeta(y)$ ). To find it, we consider the operator  $-\frac{d^2}{dy^2}$  on  $R$  with the following conditions at two points:

$$\begin{aligned} \zeta(+0) &= \zeta(-0), \\ \zeta(L+0) &= \zeta(L-0), \\ \frac{d\zeta}{dy}(+0) - \frac{d\zeta}{dy}(-0) &= -\alpha\zeta(-0), \\ \frac{d\zeta}{dy}(L+0) - \frac{d\zeta}{dy}(L-0) &= -\alpha\zeta(L-0), \end{aligned} \tag{2}$$

**Theorem 1.** *The lower bound of the continuous spectrum of the operator  $\hat{H}$  is  $-\max_j \kappa_j^2$ , where  $\kappa_j$  are real roots of the spectral equation:*

$$\frac{4}{\alpha^2} \kappa (\kappa + L) = e^{2\kappa L} - 1 \tag{3}$$

*Proof.* Differential equation for transversal eigenfunction  $\zeta(y)$  of  $-\frac{d^2}{dy^2}$  corresponding to eigenvalue  $k^2$  at each part of is as follows:  $-\frac{d^2\zeta}{dy^2} = k^2\zeta$ . Taking its solutions  $e^{\pm ik y}$  and satisfying conditions (2), one obtains (3), where  $\kappa = ik \in R_-$ .

To have an eigenvalue, one needs a decay at infinity, i. e.,  $\kappa < 0$ . Keeping in mind that the function in the left-hand side of (3) takes minimal value  $-1$  at  $\kappa = -\frac{\alpha}{2}$ , one concludes that there is a root  $\kappa_1$  of (3),  $-\alpha < \kappa_1 < -\frac{\alpha}{2}$ .

**Remark.** It is known that in the case of a single line, the lower bound of the continuous spectrum is  $-\frac{\alpha^2}{4}$ . In case of two lines with conditions (2), the limit of the threshold determined by (3) tends to  $-\alpha_2$  when  $L \rightarrow 0$ . It corresponds to potential  $-2\alpha$  at single line. Hence, for conditions (2), one has a summation of the two-line potentials.

### Test functions

To find the discrete spectrum, we use a variational technique. We consider the ratio

$$E = \frac{(\hat{H}\psi, \psi)}{(\psi, \psi)}$$

which minimal value is the minimal eigenvalue of the operator  $\hat{H}$ . If a test function  $\psi$  is such that the value of the ratio is smaller than the lower bound of the continuous spectrum of  $\hat{H}$ , then there is an eigenvalue of  $\hat{H}$  below the continuous spectrum and the value of the ratio gives one an upper estimation for this eigenvalue.

We will construct test functions which satisfy the condition (1) on the lines, but are not continuous along the  $X$  axis. However, it can be approximated with arbitrary accuracy by the functions from the operator domain. Specifically, we assume  $\psi(x,y) = \chi(x)\zeta_x(y)$ , where  $\zeta_x(y)$  are five eigenfunctions of  $-\frac{d^2}{dy^2}$ , satisfying condition (2), one for each vertical strip with unique delta potentials on lines (denoted by Roman numerals in Fig. 1).

First, let us consider a transversal part  $\zeta_x(y)$ . There are 5 of them, with three unique sets of conditions  $(u_1, u_1)$ ,  $(u_1, u_2)$ ,  $(u_2, u_2)$ . Let each of  $a_1$  and  $a_2$ ,  $a_1 \leq a_2$  take value of  $u_1$  or  $u_2$ . The problem sometimes referred to as double delta-function potential in 1D. For the  $L > L_0 = \frac{a_1 + a_2}{a_1 a_2}$ , there are two solutions. When continually changing delta-function intensities to make them equal, one of them transforms into a symmetrical solution, and the other into an asymmetrical one. We will refer to them as solutions of symmetrical and asymmetrical types respectively. The restrictions on transversal energy levels  $\tilde{E} = (0.5p)^2$  are as follows:

$$e^{-pL} = \frac{(p - a_1)(p - a_2)}{a_1 a_2}$$

Now, let us consider a longitudinal component  $\chi(x)$  for the test function. The transversal variants create five regions with different energy  $\tilde{E}_x$  each. These energies can be converted into a step-like potential for the longitudinal component constant in each region. We will consider two specific cases, corresponding to all transversal functions being either of symmetric or asymmetric types, which produces symmetric potentials with 3 different levels: a variation on square well potential, with additional step, hereafter referred to as step-well potential (see the example of potential, produced by symmetric type  $\zeta_x(y)$ , Fig. 2). Let  $V_1, V_2, V_3$  denote constant levels of a potential, from the lowest to the highest. The solutions for  $V_1 < E < V_2$  and  $V_2 < E < V_3$ , which we refer to as bottom and top ones respectively, satisfy different restrictions on energy levels. Let  $k_1 = \sqrt{E - V_1}$ ,  $k_2 = \sqrt{E - V_2}$ ,  $k_3 = \sqrt{V_3 - E}$  and

$$T_r(E) = \tan(k_1 r) \tag{4}$$

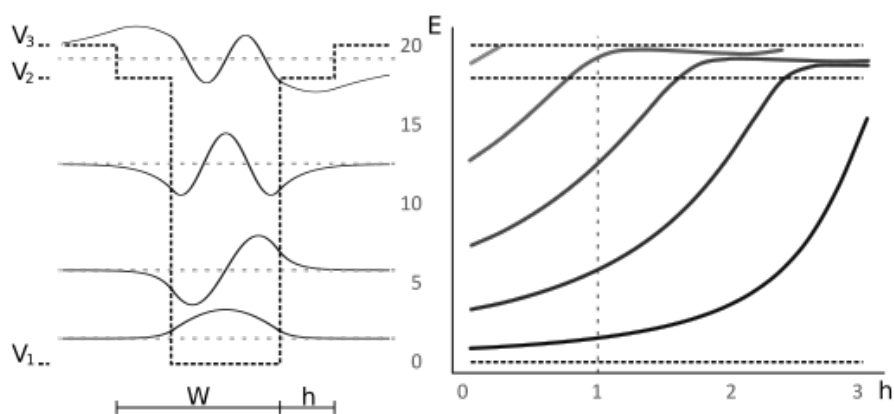


Fig. 2. Longitudinal component of the constructed function for the symmetric type  $\zeta_x(y)$ . Fixed values:  $W = 3, V_1 = 0, V_2 = 18, V_3 = 20$ . The plot shows dependence of energy levels on shift  $h$ . The left part shows a specific step-well potential, for  $h = 1$ , with energy levels and corresponding eigenfunctions.

The restrictions for energies of symmetric and asymmetric solutions are as follows:

$$T_r(E) = \frac{k_2}{k_1} \tan \left( \arctan \left( \frac{k_3}{k_2} \right) - k_2 h \right) \tag{5}$$

$$T_r(E) = -\frac{k_2}{k_1} \cot \left( \arctan \left( \frac{k_3}{k_2} \right) - k_2 h \right)$$

Let us denote the right-hand side of (5), as  $K(E)$ . These equations cover the case of  $E < V_2$  with complex  $k_2$ . However, it might be convenient to use other expression for  $K(E)$  with  $\tilde{k}_2 = \sqrt{V_2 - E}$ , which eliminates complex numbers:

$$K(E) = \frac{\tilde{k}_2}{k_1} \tanh \left( \operatorname{arctanh} \left( \frac{k_3}{\tilde{k}_2} \right) + \tilde{k}_2 h \right) =$$

$$= \frac{\tilde{k}_2}{k_1} \operatorname{coth} \left( \operatorname{arccoth} \left( \frac{k_3}{\tilde{k}_2} \right) + \tilde{k}_2 h \right)$$

## Existence of bound states

The constructed functions can be used to create an upper bound on the discrete spectrum of  $\hat{H}$ .

**Theorem 2.** *The step-well potential (see Fig.2) always has at least one discrete eigenvalue below the essential spectrum  $\sigma_{ess}$ .*

*Proof.* We will prove that there is an interval where  $T(E) - K(E)$  is continuous and takes values of different sign at the borders, where  $T(E)$  (determined as (4)) and  $K(E)$  are the left hand side and the right hand side of (5). Note, that for the edge cases  $V_2 = V_1$ ,  $V_2 = V_3$ ,  $h = 0$  or  $h = W$ , the problem turns into a square well potential situation, for which the existence of an eigenvalue is proven.

First, let us note that  $T(V_1) = 0$  and  $K(+0) = +\infty$ . The only discontinuities for the functions are the vertical asymptotes. Let us denote the smallest vertical asymptotes for  $T$  and  $K$  as  $A_T$  and  $A_K$ . Then  $T(A_T - 0) = +\infty$ ,  $K(A_K - 0) = -\infty$ , and therefore, if  $\min(A_T, A_K) \leq V_3$ , then the interval  $(0, \min(A_T, A_K))$  is the required one.

Now, let us consider the case  $\min(A_T, A_K) \leq V_3$ . Fix some values of  $W$  and  $V_2$ . Here,  $T(V_3) > 0$ , let us prove that  $K(V_3) \leq 0$  for all relevant  $h$ . The equation for the asymptotes of  $K(E)$  can be written as

$$\cot(k_2 h) = -\frac{k_3}{k_2},$$

which shows that as  $h$  increases,  $A_K$  monotonically decreases, thus  $K(E)$  continuous on  $(V_1, V_3)$ , only for  $h$  from 0 to the point at which  $A_K = V_3$ . The function  $K(V_3) = -\frac{k_2}{k_1} \tan(k_2 h)$  is a monotonically decreasing function and when  $h = 0$ , one has  $K(V_3) = 0$ . That proves  $K(V_3) \leq 0$ , when  $A_K > V_3$ , and, therefore, interval  $(V_1, V_3)$  is the necessary one.

**Corollary 1.** *The main operator  $\hat{H}$  has at least one bound state.*

*Proof.* The essential spectrum of an operator is  $\sigma_{ess}(\hat{H}) = (V_3, +\infty)$ . The constructed function satisfies  $\frac{(\hat{H}\psi, \psi)}{(\psi, \psi)} = E$ , and can be approximated to an arbitrary degree by the functions from the operator domain.

Therefore, the value  $E$  from Theorem 2 is the upper bound for the discrete spectrum of  $\hat{H}$ .

## Results

Now let us consider the constructed function energy levels as functions of  $h$ . As  $V_2$  changes, note, that edge cases  $V_2 = V_1$  and  $V_2 = V_3$ , produce square well potentials of widths  $W + h$  and  $W - h$ , which, with an increase of  $h$ , get wider and narrower respectively. With  $V_2$  fixed, an increase of  $h$  from 0 to  $W$ , transforms a narrow well  $(W, V_3)$ , into a wide well  $(2W, V_2)$ , while continuously changing their energy levels.

As has been described above, the constructed functions, given large enough  $L$ , allow us to choose one of two transversal eigenvalues:  $\tilde{E}_1 < a_1$  and  $\tilde{E}_2 > a_2$  for each region, and while regions with  $a_1 = a_2$  produce close values, regions with different intensities, which correspond to  $V_2$ , have a large gap between them. The choice between two values in each region corresponds to  $\psi$  of symmetric and asymmetric types. Using the results, we can conclude that their energy levels transform in different ways. Considering a symmetric type, we can see from Fig. 2 that the lowest eigenvalue is monotonically rising, until it escapes the strip below  $V_2$  and reaches the lowest level of the wide square well  $(2W, V_2)$ . As for real systems, a larger gap between the eigenvalue and  $\sigma_{ess}$  ensures larger stability of the eigenstate in respect to perturbations. This means that the bound states with that behavior are more stable for small  $h$ .

As we mentioned in the Introduction, the considered system can be treated as a rough model for the description of some features of line molecules (e. g., DNA-like or protein-like) interactions. Particularly, it can be useful for understanding of the first stage of interaction between a virus and an organism molecule (recognition of a "label" and fixation near the molecule), see, e. g., (Li 2016; Shang et al. 2020).

## Conflict of Interest

The authors declare that there is no conflict of interest, either existing or potential.

## Authors contribution

The authors have made an equal contribution to the paper.

## References

- Bagmutov, A. S., Popov, I. Yu. (2020) Window-coupled nanolayers: Window shape influence on one-particle and two-particle eigenstates. *Nanosystems: Physics, Chemistry, Mathematics*, 11 (6), 636–641. <https://doi.org/10.17586/2220-8054-2020-11-6-636-641> (In English)
- Behrndt, J., Exner, P., Holzmann, M., Lotoreichik, V. (2017a) Approximation of Schroedinger operators with delta-interactions supported on hypersurfaces. *Mathematische Nachrichten*, 290 (8–9), 1215–1248. <https://doi.org/10.1002/mana.201500498> (In English)
- Behrndt, J., Frank, R. L., Kuhn, C. et al. (2017b) Spectral theory for schrodinger operators with  $\delta$ -interactions supported on curves in  $\mathbb{R}^3$ . *Annales Henri Poincare*, 18 (4), 1305–1347. <https://doi.org/10.1007/s00023-016-0532-3> (In English)
- Behrndt, J., Langer, M., Lotoreichik, V. (2016) Boundary triples for Schrodinger operators with singular interactions on hypersurfaces. *Nanosystems: Physics, Chemistry, Mathematics*, 7 (2), 290–302. <https://doi.org/10.17586/2220-8054-2016-7-2-290-302> (In English)
- Brasche, J., Exner, P., Kuperin, Yu. A., Seba, P. (1994) Schroedinger operator with singular interactions. *Journal of Mathematical Analysis and Applications*, 184 (1), 112–139. <https://doi.org/10.1006/jmaa.1994.1188> (In English)
- Brasche, J., Teta, A. (1992) Spectral analysis and scattering theory for Schrodinger operators with an interaction supported by a regular curve. In: *Ideas and Methods in Quantum and Statistical Physics*. Cambridge: Cambridge University Press, pp. 197–211. (In English)
- Exner, P., Ichinose, T. (2001) Geometrically induced spectrum in curved leaky wires. *Journal of Physics A: Mathematical and General*, 34 (7), 1439–1450. <https://doi.org/10.1088/0305-4470/34/7/315> (In English)
- Exner, P., Jex, M. (2013) Spectral asymptotics of a strong  $\delta'$  interaction on a planar loop. *Journal of Physics A: Mathematical and Theoretical*, 46 (34), article 345201. <https://doi.org/10.1088/1751-8113/46/34/345201> (In English)
- Exner, P., Kondej, S. (2002) Curvature-induced bound states for a  $\delta$  interaction supported by a curve in  $\mathbb{R}^3$ . *Annales Henri Poincaré*, 3 (5), 967–981. <https://doi.org/10.1007/s00023-002-8644-3> (In English)
- Exner, P., Kondej, S. (2004) Strong-coupling asymptotic expansion for Schroedinger operators with a singular interaction supported by a curve in  $\mathbb{R}^3$ . *Reviews in Mathematical Physics*, 16 (5), 559–582. <https://doi.org/10.1142/S0129055X04002084> (In English)
- Exner, P., Kondej, S. (2005) Scattering by local deformations of a straight leaky wire. *Journal of Physics A: Mathematical and General*, 38 (22), 4865–4874. <https://doi.org/10.1088/0305-4470/38/22/011> (In English)
- Exner, P., Kondej, S. (2015) Gap asymptotics in a weakly bent leaky quantum wire. *Journal of Physics A: Mathematical and Theoretical*, 48 (49), article 495301. <https://doi.org/10.1088/1751-8113/48/49/495301> (In English)
- Exner, P., Kondej, S., Lotoreichik, V. (2018) Asymptotics of the bound state induced by  $\delta$ -interaction supported on a weakly deformed plane. *Journal of Mathematical Physics*, 59 (1), article 013051. <https://doi.org/10.1063/1.5019931> (In English)
- Exner, P., Pankrashkin, K. (2014) Strong coupling asymptotics for a singular Schrodinger operator with an interaction supported by an open arc. *Communications in Partial Differential Equations*, 39 (2), 193–212. <https://doi.org/10.1080/03605302.2013.851213> (In English)
- Exner, P., Vugalter, S. (2016) On the existence of bound states in asymmetric leaky wires. *Journal of Mathematical Physics*, 57 (2), article 022104. <https://doi.org/10.1063/1.4941139> (In English)
- Exner, P., Yoshitomi, K. (2002) Asymptotics of eigenvalues of the Schroedinger operator with a strong delta-interaction on a loop. *Journal of Geometry and Physics*, 41 (4), 344–358. [https://doi.org/10.1016/S0393-0440\(01\)00071-7](https://doi.org/10.1016/S0393-0440(01)00071-7) (In English)
- Li, F. (2016) Structure, function, and evolution of coronavirus spike proteins. *Annual Review of Virology*, 3, 237–261. <https://doi.org/10.1146/annurev-virology-110615-042301> (In English)
- Popov, I. Yu. (1993) The helmholtz resonator and the theory of operator extensions in a space with indefinite metric. *Russian Academy of Sciences. Sbornik Mathematics*, 75 (2), article 285. <https://doi.org/10.1070/SM1993v075n02ABEH003386> (In English)
- Popov, I. Yu. (1992a) The extension theory and the opening in semitransparent surface. *Journal of Mathematical Physics*, 33 (5), 1685–1689. <https://doi.org/10.1063/1.529697> (In English)
- Popov, I. Yu. (1992b) The resonator with narrow slit and the model based on the operator extensions theory. *Journal of Mathematical Physics*, 33 (11), 3794–3801. <https://doi.org/10.1063/1.529877> (In English)
- Posilicano, A. (2001) A Krein-like formula for singular perturbations of self-adjoint operators and applications. *Journal of Functional Analysis*, 183 (1), 109–147. <https://doi.org/10.1006/jfan.2000.3730> (In English)
- Posilicano, A. (2004) Boundary triples and weyl functions for singular perturbations of self-adjoint operators. *Methods of Functional Analysis and Topology*, 10 (2), 57–63. (In English)
- Shang, J., Wan, Y., Liu, C. et al. (2020) Structure of mouse coronavirus spike protein complexed with receptor reveals mechanism for viral entry. *PLOS Pathogens*, 16 (3), article e1008392. <https://doi.org/10.1371/journal.ppat.1008392> (In English)
- Vorobiev, A. M., Trifanova, E. S., Popov, I. Yu. (2020) Resonance asymptotics for a pair quantum waveguides with common semitransparent perforated wall. *Nanosystems: Physics, Chemistry, Mathematics*, 11 (6), 619–627. <https://doi.org/10.17586/2220-8054-2020-11-6-619-627> (In English)



Check for updates

Physics of Semiconductors.  
Physics of Low-Dimensional Structures  
and Nanostructures

UDC 536.42+539.19

<https://www.doi.org/10.33910/2687-153X-2022-3-1-43-50>

## Dielectric spectroscopy of VO<sub>2</sub> nanocrystalline films

R. A. Castro Arata<sup>✉1</sup>, A. V. Ilinskiy<sup>2</sup>, V. A. Klimov<sup>2</sup>, M. E. Pashkevish<sup>3</sup>, E. B. Shadrin<sup>2</sup>

<sup>1</sup> Herzen State Pedagogical University of Russia, 48 Moika Emb., Saint Petersburg 191186, Russia

<sup>2</sup> Ioffe Institute, 26 Politekhnicheskaya Str., Saint Petersburg 194021, Russia

<sup>3</sup> Peter the Great St. Petersburg Polytechnic University,  
29 Politekhnicheskaya Str., Saint Petersburg 195251, Russia

### Authors

Rene Alejandro Castro Arata, ORCID: 0000-0002-1902-5801, e-mail: [recastro@mail.ru](mailto:recastro@mail.ru)

Aleksandr V. Ilinskiy, e-mail: [ilinskiy@mail.ioffe.ru](mailto:ilinskiy@mail.ioffe.ru)

Vladimir A. Klimov, ORCID: 0000-0002-9096-7594, e-mail: [vlad.a.klimov@mail.ioffe.ru](mailto:vlad.a.klimov@mail.ioffe.ru)

Marina E. Pashkevish, ORCID: 0000-0002-3373-4129, e-mail: [marpash@yandex.ru](mailto:marpash@yandex.ru)

Evgeniy B. Shadrin, ORCID: 0000-0002-1423-2852, e-mail: [shadr.solid@mail.ioffe.ru](mailto:shadr.solid@mail.ioffe.ru)

**For citation:** Castro Arata, R. A., Ilinskiy, A. V., Klimov, V. A., Pashkevish, M. E., Shadrin, E. B. (2022) Dielectric spectroscopy of VO<sub>2</sub> nanocrystalline films. *Physics of Complex Systems*, 3 (1), 43–50. <https://www.doi.org/10.33910/2687-153X-2022-3-1-43-50>

**Received** 20 December 2021; reviewed 12 January 2022; accepted 12 January 2022.

**Funding:** The reported study was funded by Russian Foundation for Basic Research (RFBR), Project No. 20-07-00730.

**Copyright:** © R. A. Castro Arata, A. V. Ilinskiy, M. E. Pashkevish, E. B. Shadrin (2022). Published by Herzen State Pedagogical University of Russia. Open access under [CC BY-NC License 4.0](https://creativecommons.org/licenses/by-nc/4.0/).

**Abstract.** The article describes the first reported case of applying dielectric spectroscopy to study nontrivial details of size dependences of phase transformation parameters in nanocrystallites of VO<sub>2</sub> films. The method allows to identify the electrophysical parameters of nanocrystalline sets of different sizes and random location on the VO<sub>2</sub> substrate. The article investigates the martensitic nature of the Mott-Peierls semiconductor-metal phase transition in crystalline VO<sub>2</sub> films.

**Keywords:** dielectric spectroscopy, vanadium dioxide films, VO<sub>2</sub>, semiconductor-metal phase transition, correlation effects

### Introduction

When studying the parameters of the electrical response of a material (Prokhorov 1994), dielectric spectroscopy pays special attention to the tangent of the dielectric loss angle  $\delta$ — $\tan\delta$ . For an ideal dielectric between the capacitor plates, the bias current outstrips the hesitation phase of the applied alternating voltage by an angle  $\psi = \pi/2$ . For a non-ideal dielectric, this angle is smaller according to the law  $\delta + \psi = \pi/2$ . The smaller the angle  $\delta$ , the less energy is lost for heat generation. This is essential for the production of large high-quality capacitors. Data on frequency dependence of  $tg(f)$  is instrumental in the design of insulators for high-voltage power lines as well as for many other practical applications.

The development of highly sensitive dielectric spectrometers with high-speed computers has led to the emergence of dielectric spectroscopy as a method of scientific research.

The aim of our article was to explore semiconductor-metal phase transition (SMPT) in nanocrystalline VO<sub>2</sub> films using dielectric spectroscopy. These films undergo SMPT with an increase of temperature near  $T = 340$  K. This transition has a combined nature (Ilinskiy et al. 2012; Shadrin, Il'inskiy 2000) which is of interest from both applied and fundamental points of view.

### Experimental technique

The samples studied by dielectric spectroscopy included vanadium dioxide thin films (100 nm) synthesized on insulating glass substrates with a thickness of  $d = 1 \text{ mm}$ . The samples were placed in the measuring cell of a dielectric spectrometer shaped as a cylinder with two flat metal electrodes. The cell capacity without a sample was  $C_0 = \epsilon_0 S/d$ , where  $S$  is the area of mutual overlap of the electrodes and  $\epsilon_0$  is the dielectric constant. A sinusoidal electric voltage  $U_0$  of frequency  $f$  was applied to the electrodes. In this case, an alternating current  $I_0$  of the same frequency flowed through the sample, but with a phase shift  $\psi$  with respect to the phase of the applied voltage oscillations. Dielectric spectroscopy was applied to measure the following parameters: the amplitude  $U_0$  of the applied voltage, the frequency dependences of the amplitude of the current  $I_0(f)$  flowing through the sample, and the frequency dependences of the phase difference  $\psi(f)$ . The spectrometer cell with the sample is a flat capacitor. This means that the computer built into the spectrometer can obtain the following characteristics of dielectric spectra based on the measured values  $U_0$ ,  $I_0(f)$ , and  $\psi(f)$ :

- 1) the frequency dependence of the tangent of the dielectric loss angle  $\tan\delta(f)$  ( $\delta = \pi/2 - \psi$ ) and the frequency dependence of the current amplitude  $I_0(f)$ ;
- 2) frequency dependences of the real  $z'$  and imaginary  $z''$  parts of the total impedance of the sample;
- 3) frequency dependences of the real  $\epsilon'$  and imaginary  $\epsilon''$  parts of the dielectric constant of the sample;
- 4) frequency dependence of  $\tan\delta(f)$  together with Cole-Cole diagram  $\epsilon''(\epsilon')$ .

### Experimental results

As an initial result, the article presents data on the morphology of the studied film. Fig. 1 shows the atomic-force image of an undoped VO<sub>2</sub> film, and Fig. 2 shows a histogram of the size distribution of film nanocrystallites. It should be noted that the study found two types of nanocrystallites significantly different in their average size. They can be called “large” and “small”.

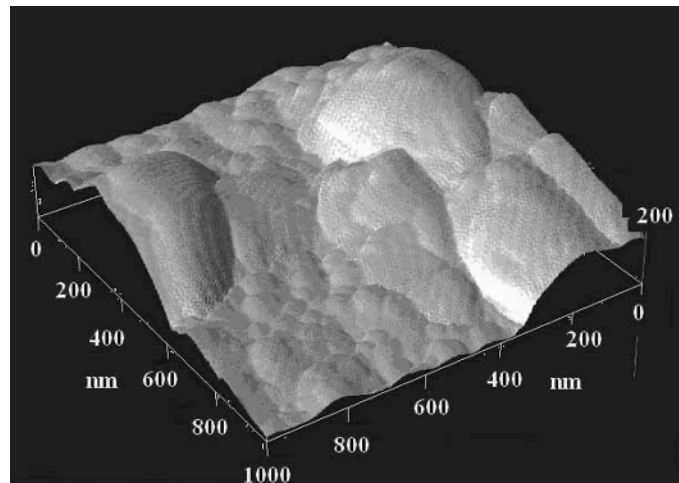


Fig. 1. Atomic force image of the surface of a vanadium dioxide film

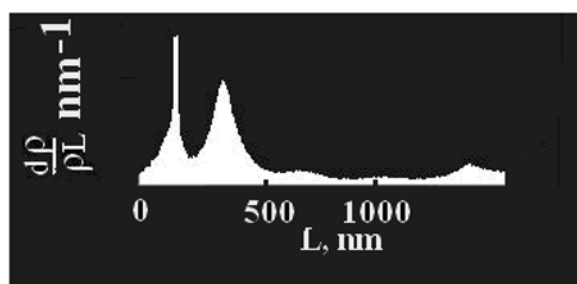


Fig. 2. Size distribution histogram of nanocrystallites

In what follows we discuss:

- 1) frequency dependence of  $\tan\delta(f)$ ;
- 2) Cole-Cole diagram  $\varepsilon''(\varepsilon')$ .

These results were obtained at different temperatures. As practice shows, these data most effectively reflect both frequency and thermal parameters of the sample (Fig. 3).

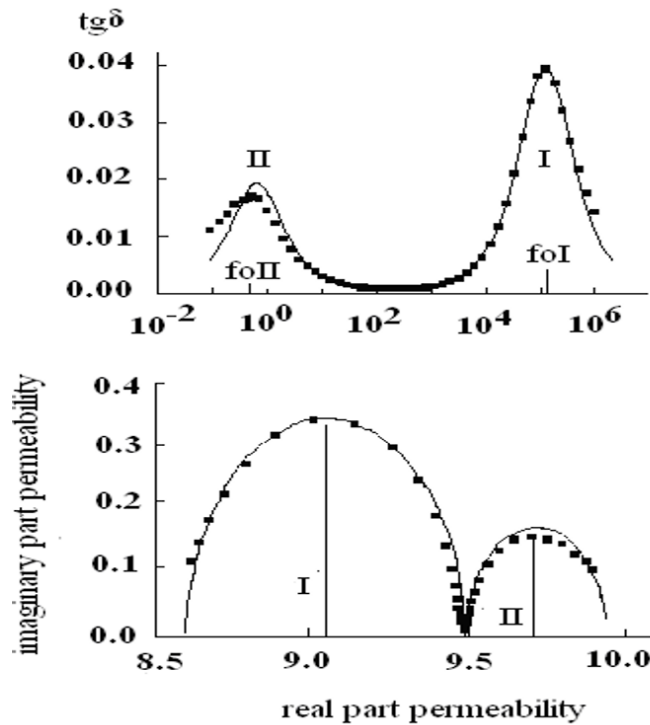


Fig. 3. Frequency dependences of the tangent of the dielectric loss angle  $\tan\delta(f)$  and Cole-Cole diagram for a  $\text{VO}_2$  film at a temperature of  $T = 303$  K. Dots are the result of the experiment, solid lines are the result of the calculation ( $C_b = 6.2$  pF,  $CI = 33$  pF,  $RI = 56.8$  k $\Omega$ ,  $Cm = 7.5$  pF,  $CII = 127$  pF,  $R_{II} = 2.8$  G $\Omega$ ,  $CO = 1.4$  pF)

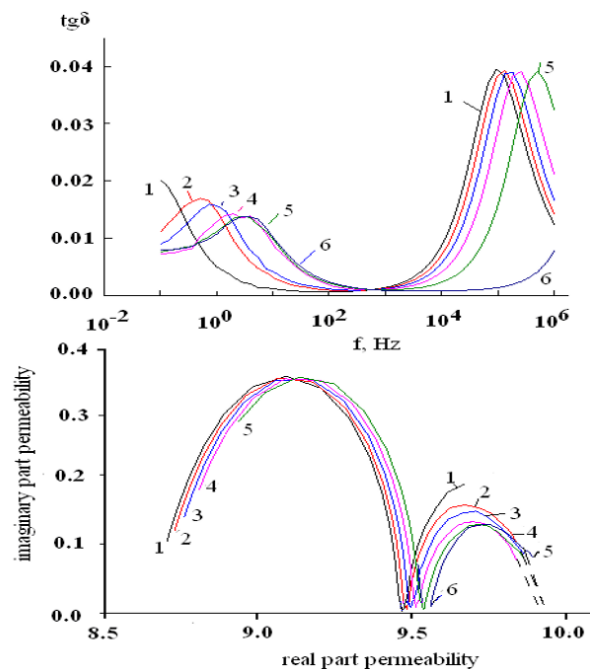


Fig. 4. Frequency dependences of the tangent of the dielectric loss angle  $\tan\delta(f)$  and Cole-Cole diagrams for an undoped  $\text{VO}_2$  film at different temperatures (experiment): 1–293 K, 2–303 K, 3–313 K, 4–323 K, 5–333 K, 6–343 K

Fig. 3 provides experimental data for the sample temperature  $T = 303$  K. Dots are the result of the experiment, solid lines are the result of the calculation. It is interesting that two maxima of the function  $\tan\delta(f)$  are observed at frequencies  $f_{oi} = 50$  kHz and  $f_{oii} = 1$  Hz. The Cole-Cole diagram has two semi-circles: a high-frequency semicircle of a large diameter and a low-frequency semicircle of a smaller diameter.

Fig. 4 shows the experimental data for  $\tan\delta(f)$  and  $\varepsilon''(\varepsilon')$  in the range 293–343 K. With an increase in temperature, the maxima shift unevenly towards high frequencies. The high-frequency maximum in the range 293–323 K shifts to high frequencies by a smaller interval than in the range 323–343 K. The low-frequency maximum shifts in the range  $T = 293$ –323 K by a larger frequency interval than in the range  $T = 323$ –343 K. The Cole-Cole diagram does not change with temperature.

### Mathematical modeling

Dielectric spectroscopy makes it possible to experimentally determine the frequency dependences (dielectric spectra)  $\tan\delta(f)$ ,  $\varepsilon'(f)$  and  $\varepsilon''(f)$ , that is, construct  $\varepsilon''(\varepsilon')$  regardless of the equivalent electrical circuit of the sample. The theory makes it possible to simulate the electrical response of a sample and find analytical expressions that correlate the values  $\tan\delta$ ,  $\varepsilon'$  and  $\varepsilon''$  with specific parameters of the samples. By comparing the experimental spectra with the calculated ones, the validity of the application of a particular scheme is tested and the numerical values of the parameters of the equivalent circuit model are determined.

In our case, there are two maxima of the function  $\tan\delta(f)$  and two semicircles on the Cole-Cole diagram. Therefore, the approach shown in Fig. 5, may be applied in modelling.

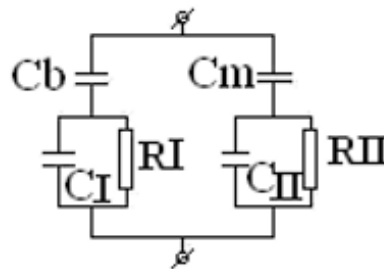


Fig. 5. Equivalent schema

The use of this approach is also justified by the structure of the sample. It takes into account the presence of two sets of film nanocrystallites with very different parameters. These sets are randomly mixed with each other on an insulating substrate. Capacities  $C_b$  and  $C_m$  are the total capacities of those parts of the substrate on which large and small nanocrystallites are synthesized. Capacities  $C_p$ ,  $C_{II}$  represent the electrical capacities of the sets of nanocrystallites themselves. Electric resistances  $R_i$  and  $R_{II}$  are connected in parallel to these capacitors in the equivalent circuit, which characterise the through-current flow through the sample.

Mathematical modeling is as follows. The symbolic method of calculation is used to obtain formulas for the frequency dependence of the tangent of the dielectric loss angle, that is, the function  $\tan\delta(f)$ . After these we obtain formulas for the frequency dependences of  $\varepsilon''(\omega)$  and  $\varepsilon'(\omega)$  of the sample ( $f = 2\pi\omega$ ) (Ilinskiy et al. 2020).

$$\tan\delta(f) = - (DW + FV) / (FW - DV), \tag{1}$$

$$\varepsilon'(\omega) = (FW - DV)(W^2 + V^2) / \omega C_o [(DW + FV)^2 + (FW - DV)^2], \tag{2}$$

$$\varepsilon''(\omega) = (DW + FV)(W^2 + V^2) / \omega C_o [(DW + FV)^2 + (FW - DV)^2], \tag{3}$$

where

$$D = AGM - BGN - BMH - ANH$$

$$F = AGN + AMH + BGM - BHN$$

$$W = MG - NH + AG - BH + AM - BN$$

$$V = NG + MH + BG + AH + BM + AN,$$

where

$$A = R_I / (\omega^2 R_I^2 C_I^2 + 1)$$

$$B = - [\omega^2 R_I^2 C_I (C_I + C_b) + 1] / (\omega^3 R_I^2 C_I^2 C_b + \omega C_b)$$

$$M = R_{II} / (\omega^2 R_{II}^2 C_{II}^2 + 1)$$

$$N = - [\omega^2 R_{II}^2 C_{II} (C_{II} + C_m) + 1] / (\omega^3 R_{II}^2 C_{II}^2 C_m + \omega C_m)$$

Expression (1) gives two maxima on the graph of the frequency dependence  $\tan\delta(f)$ , and expressions (2), (3) — two semicircles on the Cole-Cole — diagram (solid curves in Fig. 3). By varying the values of  $C_p, C_b, R_p, C_{II}, C_m, R_{II}$  in accordance with the algorithm (Castro et al. 2021), the best agreement of the experimental data with the calculated data is obtained. The result of the fitting determines the sought values  $C_p, C_b, R_p, C_{II}, C_m, R_{II}$  (specific numerical values for the VO<sub>2</sub> film sample are given in the caption to Fig. 3).

Calculations show that as Cole-Cole diagrams do not depend on temperature (Fig. 4), it follows that the temperature shift of both maxima  $\tan\delta(f)$  is determined only by the values  $R_I$  and  $R_{II}$  and the expressions for Cole-Cole diagrams include only the electrical capacities of the sets of grains. Therefore, Fig. 6 shows the calculated temperature dependences of the conductivities  $1/R_I(T)$  and  $1/R_{II}(T)$  for two sets of film grains.

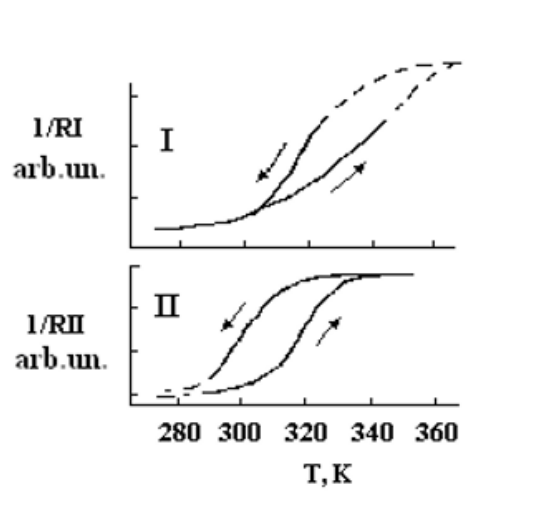


Fig. 6. Thermal hysteresis loops of the electrical conductivity of two sets of grains of the VO<sub>2</sub> film

Figure 6. shows that with an increase in  $T$ , the numerical values of  $R$  decrease. Functions  $1/R_I(T)$  and  $1/R_{II}(T)$  represent the ascending and descending branches of the temperature hysteresis loops of the conductivity of nanocrystallites. The presence of loops indicates semiconductor-metal phase transitions with different values of physical parameters in both sets of VO<sub>2</sub> nanocrystallites. We point out that the set of nanocrystallites, designated by the index I, is characterized by an average resistance  $R_I = 56 \text{ k}\Omega$ , and the elements of this set undergo the Peierls structural SMPT at an average temperature of  $T_{cl} = 340 \text{ K}$ . The elements of the set of nanocrystallites, designated by the index II, are characterized by an average resistance  $R_{II} = 10^6 \Omega$ , and the elements of this set perform the Peierls structural SMPT at an average temperature of  $T_{cII} = 320 \text{ K}$ . This indicates a difference in the physical properties of elements in type I and type II sets.

### Discussion

Function  $\tan(f)$  has two maxima ( $f_{oII} = 1 \text{ Hz}$  and  $f_{oI} = 0.5 \text{ MHz}$ ) and the Cole-Cole diagram has two semicircles. This means that the VO<sub>2</sub> film contains two types of relaxators (II and I). One type is characterised by a time constant of 1 s, and the other type is characterised by a time constant of  $10^{-5} \text{ s}$ .

These types of relaxators correspond to the two sets of nanocrystallites with significantly different electrophysical properties. In addition, the critical temperatures  $T_c$  of the Mott-Peierls SMPT are different for the elements of both sets.

For the low-frequency maximum, the SMPT temperature  $T_{cII} = 320$  K is lower than the transition temperature  $T_{cI} = 340$  K for the high-frequency maximum. This means that in a set of type II, the correlation effects narrow down the  $E_g$  of VO<sub>2</sub> nanocrystallites (lower  $T_c$  of SMPT) much more than in a set of type I (Castro et al. 2021). It also turned out that the width of the hysteresis loop (20 K) for the low-frequency maximum is almost twice the width of the hysteresis loop (11 K) of the high-frequency maximum. According to the martensitic model of the combined Mott–Peierls SMPT in VO<sub>2</sub> (Il'inskiy et al. 2017), this indicates the presence in the VO<sub>2</sub> film of two sets of nanocrystallites significantly different in their diameter.

Low frequency maximum II of function  $\tan(f)$  corresponds to nanocrystallites with a “small” diameter (wide hysteresis loop), while the high-frequency maximum I corresponds to nanocrystallites with a “large” diameter (narrow hysteresis loop). The presence of two types of nanocrystallites is also evidenced by the histogram of the size distribution of nanocrystallites (Fig. 1).

Thus, the numerical values of  $C_{II}$  and  $R_{II}$  represent the electrical capacitance and charging resistance of the entire set of “small” nanocrystallites of the film. This causes an electrical response of the film sample at a low frequency  $f_{oII} = (2^{1/2}) / R_{II}C_{II}$ . The numerical values of  $C_I$  and  $R_I$  correspond to a set of “large” film nanocrystallites at a high frequency  $f_{oI} = (2^{1/2})/R_I C_I$ .

We emphasize that the proposed algorithm used to compare the experimental results with the calculated parameters of the equivalent circuit makes it possible to obtain the numerical value of the ratio of the substrate areas  $S$  occupied by the two described sets of nanocrystallites. This ratio for the sample under study is  $S_{small}/S_{large} = 1.2$ . This result can be obtained because our method allows us to separately determine the capacitances of the substrate  $C_m = 7.5$  pF and  $C_b = 6.2$  pF from the analysis of the parameters of the Cole-Cole diagram.

The nature of SMPT is difficult to analyze because near  $T_c$  vanadium dioxide undergoes two types of SMPT: the Peierls structural transition and the Mott electronic transition (Ilinskiy et al. 2012; Shadrin, Il'inskii 2000). This significantly complicates the simple SMPT model as it is necessary to take into account many-electron interactions. This issue is discussed in detail in our earlier paper (Il'inskiy et al. 2017), therefore, here we present only those excerpts that are important for understanding the proposed statements.

So, at a temperature  $T < T_c = 340$  K vanadium dioxide is a semiconductor, not a metal. This circumstance compels us to assume (on the basis of the considerations described in our earlier papers) that as the temperature decreases to  $T < T_c$ , neighboring vanadium atoms approach each other in pairs, combining their free electrons on the  $d_{x^2-y^2}$  orbitals into a  $\sigma$ -bond.

At this moment, V-V pairs of ions, called “dimers”, are formed. The formation of dimers distorts the crystal lattice lowering its symmetry from tetragonal to monoclinic. The convergence of vanadium atoms means that the distance between vanadium ions inside a pair (or, in other words, a dimer) is less than the distance between the pairs. Therefore, the period of the crystal lattice along the one-dimensional chain of dimers during the formation of V-V pairs doubles. As a result of this structural transition from the metallic phase at  $T > T_c$  to the semiconducting phase at  $T < T_c$ , called the Peierls transition, a gap in the electronic spectrum is formed. In this case, the  $3d||$ -band of the metallic phase splits into two Hubbard subbands (Ilinskiy et al. 2012; Il'inskiy et al. 2017), each of which contains half the number of levels of the original  $d||$ -band.

The lower subband turns out to be almost completely filled with electrons, according to the Pauli principle, while the upper one remains empty (up to the thermal transfer of electrons through the energy gap). Due to the formation of a gap in the energy spectrum, the VO<sub>2</sub> crystal becomes a semiconductor. According to the experiment, the width of the forbidden zone of the semiconductor is 0.7 eV. Hence, it follows that VO<sub>2</sub> in the proposed model should remain a semiconductor at temperatures for which the energy  $K_B T = 34$  meV (at  $T = 340$  K) cannot populate the conduction band through the 700 meV gap. At the same time, the experiment says that VO<sub>2</sub> at  $T > 340$ K becomes a metal.

### *The model requires elaboration.*

There is no doubt about the formation of dimers at  $T < 340$  K, since numerous experimental data (X-ray structural analysis, EPR and NMR studies, Raman spectroscopy, etc.) confirm the formation

of dimers with a decrease in the lattice symmetry from tetragonal to monoclinic at  $T < T_c$ . But even a complicated model of a nonrigid quasi-one-dimensional chain, in which V-V dimers can appear and disappear, cannot explain the fact of thermal SMPT. Indeed, an increase in temperature to the critical value  $T_c = 340$  K at a gap of  $0.7$  eV ( $k_B T = 34$  meV) between the filled lower  $3d$  subband and the empty conduction band cannot lead to thermal destruction of the critical number of dimers required for the metallisation of the sample. That is, with the help of an energy of  $30\text{--}40$  meV bring through the gap of  $700$  meV the number of electrons that is needed to destroy the dimers is impossible. Therefore, the described model requires further elaboration.

At this stage of the construction of a complicated (SMPT) model, it is reasonable to use the well-known consideration of Mott (Mott 1997) regarding the problem of the behavior of an electron in the field of a one-dimensional chain. Such consideration is insufficient for a description in case of one-partial approximation. It is necessary to take into account the many-partial interaction, that is, the interaction between the electrons in the periodic field of the lattice. The effects caused by such interaction are defined by the term “correlation effects”, and the correction to the energy of the bands caused by them is defined as the correlation energy (Gatti et al. 2007).

To conclude, it should be noted that the correlation effects in vanadium dioxide are a consequence of the special properties of the atom V, which has an unfinished  $3d$  shell (No. 23 of the periodic table of elements). A fundamental property of the V atom is the strong dependence of the position of its energy levels on the population of electrons. As a result, the population of the  $4s$  shell with electrons lowers its energy so much that it turns out to be below the  $3d$  shell in energy. Vanadium oxides inherit the fundamental property of this element and obtain the dependence of the energy position of the energy bands on their population. This can be seen when analysing the electronic configurations of the elements K, Ca, Sc, Ti, V, and Cr located sequentially in the periodic table of elements. So, when analysing the electronic configuration K (element no. 19 with the  $3d^0 4s^1$  configuration), a “strangeness” is found: it has the overlying  $4s$  shell filled, while the underlying  $3d$  shell remains empty. That is, the  $4s$  shell, having received an electron, is located lower than the  $3d$  shell in terms of energy. Only after saturation of the  $4s$  shell with electrons does the  $3d$  shell gets filled, starting from the Sc element (21:  $3d^1 4s^2$ ) to the V element (23:  $3d^3 4s^2$ ). Ongoing from V to the element Cr (24:  $3d^5 4s^1$ ), the filling sequence is again violated. An additional Cr electron with respect to V, filling the  $3d$  level, lowers its energy and initiates the transition of an electron from the  $4s$  level to the  $3d$  level.

The reason for the decrease in energy is strong electron–electron interactions (electron–electron correlations) along with the interactions of electrons with the atomic nucleus. As a consequence, the positions of the atomic levels strongly depend on their population. This dependence is transferred to vanadium compounds, in particular, vanadium dioxide. Due to the correlation effects, the energy position of the  $\text{VO}_2$  bands depends on their electron population. This dependence is such that an increase in the population lowers the energy of the bands, and the emptying of the bands enhances their energy. Therefore, a thermal (or optical) increase in the population of the energy bands located above the Fermi level leads to a decrease in their energy, that is, to a decrease in the band gap  $E_g$ . This leads to structural SMPT in  $\text{VO}_2$  at a relatively low temperature  $T = 340$  K.

## Conclusions

The Mott–Peierls SMPT in crystalline  $\text{VO}_2$  films is determined, in addition to what is described above, by the martensitic nature of this phase transformation. As the temperature increases, the structural SMPT at the critical temperature  $T = T_{cl} + \Delta T_H$  ( $\Delta T_H$ —the half-width of the elementary hysteresis loop of the nanocrystallite) first targets “small” grains of the film despite their relatively wide elementary hysteresis loop. Following SMPT in “small” grains, structural SMPT occurs in “large” grains at  $T = T_{cl} + \Delta T_L$ .

This sequence is due to the fact that the phase equilibrium temperature  $T_{cl}$  of “small” grains, corresponding to the middle of the elementary loop, is significantly lower than  $T_{cl}$  of “large” grains. The reason is the technology behind the synthesis of nanocrystalline  $\text{VO}_2$  films.

Thus, it can be stated that the separation of nanocrystallites of the film during its synthesis into two sets—“large” and “small”—is what makes the described SMPT mechanism in  $\text{VO}_2$  films special. In this case, “small” nanocrystallites have a higher concentration of free electrons due to the presence of oxygen vacancies arising during the film synthesis. As a result, they have a smaller band gap (due to the correlation effects) and a smaller value of  $T_{cl}$ . The role of nanocrystallites of various sizes in SMPT in  $\text{VO}_2$  films has been repeatedly discussed earlier. However, our work is the first to experimentally separate the

contributions of “large” and “small” nanocrystallites to SMPT and show that these contributions really differ greatly in the value of critical temperatures. The new experimental data were possible to obtain by dielectric spectroscopy. It turned out that dielectric spectroscopy is capable of separate identification of the electrophysical parameters of various sets of nanocrystallites randomly mixed on the surface of the VO<sub>2</sub> film.

To provide evidence, our article considers a simple case in which dielectric spectroscopy makes it possible to separately study nanocrystallites of different sizes. The size distribution of nanocrystallites can also be recorded using an electron or atomic force microscope (Fig. 1). However, nanocrystallites can be approximately the same size, but have different electrical properties. For example, nanocrystallites doped with different impurities or having different concentrations of the same impurity are not likely to be distinguished by microscopic methods. Dielectric spectroscopy, in this case, turns out to be a very convenient research tool. The nontrivial results of such more complex research options are described in detail in (Ilinskiy et al. 2020).

### Conflict of interest

The authors declare that they have no conflicts of interest.

### References

- Castro, R. A., Ilinskiy, A. V., Pashkevich, M. E. et al. (2021) *Dielektricheskaya spektroskopiya soedinenij sil' nokorrelirovannykh elementov [Dielectric spectroscopy of compounds of strongly correlated elements]*. Saint Petersburg: Fora-print Publ., 54 p. (In Russian)
- Gatti, M., Bruneval, F., Olevano, V., Reining, L. (2007) Understanding correlations in vanadium dioxide from first principles. *Physical Review Letters*, 99 (26), article 266402. <https://www.doi.org/10.1103/PhysRevLett.99.266402> (In English)
- Il'inskiy, A. V., Pashkevich, M. E., Shadrin, E. B. (2017) Stage-by-stage modeling of the mechanism of semiconductor–metal phase transition in vanadium dioxide. *St. Petersburg Polytechnical University Journal: Physics and Mathematics*, 3 (3), 181–186. <https://doi.org/10.1016/j.spjpm.2017.09.002> (In English)
- Ilinskiy, A. V., Kastro, R. A., Pashkevich, M. E., Shadrin, E. B. (2020) Dielectric spectroscopy and mechanism of the semiconductor–metal phase transition in doped VO<sub>2</sub>:Ge and VO<sub>2</sub>:Mg Films. *Semiconductors*, 54 (4), 403–411. <https://doi.org/10.1134/S1063782620040077> (In English)
- Ilinskiy, A. V., Kvashenkina, O. E., Shadrin, E. B. (2012) Nature of the electronic component of the thermal phase transition in VO<sub>2</sub> films. *Semiconductors*, 46 (9), 1171–1185. <https://doi.org/10.1134/S1063782612090096> (In English)
- Mott, N. F. (1997) *Metal-insulator transitions*. London: Taylor and Francis Publ., p. 286. (In English)
- Prokhorov, A. M. (ed.). (1994) *Fizicheskaya entsiklopediya. T. 4: Pojntinga — Robertsona strimery [Physical encyclopedia. Vol. 4: Pointing—Robertson streamers]*. Moscow: Bol'shaya Rossijskaya entsiklopediya Publ., 704 p. (In Russian)
- Shadrin, E. B., Il'inskii, A. V. (2000) On the nature of metal–semiconductor phase transition in vanadium dioxide. *Physics of the Solid State*, 42 (6), 1126–1133. <https://doi.org/10.1134/1.1131328> (In English)

### Физика конденсированного состояния

#### СЕГНЕТОЭЛЕКТРИЧЕСКИЕ ПОЛИМЕРЫ С УЛУЧШЕННЫМИ ХАРАКТЕРИСТИКАМИ.

Шишкин Николай Дмитриевич, Гулякова Анна Александровна

##### Аннотация

Предложен краткий обзор уникальных свойств электроактивных полимеров на основе ПВДФ, а также областей их применения. Сегнетоэлектрические материалы широко используются в современной электронике. Терполимеры с хлорфторэтиленом проявляют релаксорные сегнетоэлектрические свойства с исчезающим гистерезисом, но значительно более высоким значением поляризации. Такие материалы являются потенциальными кандидатами для использования при создании устройств для хранения энергии (суперконденсаторов).

**Ключевые слова:** сегнетоэлектрические полимеры, поливинилиденфторид, поляризация, преобразование энергии, накопление энергии

**Для цитирования:** Shishkin, N. D., Guliakova, A. A. (2022) Ferroelectric polymers with improved performance. *Physics of Complex Systems*, 3 (1), 3–10. <https://www.doi.org/10.33910/2687-153X-2022-3-1-3-10>

#### ИСПОЛЬЗОВАНИЕ МЕТОДА КОМПЛЕКСНОГО ЭЛЕКТРИЧЕСКОГО МОДУЛЯ ДЛЯ ОПРЕДЕЛЕНИЯ РЕЛАКСАЦИОННЫХ ПАРАМЕТРОВ ДИЭЛЕКТРИКОВ С ВЫСОКОЙ ЭЛЕКТРОПРОВОДНОСТЬЮ.

Сальникова Жанна Андреевна, Кононов Алексей Андреевич, Смирнов Александр Павлович, Кастро Арата Рене Алехандро

##### Аннотация

В работе показано, что метод комплексного электрического модуля позволяет исследовать характеристики релаксационных процессов, скрытых высокой электропроводностью диэлектриков. Данный метод позволяет определять релаксационные параметры диэлектриков в случае, когда отсутствуют релаксационные пики на частотной зависимости диэлектрических потерь  $\varepsilon''(f)$ . В результате его применения на частотных зависимостях  $M''(f)$  можно выявить релаксационные пики, а также обнаружить график  $M'(f)$  с резким ростом в области частот, соответствующих максимуму  $M''$ . Аппроксимируя одновременно кривые  $M''(f)$  и  $M'(f)$  в области частот, соответствующих максимуму  $M''$  на основе уравнения Гаврильяка — Негами для электрического модуля, можно определить релаксационные параметры  $\alpha$ ,  $\beta$ ,  $\tau_0$  для исследуемого образца.

**Ключевые слова:** электрический модуль, релаксационные параметры, уравнение Гаврильяка — Негами для электрического модуля

**Для цитирования:** Salnikova, Zh. A., Kononov, A. A., Smirnov, A. P., Castro Arata, R. A. (2022) Application of the complex electrical module method for the determination of the relaxation parameters of dielectrics with high electrical conductivity. *Physics of Complex Systems*, 3 (1), 11–20. <https://www.doi.org/10.33910/2687-153X-2022-3-1-11-20>

#### ЭЛЕКТРОННАЯ СТРУКТУРА НАНОИНТЕРФЕЙСА K/AlN.

Тимошнев Сергей Николаевич, Бенеманская Галина Вадимовна

##### Аннотация

Электронная структура поверхности AlN и ультратонкого интерфейса K/AlN исследовалась с помощью фотоэлектронной спектроскопии *in situ* в условиях сверхвысокого вакуума. Спектры остовных уровней N 1s, Al 2p и K 3p и валентной зоны были исследованы для чистой поверхности AlN и для интерфейса K/AlN в режиме субмонослойных покрытий K. При адсорбции K были обнаружены существенные изменения во всех спектрах. Обнаружены поверхностные состояния в области валентной зоны ниже  $E_{VBM}$ . Установлено, что интерфейс K/AlN имеет полупроводниковый характер.

**Ключевые слова:** нитриды III группы, нитрид алюминия (AlN), интерфейсы, поверхность, фотоэлектронная спектроскопия, электронная структура

**Для цитирования:** Timoshnev, S. N., Benemanskaya, G. V. (2022) The electronic structure of the K/AlN nanointerface. *Physics of Complex Systems*, 3 (1), 21–24. <https://www.doi.org/10.33910/2687-153X-2022-3-1-21-24>

## Теоретическая физика

### К ВОПРОСУ О МЕТОДЕ ПЕРЕПРОЕКЦИРОВАНИЯ ДЛЯ НЕУПРУГИХ ПРОЦЕССОВ В АТОМНЫХ СТОЛКНОВЕНИЯХ В РАМКАХ ПОДХОДА БОРНА — ОППЕНГЕЙМЕРА.

Беляев Андрей Константинович

#### Аннотация

Метод перепроецирования для точного решения неадиабатической ядерной динамики в рамках формализма Борна — Оппенгеймера описан в деталях. В частности, обсуждается асимптотическое поведение вероятности перехода в случае, когда неадиабатический радиальный матричный элемент взаимодействия для рассматриваемого перехода имеет ненулевое асимптотическое значение, что является фундаментальным свойством подхода Борна — Оппенгеймера. Известно, что стандартный подход Борна — Оппенгеймера приводит к расходимости неупругих сечений и неупругих констант скоростей, в то время как метод перепроецирования обеспечивает сходимость. В работе описана физическая основа метода перепроецирования.

**Ключевые слова:** теория рассеяния, неупругие процессы столкновения, неадиабатические переходы, атомные данные

**Для цитирования:** Belyaev, A. K. (2022) Reprojection method for inelastic processes in atomic collisions within Born–Oppenheimer approach. *Physics of Complex Systems*, 3 (1), 25–36. <https://www.doi.org/10.33910/2687-153X-2022-3-1-25-36>

### СВЯЗАННЫЕ СОСТОЯНИЯ ДЛЯ ДВУХ ДЕЛЬТА-ПОТЕНЦИАЛОВ, СОСРЕДОТОЧЕННЫХ НА ПАРАЛЛЕЛЬНЫХ ПРЯМЫХ В ПЛОСКОСТИ.

Багмутов Александр Сергеевич, Попов Игорь Юрьевич

#### Аннотация

Мы рассматриваем сингулярные дельта-потенциалы, сосредоточенные на двух параллельных прямых в плоскости, как модель взаимодействия двух макромолекул. Потенциал имеет постоянную интенсивность на протяжении прямых, за исключением ограниченного отрезка на каждой прямой, где интенсивность уменьшена. Используя вариационный подход, мы изучаем спектр системы, а также получаем оценку лакуны между дискретным и непрерывным спектром как функцию расстояния между отрезками с вариацией потенциала. В заключении с помощью пробной функции доказывается существование хотя бы связанного состояния при любых параметрах системы.

**Ключевые слова:** спектр, вариационный принцип, потенциал на прямой

**Для цитирования:** Bagmutov, A. S., Popov, I. Y. (2022) Bound states for two delta potentials supported on parallel lines on the plane. *Physics of Complex Systems*, 3 (1), 37–42. <https://www.doi.org/10.33910/2687-153X-2022-3-1-37-42>

## Физика полупроводников

### ДИЭЛЕКТРИЧЕСКАЯ СПЕКТРОСКОПИЯ НАНОКРИСТАЛЛИЧЕСКИХ ПЛЕНОК VO<sub>2</sub>.

Кастро Арата Рене Алехандро, Ильинский Александр Валентинович, Климов Владимир Александрович, Пашкевич Марина Эрнстовна, Шадрин Евгений Борисович

#### Аннотация

Методом диэлектрической спектроскопии впервые исследованы нетривиальные особенности размерных зависимостей параметров фазовых превращений в нанокристаллитах пленок VO<sub>2</sub>. Метод позволяет идентифицировать электрофизические параметры наборов нанокристаллитов в пленках VO<sub>2</sub> разного размера, расположенных в случайном порядке на поверхности подложки. Исследована мартенситная природа механизма фазового перехода Мотта — Пайерлса полупроводник — металл в кристаллических пленках VO<sub>2</sub>.

**Ключевые слова:** диэлектрическая спектроскопия, пленки диоксида ванадия, VO<sub>2</sub>, фазовый переход полупроводник — металл, корреляционные эффекты

**Для цитирования:** Castro Arata, R. A., Ilinskiy, A. V., Klimov, V. A., Pashkevish, M. E., Shadrin, E. B. (2022) Dielectric spectroscopy of VO<sub>2</sub> nanocrystalline films. *Physics of Complex Systems*, 3 (1), 43–50. <https://www.doi.org/10.33910/2687-153X-2022-3-1-43-50>